

# DEMONSTRATION REPORT

Demonstration of Crawler-Towed Sensor Technologies in  
Challenging Nearshore Sites

ESTCP Project MR-201422

AUGUST 2017

Gregory Schultz  
White River Technologies

*Distribution Statement A*  
*This document has been cleared for public release*



*Page Intentionally Left Blank*

This report was prepared under contract to the Department of Defense Environmental Security Technology Certification Program (ESTCP). The publication of this report does not indicate endorsement by the Department of Defense, nor should the contents be construed as reflecting the official policy or position of the Department of Defense. Reference herein to any specific commercial product, process, or service by trade name, trademark, manufacturer, or otherwise, does not necessarily constitute or imply its endorsement, recommendation, or favoring by the Department of Defense.

*Page Intentionally Left Blank*

**REPORT DOCUMENTATION PAGE**

Form Approved  
OMB No. 0704-0188

The public reporting burden for this collection of information is estimated to average 1 hour per response, including the time for reviewing instructions, searching existing data sources, gathering and maintaining the data needed, and completing and reviewing the collection of information. Send comments regarding this burden estimate or any other aspect of this collection of information, including suggestions for reducing the burden, to Department of Defense, Washington Headquarters Services, Directorate for Information Operations and Reports (0704-0188), 1215 Jefferson Davis Highway, Suite 1204, Arlington, VA 22202-4302. Respondents should be aware that notwithstanding any other provision of law, no person shall be subject to any penalty for failing to comply with a collection of information if it does not display a currently valid OMB control number.  
**PLEASE DO NOT RETURN YOUR FORM TO THE ABOVE ADDRESS.**

<b>1. REPORT DATE (DD-MM-YYYY)</b> 8/31/2017		<b>2. REPORT TYPE</b> ESTCP Demonstration Report		<b>3. DATES COVERED (From - To)</b> 8/25/2014 - 2/28/2019	
<b>4. TITLE AND SUBTITLE</b> Demonstration of Crawler-Towed Sensor Technologies in Challenging Nearshore Sites				<b>5a. CONTRACT NUMBER</b> 14-C-0057	
				<b>5b. GRANT NUMBER</b>	
				<b>5c. PROGRAM ELEMENT NUMBER</b>	
<b>6. AUTHOR(S)</b> Gregory Schultz				<b>5d. PROJECT NUMBER</b> MR-201422	
				<b>5e. TASK NUMBER</b>	
				<b>5f. WORK UNIT NUMBER</b>	
<b>7. PERFORMING ORGANIZATION NAME(S) AND ADDRESS(ES)</b> White River Technologies 1242 Chestnut Street Newton, MA 02464				<b>8. PERFORMING ORGANIZATION REPORT NUMBER</b> MR-201422	
<b>9. SPONSORING/MONITORING AGENCY NAME(S) AND ADDRESS(ES)</b> Environmental Security Technology Certification Program 4800 Mark Center Drive, Suite 17D03 Alexandria, VA 22350-3605				<b>10. SPONSOR/MONITOR'S ACRONYM(S)</b> ESTCP	
				<b>11. SPONSOR/MONITOR'S REPORT NUMBER(S)</b> MR-201422	
<b>12. DISTRIBUTION/AVAILABILITY STATEMENT</b> DISTRIBUTION STATEMENT A. Approved for public release: distribution unlimited.					
<b>13. SUPPLEMENTARY NOTES</b>					
<b>14. ABSTRACT</b> The overarching goal of this demonstration project was to assess a combination of platform and sensing systems in order to deliver a UXO mapping survey and characterization technology in very challenging nearshore environments. Nearshore environments such as surf zones, salt marshes, shallow bays and tidal estuaries are particularly challenging from the standpoint of mobility and stability of sensing platforms in order to acquire high quality geophysical data.					
<b>15. SUBJECT TERMS</b> Crawler-Towed Sensor Technologies, Nearshore, Battery Management System, Explosive Ordnance Disposal Electromagnetic					
<b>16. SECURITY CLASSIFICATION OF:</b>			<b>17. LIMITATION OF ABSTRACT</b>	<b>18. NUMBER OF PAGES</b>  127	<b>19a. NAME OF RESPONSIBLE PERSON</b> Gregory Schultz
<b>a. REPORT</b>	<b>b. ABSTRACT</b>	<b>c. THIS PAGE</b>			<b>19b. TELEPHONE NUMBER (Include area code)</b> 603-678-8385
UNCLASS	UNCLASS	UNCLASS	UNCLASS		

*Page Intentionally Left Blank*

## **Acknowledgements**

This work was conducted as part of Environmental Security Technology Certification Program (ESTCP) Project MR-201422 led by White River Technologies. Dr. Gregory Schultz was the Principal Investigator. Joe Keranen of White River Technologies provided significant effort in data collection and analysis. Chet Bassani, Randall Reynolds, and Erik Russell of White River Technologies supported system engineering, mobilization, and documentation of the integrated Crawler-EM system. Drs. Jesse McNinch and Heidi Wadman of the USACE Field Research Facility in Duck, North Carolina provided technical guidance, site access/preparation and test support for the demonstration. Matthew Cook, Ed Celkis, and Dr. Tim Crandle of Seaview Systems provided engineering and operational expertise on the SurfROVER crawler system as well as on-site test support.

Funding for this project was provided by the ESTCP. We wish to express our sincere appreciation to Dr. Herb Nelson and Drs. Michael Richardson and Michael Tuley for providing support and guidance for this project.

This report was prepared under contract to the Environmental Security Technology Certification Program. The publication of this report does not indicate endorsement by the Department of Defense, nor should the contents be construed as reflecting the official policy or position of the Department of Defense. Reference herein to any specific commercial product, process, or service by trade name, trademark, manufacturer, or otherwise, does not necessarily constitute or imply its endorsement, recommendation, or favoring by the Department of Defense.

## **Executive Summary**

The overarching goal of this demonstration project was to assess a combination of platform and sensing systems in order to deliver a UXO mapping survey and characterization technology in very challenging nearshore environments. Nearshore environments such as surf zones, salt marshes, shallow bays and tidal estuaries are particularly challenging from the standpoint of mobility and stability of sensing platforms in order to acquire high quality geophysical data. To overcome the limitations of current diver/man-portable or ship-towed configurations, we evaluated both platform and sensor performance to demonstrate and characterize a tailored and integrated robotic bottom crawler-towed sensor solution in representative nearshore UXO sites. The tests and demonstrations reported on here are among the first of their kind in terms of quantification of UXO detection survey performance metrics for a system that can traverse back and forth between fully submerged and dry land environments. In this Interim Test Report, we present challenges overcome in system integration and validation, the preparation of a nearshore test site, and execution and analysis of field tests over representative UXO targets emplaced on land, underwater, and in the transitional shoreline zone.

The data collection and analyses we conducted were part of engineering validation tests and in preparation for follow-on demonstrations at current or former Department of Defense (DoD) nearshore or underwater ranges. The report includes sections on the technology used, specific applications tested, and results obtained for the crawler-towed sensing array system. The initial part of our study focused on verifying control, mobility, and stability features of the bottom crawler platform (i.e., the SurfROver crawler) and its associated sensor tow platform. This included measurements of tow forces required (total bollard pull forces), susceptibility to significant currents and hydrodynamic events (e.g., heave, sway, surge, and breaking wave impact). We then integrated the FlexEM 3D time-domain electromagnetic (EM) sensor array on a tow sled with the crawler and confirmed the combined capabilities required for EM data acquisition, communication, positioning, and control. These capabilities were tested and verified during shakedowns along the western shore of Lake Erie (Toledo Beach, Michigan) and at Blossom Point, Maryland, prior to the demonstration at the US Army Corps of Engineers (USACE) Field Research Facility (FRF) on the shoreline of the northern Outer Banks in Duck, North Carolina.

The SurfROver crawler platform and integrated tow sled system were successfully deployed multiple times and proved to be a stable operating platform with decent tractive control on all substrates on which it was tested (dry grass and gravel, soft sand, mud and silt, shelly sands, dry and saturated fine to coarse sand). Initial deployment testing yielded the need for some improvements to the fiber optic tether system, the tow point encoder and positioning system, and to the EM array sled. Analyses of EM data acquired during these preliminary tests were used to optimize system configuration and data acquisition parameters. Specifically, we made iterative modifications to the mechanical tow sled assemblies and EM system electronics to reduce the overall noise floor of the system by a factor of 6. Additionally, these tests yielded significant improvements for the mission operations and methods used to survey with the system. This included waypoint following and user interface navigation guidance software as well assessments and planning tools for turn radius and traction/trafficability potential of the system.

The majority of the results reported here are from those associated with our demonstration of the system at FRF surfzone and back-barrier sound test sites. We established small test grids comprising inert test UXO objects and standardized test objects in two different nearshore environments adjacent to the FRF site. The first test grid was located in the surfzone (0-2 m water depth) just south of the long observation pier at the FRF site. Late season offshore storms during our test window significantly challenged target emplacement and surveying in water deeper than the breaking wave trough (approximately 1-2 m water depth). Winds in excess of 30 knots and breaking waves over 2.2 m in height prevented a safe and thorough assessment of the system in the surfzone. The results of surveying that were conducted in this environment are promising however. We are able to show adequate control of system mobility and stability with advance rates exceeding 0.32 m/s (0.62 knots) and detection of all targets within 0.3 m RMS localization accuracy relative to surveyed ground truth locations. The full capability of the 3D EM array system was not completely tested because of our limited areal coverage and associated multi-angle EM illumination of targets. Even though we were not able to conduct overlapping survey transects, single pass transects over a number of the emplaced targets yielded classification quality magnetic polarizability inversions that matched our target libraries within 90% fit RMS fit metrics.

Additional testing over the target grid established in the northwestern portion of the Currituck Sound enabled efficient surveying at a rate of approximately 1.2 acres/hour. Targets were readily detected with an overall probability of detection of 100%. Follow on classification using three-axis polarizability inversion was adequate to correctly classify many of the anomalies as targets of interest and as clutter.

Overall, the tests reported on here proved that the system could: (i) be transported, launched, and operated for nearshore and marine UXO applications, (ii) survey effectively with adequate stability and mobility in the surf and traction control on the soft muds in the sound, (iii) provide high quality data to topside operators and analysts for detection and localization of UXO of size 60mm to 155mm within 30 cm of surveyed locations, and (iv) discriminate targets of interest from clutter in many cases when EM array positioning control and coverage permitted. Two technical implementation issues were observed during our demonstration. The first was related to the battery management system for the subsea crawler power supply. We observed frequent faults due to potential overcurrent or overvoltage indicators that moderately impacted operations and should be addressed in future tests/operations. The second issue was related to operations with fiber optic system. The tether and related subsea topside-subsea communications system functioned without exception, but management of the tether while make turns required some additional procedures for preventing the tether from getting wrapped around the GPS mast. Although, the operator control of the crawler system was relatively straightforward, continuous turning with the tow system took some practice. Optimization of the crawler track drive motors may be required to improve continuous turning and overall maneuverability of the integrated system.

# Table of Contents

---

1.0 INTRODUCTION .....	1
1.1 BACKGROUND.....	1
1.2 OBJECTIVE OF THE DEMONSTRATION .....	2
1.3 REGULATORY DRIVERS.....	2
2.0 TECHNOLOGY .....	3
2.1 TECHNOLOGY DESCRIPTION .....	3
2.1.1 Amphibious Robotic Crawler Platform .....	3
2.1.2 Electromagnetic Induction Sensor Array.....	5
2.1.3 Positioning and Vehicle Control.....	9
2.2 TECHNOLOGY DEVELOPMENT .....	12
2.2.1 Trafficability Assessment and Crawler Pull-Force Optimization.....	12
2.2.2 Towed Sled Configuration.....	17
2.2.3 FlexEM Array Characterization.....	22
2.2.4 Topside Operator Interface .....	23
2.2.5 Launch and Recovery System.....	26
2.2.6 Preliminary Shakedown Tests: Blossom Point, Maryland & Toledo Beach, Michigan .....	27
2.3 ADVANTAGES AND LIMITATIONS OF THE TECHNOLOGY .....	33
3.0 PERFORMANCE OBJECTIVES .....	34
3.1 OBJECTIVE: SURFZONE STABILITY .....	36
3.1.1 Metric.....	36
3.1.2 Data Requirements.....	36
3.1.3 Success Criteria.....	36
3.2 OBJECTIVE: AREA COVERAGE RATE .....	36
3.2.1 Metric.....	37
3.2.2 Data Requirements.....	37
3.2.3 Success Criteria.....	37
3.3 OBJECTIVE: ON- AND OFF-SHORE MOBILITY .....	37
3.3.1 Metric.....	37
3.3.2 Data Requirements.....	38
3.3.3 Success Criteria.....	38

3.4	OBJECTIVE: UXO DETECTION PERFORMANCE.....	38
3.4.1	Metric.....	38
3.4.2	Data Requirements.....	38
3.4.3	Success Criteria.....	38
3.5	OBJECTIVE: UXO DETECTION LOCATION ACCURACY.....	38
3.5.1	Metric.....	39
3.5.2	Data Requirements.....	39
3.5.3	Success Criteria.....	39
3.6	OBJECTIVE: UXO CLASSIFICATION .....	39
3.6.1	Metric.....	39
3.6.2	Data Requirements.....	39
3.6.3	Success Criteria.....	39
3.7	OBJECTIVE: EASE OF USE AND OPERATOR INTERFACE .....	39
3.7.1	Metric.....	40
3.7.2	Data Requirements.....	40
3.7.3	Success Criteria.....	40
3.8	OBJECTIVE: LAUNCH AND RECOVERY .....	40
3.8.1	Metric.....	40
3.8.2	Data Requirements.....	40
3.8.3	Success Criteria.....	40
4.0	SITE DESCRIPTION .....	41
4.1	SITE SELECTION.....	41
4.2	SITE HISTORY .....	46
4.3	SITE GEOLOGY .....	47
4.4	MUNITIONS CONTAMINATION .....	50
5.0	TEST DESIGN .....	54
5.1	CONCEPTUAL EXPERIMENTAL DESIGN.....	54
5.2	SITE PREPARATION.....	57
5.3	SYSTEM SPECIFICATION .....	64
5.3.1	SurfROVer Crawler System .....	64
5.3.2	Flex-EM Sensor Array and Tow Platform.....	66
5.3.3	Dual-heading RTK-GPS and GPS Mast System .....	66
5.3.4	Auxiliary Platform Characterization Sensors .....	66
5.3.5	Top-side Control and Display .....	67

5.4	CALIBRATION ACTIVITIES .....	67
5.4.1	Encoder and GPS Calibration .....	67
5.4.2	IVS Surveys .....	69
5.4.3	Flex-EM Calibration .....	70
5.5	DATA COLLECTION .....	70
5.5.1	Scale and Sampling.....	70
5.5.2	Quality Checks.....	71
5.5.3	Data Summary .....	72
6.0	DATA ANALYSIS AND PRODUCTS .....	72
6.1	PREPROCESSING.....	72
6.1.1	Navigation and Control Data .....	72
6.1.2	EM Sensor Data .....	73
6.2	DETECTION .....	73
6.3	PARAMETER ESTIMATION .....	73
6.4	CLASSIFIER TRAINING AND DISCRIMINATION .....	74
6.5	DATA PRODUCTS.....	74
6.5.1	Stability and Mobility Data.....	74
6.5.2	Detection Accuracy.....	75
6.5.3	EMI Sensor Data.....	75
7.0	PERFORMANCE ASSESSMENT .....	77
7.1	SYSTEM STABILITY .....	77
7.2	AREA COVERAGE RATE.....	85
7.3	ON- AND OFF-SHORE MOBILITY.....	86
7.4	DETECTION .....	86
7.5	LOCALIZATION ACCURACY .....	90
7.6	UXO CLASSIFICATION.....	91
7.7	OPERATIONAL EASE OF USE.....	95
7.8	LAUNCH AND RECOVERY .....	97
8.0	COST ASSESSMENT.....	97
8.1	COST MODEL .....	97
9.0	SYNTHESIS AND CONCLUSIONS .....	100
10.0	REFERENCES .....	103

## List of Figures

Figure 1. Photograph of the SeaView SurfROver crawler system. The platform sits on 4 rubber tracks with an axle baseline of 142 cm and total track base width (i.e., width of the platform) of 203 cm. The system is driven by 2 x 3 kW hydraulic geroller drives powered by two 7.5 kWh subsea lithium ion battery array (the two center cylinders on the platform). The frame and mechanical fixtures are comprised of anodized aluminum. The GPS mast extends from the center of platform and can accommodate a telescoping mast of up to 6.5 meters tall.....	4
Figure 2. Photographs of the cylindrical battery pod pressure vessels and battery cell stacks. Each stack contains 600 Li-ion cells to produce a total of 7.5 kWh power supply. ....	4
Figure 3. Photograph of the SeaView SurfROver crawler system with annotations describing the system features and subunits.....	5
Figure 4. Top: Plan view drawing of the Flex-EM array layout with 6 triaxial receivers mounted in pressure vessels and surrounded by 2 transmitter coils that operate in series. Bottom: Photograph of half of the FlexEM array including the transmitter and receivers.....	6
Figure 5. Photograph (top) and solid models (bottom) of the sensor tow sled. All non-metallic materials are used including the 6-meter long tow boom and delrin inserts. ....	7
Figure 6. Photograph of the FlexEM array including the transmitter (foreground, right side) and receiver (foreground, left side) electronics pressure vessels, the sled attachment, and transmitter and receiver components mounted to the FRP sled system.....	8
Figure 7. In April 2014, the prototype EMPACT system conducted data collections at the Aberdeen Proving Ground (APG) Standardized UXO Test Sites. Excellent signal-to-noise was attained over small targets and deeply buried larger munitions. ROC and associated analyses were performed by independent DOD analysts that support the Army's Standardized UXO Test Site.....	8
Figure 8. Example triaxial magnetic polarizability response curves inverted from Flex-EM data over a 60mm UXO and medium schedule 40 ISO oriented in all three primary directions. The blue curves show the primary polarizabilities with red and green illustrating the secondary and tertiary polarizabilities. ....	9
Figure 9. Photograph of the 3 DOF tow point hitch and incremental angle encoder on the aft portion of the crawler. The marine-grade encoder supplies serial data to the multiplexer and fiber optic tether modem for topside data logging and integration with other navigation and positioning information.....	10
Figure 10. Photograph of the Hemisphere V320 GNSS Smart Antenna RTK DPGS system (Left) and drawing of the plan view aspect of the rover antenna (Right).....	11
Figure 11. Photograph of the crawler system with dual heading RTK DGPS rover attached to its mast (Left). The extended GPS mast and tensioned stays are shown with antenna 6.5 meters above the ground (Right). ....	11
Figure 12. Solid model design showing the sled mount and tow boom configuration attached to the crawler.....	13
Figure 13. The effect of varying track width on tractive efficiency in different soil types represented by cohesive strengths of 10, 30, 50, and 70 kPa.....	14
Figure 14. Estimated tractive force as a function of total system weight on various soils. The ratio of maximum tractive force to weight is also shown by the dashed curves relative to the values on the righthand side axis. ....	15

Figure 15. The relationship between traction efficiency and slip is shown for varying track widths. Simulations were conducted assuming a nominal beach sand substrate of 30 kPa cohesive strength.....	15
Figure 16. Drawbar pull force across varying soil cohesive strengths using tracks with different grouser heights. As expected, larger grousers increase the drawbar pull capacity by about the same ratio regardless of the soil cohesion.....	16
Figure 17. Photographs of the bollard pull force test set up and configuration.....	17
Figure 18. Solid model design showing the sled mount and tow boom configuration attached to the crawler.....	18
Figure 19. A. Photograph of the array sled prior to installation of the Flex-EM transmitter coils and receivers. ....	18
Figure 20. Photographs of the preliminary tow sled configuration tests performed at the FRF Duck, NC site.....	19
Figure 21. Profile of the topography across the CRAB transects extending from shore through the surf zone just north of the FRF pier. Depicted are the locations of lower beach, surf zone (near wave trough), and sand bar along the profile where both static and dynamic measurements were taken. ....	20
Figure 22. Load force data along various parts of the shore normal transect. The top two plots show both the raw (red trace) and filtered (blue trace) load force as measured at the tow point of the sled (by a strain gauge). The top plot shows the shore to surf zone portion of the profile and the middle plot shows the profile extending from trough out through the surf and onto the sand bar offshore. The bottom plot shows the time evolution of the load forces while the sled sat in the trough and was repeatedly forced by waves. The local pressure is also plotted showing a strong correlation between wave pressure and load force as expected. ....	20
Figure 23. Comparisons of the light and heavy versions of the sled. The top plots show the load force for the light (approximately 40 lbs weight in saltwater) and heavy (approximately 150 lbs weight in saltwater) sled pulls from offshore to onshore. Although it was not possible to traverse the exact same offshore-to-onshore transect for both experiments, similar vertical relief and wave conditions were experienced by both. The roll and pitch angles were slightly more exaggerated for the light sled.....	21
Figure 24. Left: Load force (bottom) and water depth / altitude off bottom (top) are correlated with single beam acoustic backscatter intensity (middle). Transition from offshore sandy substrates to larger grain size gravely material in the surf and swash zone are evident in the backscatter range versus distance profile. Right: Echologger EA400 sonar mounted on the test sled during FRF data collection.....	22
Figure 25. Photographs of the experimental test stand and dynamic test area for dry characterization tests. A select set of targets were used to characterize the array performance in both the test stand and buried in the test field. ....	23
Figure 26. Block diagram of the overall system configuration split between topside and subsea components. Subsea systems that travel with the crawler include the bottomside motor drive and multiplexer unit, the FlexEM array, and the power and mobility subsystem. Topside comprises the demultiplexer, handheld operator controller, GPS base station, and data processing and visualization computers and monitors. ....	24
Figure 27. The topside operator control station with multiple operator displays. These include (from left to right) the navigation and mission control user interface, 3 crawler-based	

cameras, the FlexEM array data acquisition and real-time display, the power management system interface and scanning sonar display. ....	24
Figure 28. Close-up views of some of the operator displays. The top two monitors show camera views from the crawler, while the bottom two monitors display the navigation and control interface software and the battery management and scanning sonar information to the operator. ....	25
Figure 29. The standalone FlexEM data UI showing navigation information panel on top and real-time waterfall display on the bottom. Additional configuration and diagnostic feedback from the sensor system are displayed to the analyst. In this example, a clear anomaly is displayed (centered) for all axial components for the 6 receiver units across the array. ....	26
Figure 30. Photographs of the open and closed trailer launching of the crawler system. The operators are able to launch and operate the crawler within minutes of arriving on site. The enclosed trailer system houses the crawler for transport and is converted into a fully functioning operator control station once launched. The OCS is completely outfitted for operations included all data displays, rack-mounted computers and data interface modules, dry and wet lab benches, and crawler control systems. ....	27
Figure 31. Power spectral density plots of the estimated noise from measurements during shakedown tests. The plot on the left shows the PSD for all axial components of one receiver channel (Rx-2) on the array prior to noise cancellation while the plot on the right shows the results of noise mitigation methods described. Note the higher than expected noise in the Z-oriented receiver prior to noise cancellation. Noise across the band is similar for all axial components and reduced after application of noise cancellation methods. ....	28
Figure 32. Maps depicting the area on the far western shore of Lake Erie where we conducted shakedown tests with the integrated system. Testing was conducted at Toledo Beach, Michigan on a rocky, sandy shoreline adjacent to shallow waters of Lake Erie. ....	29
Figure 33. The shakedown test area including target strip at the initial water line (the water line shifted or receding during our tests). The locations of the 5 targets we used are shown in the photograph parallel to the shoreline. ....	29
Figure 34. Photographs of the integrated system in operation during shakedown tests in Lake Erie. ....	30
Figure 35. Example GPS heading track data from a shore-normal transect. The profile extends from the shoreline beach area into the water until fully submerged. The dual heading GPS system provides a true-track and magnetic track from the magnetic compass and IMU as well as an independent location-based track from point-to-point GPS motion (course over ground). The best track is the heading based on calculated true vessel heading (HDT) from the dual antenna system. ....	31
Figure 36. Example of raw three component (X, Y, Z) receiver signals for nominal target buried during shakedown tests. ....	32
Figure 37. Example array signature maps showing the integrated Z-axis response for early-to-intermediate time gates over the test string along Lake Erie. Data were processed using the Geosoft Oasis Montaj UX-Detect modules and overlain on a Google Earth image of the site. The bottom plot shows more detail of the target responses - all of which had excess signal-to-noise for detection and mapping. ....	32
Figure 38. Example analyst display of selected target magnetic polarizability classification. The selected target was a 3" diameter steel sphere exhibiting good triaxial symmetry in the	

polarizabilities. The BLU-26 target match is expected due to the spherical nature of that submunitions target, which is also similar in size to our test sphere. .... 33

Figure 39. Regional map of the North Carolina Outer Banks and general site area location at the US Army Corps of Engineers (USACE) Environmental Research and Developmental Center (ERDC) Field Research Facility in Duck. The demonstration is along the beach and seaward shore of the barrier island adjacent to the FRF pier..... 42

Figure 40. Photograph of the FRF pier extending 560 meters into the Atlantic Ocean. Not also the extensive surf zone at the site..... 43

Figure 41. Annotated bathymetric profile in 2015 during preliminary testing at the site. This profile was acquired along a shore-perpendicular transect from the CRAB platform approximately 75 meters north of the FRF pier..... 44

Figure 42. Left: Location of the FRF site and pier annotated over the NOAA nautical chart for this part of the Outer Banks. Right: An aerial photograph looking west over the FRF site with pier in the foreground and facility buildings beyond the dune ridge. The Currituck Sound is the background part of the photo. The general site area is outlined in red. .... 44

Figure 43. FRF site data showing detailed very near-shore bathymetry maps for the general area offshore of Duck (Left) and areas directly north and south of the FRF pier (Right)..... 45

Figure 44. Tidal water level predictions for the Duck FRF Pier (Station ID: 8651370) for early November 2016..... 46

Figure 45. Significant wave height statistical data compiled over the period from June 1995 to April 2000 at the FRF site. Wave heights for October and November are highlighted..... 46

Figure 46. Bathymetry focus map near the study area (from USACE, 2000). The Town of Kitty Hawk in cooperation with the state of North Carolina, USACE, and BOEM conducted studies on sand barrow areas and beach renourishment in 2005 and a comprehensive study was undertaken in 2014 by the towns of Duck, Kitty Hawk, and Kill Devil Hills..... 48

Figure 47. Shallow chirp seismic cross-section acquired approximately 3 km offshore from the FRF pier and extending to 5.5 km (from Walsh and Piatkowski, 2014). .... 48

Figure 48. Wave direction rose diagram from the Wave Information System (WIS) Station 63221 aggregating offshore winds between 1980 and 1999..... 49

Figure 49. Map highlighting the locations of Formerly Used Defense Sites (FUDS) in North Carolina with inset showing those in the far northeast part of the site and along the northern Outer Banks. .... 51

Figure 50. Maps and overlay diagrams depicting the former Duck Target Facility range fan and munitions response site. .... 51

Figure 51. Overview conception site model diagram developed by USACE..... 52

Figure 52. Previous UXO and site characterization investigations at the FRF. .... 54

Figure 53. Top: GIS layer map showing recently acquired (August 2016) LiDAR nearshore bathymetry at the FRF site along with wind and wave vector information from the in-shore array. Two high-resolution bathymetric profiles sampled from ~50 and ~100 meters south of the FRF pier are shown in the bottom. Note the beach slope extending toward a trough and bar sequence before shoaling more gradually seaward. The area 100 to 300 meters along the shore-normal baseline (x-axis) is the area targeted for our demonstration. .... 55

Figure 54. Conceptual overview schematic of the crawler-EM demonstration..... 56

Figure 55. Google Earth image showing the location of target emplacement areas across the surf zone. Site areas are outlined in blue with target emplacement transects indicated in red. The inset shows the shore-perpendicular bathymetric profile scaled to the image easting. A

50 m transect from the shoreline to past the wave breaking zone will be established with UXO targets buried along it. In addition, a small target grid will be set up just seaward from the shore-perpendicular transect..... 57

Figure 56. Surf weather during our demonstration presented significantly challenges for target emplacement and safe operations. Surf waves were typically greater than 5 feet tall and in some cases were 8 or more feet. Strong winds persisted during most of our available testing window..... 58

Figure 57. Annotated photograph from the upper beach looking seaward at the 4x4 target grid extending from the water line to the surf zone. The IVS strip is also shown in the foreground on the left side. .... 58

Figure 58. Schematic diagrams of the target emplacement areas at the FRF demonstration site: Instrument Verification Strip (IVS), shore-normal transect, and 20x20 m target grid area. 59

Figure 59. Photographs of the simulant targets used in the demonstration. These include ISO's, simulant UXO from the Aberdeen Test Center (ATC) test set, clutter objects, and other canonical metal objects for assessing the performance of the overall system. .... 59

Figure 60. Left: Diagram of the 4x4 offshore target grid used for area coverage and UXO target detection and localization testing. The site consisted of 20 by 20 meter grid with 4 target lines buried below the seafloor at nominal depths of 15-45 cm. Sixteen items were emplaced including 12 UXO simulants and 4 ISO objects..... 60

Figure 61. Left: Photograph and dimensions of the BlueDrop free-fall penetrometer. Middle: Summary of BlueDrop specifications. Right: Example of processed data estimated from raw BlueDrop deceleration and pressure distributions with penetration depth. The instrument produces the velocity and deceleration data needed to estimate the quasi-static bearing capacity (QSBC) profile as a function of probe penetration depth..... 61

Figure 62. Photographs of BlueDrop free fall data collection and associated sediment sampling during preliminary site assessment work. .... 61

Figure 63. Aerial view of the BlueDrop sounding locations along the Duck FRF pier. Additional sounds were acquired on the beach and in the swash zone adjacent to the pier. .... 62

Figure 64. Data acquired from foreshore and beach geotechnical sampling and surveying during preliminary site assessment. A) Beach and surf zone bathymetric profile relative to the mean water level across shore-normal transect. Data were acquired with the CRAB bathymetric survey platform. Select penetrometer and sediment grab sample locations are indicated by a-g. B) Average slope computed across the profile showing variability of ~0-10cm/m. Slopes at select locations were used to estimate cone index using the method of Jenkins [1985]. C) Grain size distribution estimates from sediment samples at select locations along the shore-normal transect. Coarsest sediments (1-5mm) were found in the shallow swash and surf zone areas, with largest grain sizes accumulating in the wave break trough in approximately 0.3-1.3 meters water depth. D) Table of average grain size (D50) and estimated cone index for select locations along the shore-normal transect. .... 63

Figure 65. Data acquired from foreshore and beach geotechnical sampling and surveying during preliminary site assessment. A) Beach and surf zone bathymetric profile relative to the mean water level across shore-normal transect..... 64

Figure 66. Configuration diagram of the crawler-based EM system used for the initial demonstrations. The bulk dimensions configuration are shown..... 66

Figure 67. Diagram of GPS rover and tow point encoder calibration. .... 69

Figure 68. Scale and ground sampling metrics from demonstrated survey data collection in the surfzone. Left-to-Right: Overview map of the surfzone transects over which the statistics were calculated; instantaneous speed of the platform computed from GPS time and position; and histogram of the computed ground sampling distance of EMI data coverage. .... 71

Figure 69. Scale and ground sampling metrics from demonstrated survey data collection in the sound. Left-to-Right: Overview map of the sound transects over which the statistics were calculated; instantaneous speed of the platform computed from GPS time and position; and histogram of the computed ground sampling distance of EMI data coverage. .... 71

Figure 70. Examples of stability and mobility data products. .... 75

Figure 71. Data product illustrating the detection location accuracy metric. .... 75

Figure 72. Survey map created using a single pass over six emplaced targets. .... 76

Figure 73. Example data product illustrating the map and inverted polarizability analysis information to be supplied along with the EMI array data quality checks. .... 76

Figure 74. Example map of GPS profile transect parallel to the wave break in the surfzone. The crawler and towed EM array transited into the surf to approximately 50 cm water depth before turning north along the shoreline for ~80 meters. The location of the approximate water line is shown notionally and was not measured. .... 78

Figure 75. Plots of measured sled yaw (top), roll (middle) and pitch (bottom) are shown in blue. The solid red line is the yaw, roll, and pitch of the crawler. Dashed red lines indicate the performance objectives. Objectives were met for roll and pitch but exceeded in yaw. .... 79

Figure 76. Example of heading deviations between the crawler and the towed EM array during shore-parallel survey maneuvers. Left: Crawler and EM array heading during the transect are shown with a turn from southeast to northwest between 0 and 100 seconds and shore-parallel maneuver from 150 seconds on. Right: Measured deviation between crawler and EM array heading. .... 80

Figure 77. Example survey transect roll, pitch, and yaw stability during surfzone demonstrations on 11/7/2016. .... 81

Figure 78. Compilation of ~2 line km of transects conducted in or around the surfzone on 11/7/2016. The western-most transect extending from northwest to southeast was performed in the shallow swash zone and the eastern-most transect extending from northwest to southeast was performed just landward of the wave break area. Compiled statistics for angular stability in terms of roll and pitch are exemplified in the histograms along with the  $\pm 6$  degrees objectives. .... 82

Figure 79. Roll and pitch deviations over the surfzone surveying transects. A variety of crawler system maneuvers and events are represented: from extended durations of the static surveying (400-600 seconds) to rapid maneuvers in high energy surf areas (1200-1400 seconds). .... 82

Figure 80. Maximum instantaneous translational motion measured from GPS and IMU data on the EM array sled. These data include motions associated with normal "straight & level" survey transiting, so a 0.1 m forward translation bias was subtracted from the overall motions to reflect the translational motion deviation. .... 83

Figure 81. Map of the selected GPS profile transect (red) across the Currituck Sound target area transects (blue) used for analysis of array sled stability. .... 83

Figure 82. Rotational angle variation of the system during survey operations in the sound. Plots of measured sled yaw (top), roll (middle) and pitch (bottom) are shown in blue. The solid

red line is the yaw, roll, and pitch of the crawler. Dashed red lines indicate the performance objectives. Objectives were met for roll and pitch but exceeded in yaw. .... 84

Figure 83. Compilation of ~3 line km of transects surveyed in the Currituck sound directly adjacent to the FRF site on 11/9/2016. Water depths extended from 1.4 to 2.6 meters in this area. Compiled statistics for angular stability in terms of roll and pitch are exemplified in the histograms along with the  $\pm 6$  degrees objectives. Both roll and pitch deviations were very small (within 1.5 degrees). Yaw stability was also much better than that exhibited in the surfzone, although multiple turns led to offsets between crawler and tow sled yaw (i.e., crabbing). .... 84

Figure 84. Roll and pitch deviations over the sound surveying transects. Multiple turns and maneuvers were conducted while the roll and pitch remained relatively stable. .... 85

Figure 85. Compilation of offshore and onshore transects used for computing coverage metrics. Left: transects divided into shore parallel (red) and shore-normal (green) transects. Histograms of averaged advance rate for both directions of transects are shown in the middle and right. Shore perpendicular speeds were noticeable slower and had a wider variation compared to shore parallel speeds. .... 85

Figure 86. Example EM data map from Z-oriented receiver data along the shoreline and during shore-parallel surveys in the surfzone. Photographs of the system on the beach and in the surf during EM surveying. .... 87

Figure 87. Detection performance results. The signal-to-noise ratio (SNR) is plotted against target index showing that all detections exceeded the 9 dB SNR objective. Targets in the surf yielded lower SNR values as might be expected. We attribute this to the targets extending deeper below the seafloor than originally planned due to wave induced scour. In addition, lack of horizontal control prevented multiple passes for full coverage surveying. 88

Figure 88. Left: Zoom-in of coverage map over emplaced surfzone targets. Right: Zoom-in showing calculated EM array location while surveying in the surfzone. Fast changes in the sled yaw were due to sudden lateral movements due to breaking waves and swash. .... 88

Figure 89. Coverage map over the Currituck Sound. Emplaced target locations are shown by the magenta Xs. The survey reveals large amounts of clutter in the sound. .... 89

Figure 90. Detection performance results for the sound target grid surveys based on the signal-to-noise ratio (SNR). All target SNR values exceeded the 9 dB SNR objective. .... 90

Figure 91. Detection location errors for IVS (red circles) and emplaced surfzone grid targets (blue circles) location estimates. .... 90

Figure 92. EM anomaly map with GPS groundtruth survey locations and estimated detection locations overlain. Numerous clutter items, densely cluttered areas, and a linear anomaly are evident in addition to the 16 emplaced UXO simulant and ISO targets. Detection location errors for IVS (red circles) and emplaced sound grid targets (blue circles) location estimates. All targets were localized to within 1m of the groundtruth locations and all but two were within 50 cm. .... 91

Figure 93. Example of the classification analysis user interface for the FlexEM crawler system. The map view region-of-interest (ROI) is shown in the upper left with threshold alarm and inverted location markers overlain on the Z-axis data image. Bottom left shows the raw EM data profile over the ROI. The upper right panels show a basic set of four polarizability time evolution libraries (gray curves) with the current set of inverted triaxial polarizabilities overlain (red, green, and blue curves). The bottom right panels show map view and cross-

section views of the inverted target (here a 60 mm mortar) location relative to the array center.....	92
Figure 94. Polarizability library match for a medium ISO target from surfzone grid coverage data.....	93
Figure 95. Polarizability library match for a 105 mm projectile based on target grid coverage data in the surfzone.....	93
Figure 96. Polarizability library match for a 60 mm mortar based on target grid coverage data in the sound. The target was estimated to be 37cm below the array based on the inversion...	94
Figure 97. Polarizability library match for a 81 mm mortar based on target grid coverage data in the sound. The target was estimated to be 38cm below the array based on the inversion...	94
Figure 98. Feature space scatter plot comparing the size and decay distribution computed from polarizability curve characteristics. Cluster analysis was used to group anomalies into 4 classes. ....	95
Figure 99. Comparisons of groupings of polarizability curves determined from analysis of size and decay amongst all anomalies identified in the sound surveys.....	95
Figure 100. Operator control station showing the helmsman with joystick control and multiple screens with camera views and system feedback.....	97

---

## List of Tables

Table 1. Comparison of commercial rubber track systems.....	14
Table 2. Performance Objectives.....	35
Table 3. Summary of MPPEH items removed from the Duck munitions response site.....	53
Table 4. SurfROVER System Specifications.....	65
Table 5. Summary of target objectives, metrics, and results. ....	77
Table 6. Cost Model for a Detection/Discrimination Survey Technology .....	98

---

## List of Acronyms

°C:	Degrees Celsius
ADC:	Analog to Digital Conversion
AFB:	Air Force Base
BLDC:	BrushLess Direct Current
BMS:	Battery Management System
CERCLA:	Comprehensive Environmental Response, Compensation and Liability Act
CH:	Channel
cm:	Centimeter
COTS:	Commercial Off The Shelf
CPA:	Closest Point of Approach
CRAB:	Coastal Research Amphibious Buggy
CST:	Conductivity, Salinity, Temperature
CTD:	Conductivity, Temperature, Depth
dB:	Decibels
DC:	Direct Current
DD:	Dynamic Discriminator
DERP:	Defense Environmental Restoration Program

DGPS: Differential Global Positioning System  
 DOD: Department of Defense  
 DVL: Doppler Velocity Log  
 E: Easting  
 EE/CA: Engineering Evaluation and Cost Analysis  
 EOD: Explosive Ordnance Disposal  
 EM: Electromagnetic  
 EMI: Electromagnetic Induction  
 EMF: Electromotive Force  
 EMPACT: Packable Electromagnetic Technology  
 ERDC: Environmental Research and Development Center  
 ESTCP: Environmental Security Technology Certification Program  
 FA: False Alarms  
 FRF: Field Research Facility  
 FREQ: Frequency  
 FUDS: Formerly Used Defense Sites  
 GNSS: Global Navigation Satellite System  
 GPS: Global Positioning System  
 GUI: Graphical User Interface  
 HDT: Heading Made True  
 HDOP: Horizontal Dilution of Precision  
 HPU: Hydraulic Power Drive Unit  
 Hz: Hertz  
 INS: Inertial Navigation System  
 IVS: Instrument Verification Strip  
 ISO: Industry Standard Objects  
 Kbps: Kilobits Per Second  
 kg: Kilogram  
 kgf: Kilogram Force  
 kHz: Kilohertz  
 kph: Kilometers Per Hour  
 kW: Kilowatt  
 kWh: Kilowatt-hour  
 LAR: Launch and Recovery  
 LARC: Light Amphibious Resupply Cargo  
 LED: Light Emitting Diode  
 LBL: Long Baseline  
 Li-Ion: Lithium Ion  
 m: Meter  
 MEC: Munitions and Explosives of Concern  
 MMRP: Military Munitions Response Program  
 MPPEH: Material Potentially Presenting an Explosive Hazard  
 MR: Munitions Response  
 N: Northing  
 NAVD88: North American Vertical Datum of 1988  
 NCS: Navigation and Control System

NMEA: National Marine Electronics Association  
NOAA: National Oceanic and Atmospheric Administration  
OCS: Operator Control Station  
OEM: Original Equipment Manufacturer  
PCB: Printed Circuit Board  
Pclass: Probability of Classification  
Pd: Probability of Detection  
Pfa: Probability of False Alarm  
ppt: parts per thousand  
PSI: Pounds Per Square Inch  
RA: Removal Action  
RGB: Red Green Blue  
RMS: Root Mean Square  
ROC: Receiver Operating Characteristic  
ROI: Region of Interest  
ROV: Remotely-Operated Vehicle  
RPM: Revolutions Per Minute  
RTCM: Radio Technical Commission for Maritime Services  
RTK: Real-time Kinematic  
Rx: Receiver  
S: Siemens  
SBIR: Small Business Innovative Research  
SI: Site Investigation  
SNR: Signal to Noise Ratio  
SWAP: Size, Weight, and Power  
TCRA: Time Critical Removal Action  
TDOP: Time Dilution of Precision  
TOI: Target of Interest  
UDP: User Datagram Protocol  
UI: User Interface  
USACE: US Army Corps of Engineers  
USBL: Ultra-Short Baseline  
UTC: Coordinated Universal Time  
UTM: Universal Transverse Mercator  
UTV: All-Terrain Utility Vehicle  
UUV: Unmanned Undersea Vehicle  
UXO: Unexploded Ordnance  
WIS: Wave Information System  
WRT: White River Technologies, Inc.  
WWII: World War II

## 1.0 INTRODUCTION

The boundary between land and sea has historically been a key strategic military environment and thus numerous training ranges have been established in these areas (e.g., Camp Lejeune, Cherry Point, Raritan Arsenal, Duck, New River Estuary, Vandenberg AFB). Not only are many of these sites highly contaminated with UXO due to their pervasive use in live fire training, they also pose special risks due to their geographic and/or ecological importance. Nearshore environments such as salt marshes, coastal wetlands, surf zones, shallow bays and tidal estuaries present a number of unique and challenging technical problems for detection and classification of UXO:

- These environments can be fully or partially submerged, or a mix of the two depending on wave and/or tidal conditions.
- UXO can be shallow or deeply buried in cohesive substrates beneath coastal vegetation, typically found in marsh or lagoon environments, or under unconsolidated sand and gravel of the surf zone.
- The geologic and hydrodynamic spatio-temporal conditions tend to vary much more than in pure offshore or terrestrial environments (e.g., highly variable shallow lithology; strong and highly dynamic wave energy and tidal currents).

Currently, only helicopter-based magnetometer or electromagnetic arrays are able to efficiently survey these areas, but they do not provide the detail necessary to both detect all hazardous munitions (due to range limitations) and provide some clutter rejection or classification potential. Conventional offshore and terrestrial methods are not appropriate for these environments due to the deployment methods and vehicles used to transport sensor arrays, the sensor modalities used, and the logistics required. Marine methods that rely on EOD-trained divers or thruster-driven remotely operated vehicles for sonar and/or visual inspection will be severely limited in these environments. Previously demonstrated towed sensor systems, limited to water depths greater than 1 meter, were not amphibious and were therefore unable to perform surveys offshore to onshore (e.g., ESTCP MR-200935). Our goal is to demonstrate a UXO detection system that addresses these challenges and presents a new integrated amphibious sensor technology for challenging nearshore UXO sites.

## 1.1 BACKGROUND

Environmental remediation in nearshore environments is significantly complicated by the dynamics of the environment. Applications related directly to detection and characterization of UXO in nearshore environments as well as those required to support UXO surveys are challenging due to the nature of the environment. There are a wide variety of problems presented:

- Limited mobility, traction and control,
- Poor visibility and overall situational awareness,
- Various physics-based challenges for sensing, such as acoustic backscatter and multi-path propagation, lack of radio frequency transmission, and moving free surface,
- Accurate positioning and navigation,

Despite these challenges, there is a need for geophysical surveying in very nearshore areas. Underwater munitions are becoming increasingly problematic as ports & harbors, seashores, and other underwater environments are commercially developed or utilized for work or recreational activities. These environments vary significantly with respect to depth, morphology, geology, munitions density and human exposure scenarios.

Our focus is on relatively shallow-water conditions – where elevated DoD liability exists due to increased probability of human encounter. These areas include surf zones, marshes, mudflats, swamps, intertidal/littoral zones, and other water bodies of less than 10 m deep such as ponds, streams and shallow lakes. Concentrated human activities and potential intrusive interactions occur in these areas due to fishing, shellfish gathering, swimming, surfing, bathing, jet-skiing, etc. Additionally, construction activity (i.e., dredging, infrastructure repair, pipeline installations) occur in these settings. These areas are also settings for munitions constituent pathways through direct consumption or via consumption of fish or shellfish.

While critical for DoD liability, these areas fall outside present paradigms for terrestrial and underwater detection and characterization. Ground-based methods are ineffectual due to platform inadequacies related to limitations of standoff, cost, mobility/capability, and destruction of the environment. Underwater methods based on acoustic sensors and/or towed arrays are challenged by limited or absent water conditions. Through this pre-proposal, we present ESTCP an efficient and innovative underwater mapping technology that advances current capabilities and provides significant added benefits to DoD.

## **1.2 OBJECTIVE OF THE DEMONSTRATION**

The primary objective of this demonstration is to validate the integration of the EMI array sensor tow, navigation and control system, and the robotic crawler mobility platform in a realistic underwater environment. Validation is conducted through analysis of integrated EMI array, position, and attitude data collected during execution of several dry (beach) and submerged survey profiles. We tracked the cost and time of using the demonstrated system to complete the various missions for comparison against the cost and time efficiency of currently used methods. The final objective of this demonstration is to identify shortcomings and areas of improvement in the hardware, software, and operation of the integrated system.

## **1.3 REGULATORY DRIVERS**

The Department of Defense (DoD) is responsible for assessment and remediation of numerous munitions sites, many containing in-water areas, in the United States. When the transfer of responsibility to other government agencies or to the civilian sector takes place, the DoD lands fall under the compliance requirements of the Superfund statutes. Section 2908 of the 1993 Public Law 103-160 requires adherence to Comprehensive Environmental Response, Compensation, and Liability Act (CERCLA) provisions. The basic drivers are related to assumption of liability for ordnance contamination on the previously DoD-controlled sites.

Site cleanup is performed using the Superfund CERCLA process, which provides the liability of persons responsible for waste at these sites and provides details on the steps required for site

cleanup from initial assessment to redevelopment. EMI and magnetic detection sensors are standard technology used in various stages of the CERCLA process in cleanup of ground sites. The technology demonstrated is towards implementation of a similar technology set for the cleanup of in-water sites.

There are no explicit regulatory drivers or considerations associated directly with this preliminary demonstration. All demonstration activities were conducted in waters regulated by federal and state (Florida) laws and outside of any military areas or regulated by special munitions contamination provisions.

## **2.0 TECHNOLOGY**

We demonstrated an amphibious robotic crawler system integrated with an EMI sensor tow sled that, together, are capable of detecting UXO in challenging nearshore environments. The crawler system is the SeaView SurfROver amphibious robot with integrated fiber optic tether system, track controller, lights and cameras, and GPS/INS positioning system. The primary EMI sensor payload technology is the FlexEM system suitable for underwater UXO detection and some level of clutter rejection and target classification.

### **2.1 TECHNOLOGY DESCRIPTION**

#### **2.1.1 Amphibious Robotic Crawler Platform**

The SeaView Systems SurfROver crawler incorporates the ability to carry the UXO sensor payload and other cameras and sensors in a wide range of marine environments including littoral environments and surf zones. The basic platform sits on a set of crawler tracks, each driven by a 3 kW hydraulic power drive unit (HPU). The tracks are comprised of 4 individual "Mattracks" made of mild steel, composite and rubberized plastic guide wheels, and 330mm wide (13-inch wide) rubber tracks. The contact area of each track is approximately 1200mm x 220mm, which is estimated to exhibit a modest ground pressure of around 10KPa (1 psi). This prevents the system from sinking into all seabed materials but soft mud. The vehicle has been designed to accept more ballast should operations prove to warrant an increase. Each track is driven by a hydraulic propulsion unit that combines BLDC motors and gerotor drives for hydraulic control of forward and backward motion. The ge-roller is a "generated roller rotor" consisting of concentric inner and outer rotors that act as a positive displacement pump (Ivantysynova, 2000). Figure 1 shows a photograph of the SurfROver crawler system.



**Figure 1. Photograph of the SeaView SurfROVer crawler system. The platform sits on 4 rubber tracks with an axle baseline of 142 cm and total track base width (i.e., width of the platform) of 203 cm. The system is driven by 2 x 3 kW hydraulic geroller drives powered by two 7.5 kWh subsea lithium ion battery array (the two center cylinders on the platform). The frame and mechanical fixtures are comprised of anodized aluminum. The GPS mast extends from the center of platform and can accommodate a telescoping mast of up to 6.5 meters tall.**

SeaView utilize a “ROV Backbone” system which has been designed to aid in the rapid development of custom underwater vehicles such as tunnel crawlers, customized ROVs, and articulated underwater robots. The ROV backbone provides power, fiber optic telemetry and peripheral device control options. Power is provided subsea (on the crawler) through two 7.5 kWh battery pods that yield a nominal 12-16 hours of endurance (Figure 2).



**Figure 2. Photographs of the cylindrical battery pod pressure vessels and battery cell stacks. Each stack contains 600 Li-ion cells to produce a total of 7.5 kWh power supply.**

System control is performed using an ethernet and RS-485 control protocol common to SeaView systems called ROVbus. This protocol is used to control devices such as the drive motor speed and direction, camera pan and tilt units, LED lights and dimmers, drive actuators (antenna poles, UXO sensor arm etc.). The fiber optic tether system is a proven and rapidly customizable technology used in multiple SeaView systems. Figure 3 illustrates the overall layout of the system including location of subunits and auxiliary sensors.

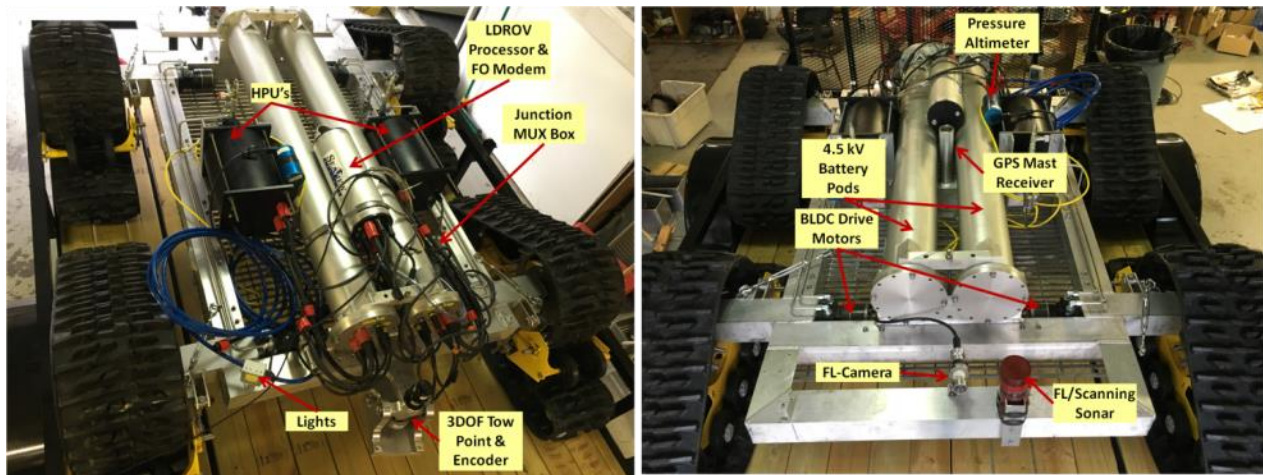


**Figure 3. Photograph of the SeaView SurfROVER crawler system with annotations describing the system features and subunits.**

The crawler system is stable in sea states up to SS3 and sustained current conditions of 3 knots. One hundred liters of payload volume is available for carrying up to 150 kg of equipment or sensors. A range of payload power and data communication formats are available to accommodate most types of towed or rigidly attached sensors such as pipe/cable trackers, EM systems, sonar systems, optical systems, and sampling instrumentation. The maximum ground speed is approximately 5 kph with over 350 kgf of drawbar pulling force available for towing. Standard auxiliary sensing includes three RGB fixed view cameras, two sets of LED lamps, forward scanning sonar, obstacle avoidance camera, inertial measurement unit, pressure depth sensor, and compass. The position of the crawler is determined from a GNSS-enabled RTK-DGPS dual heading system mounted on a 6-meter mast for shallow water operations. Inertial guided underwater positioning can be readily augmented with USBL or LBL positioning systems.

### 2.1.2 Electromagnetic Induction Sensor Array

In conjunction with previous efforts (e.g., ESTCP MR-201225 and Army SBIR Topic A12-040) WRT has developed the Flex-EM marine array as a configurable high-resolution digital geophysical mapping system. The Flex-EM was developed as a marine version of the EMPACT Dynamic Discriminator (DD) time-domain EMI array (Laudato et al., 2016; Schultz et al., 2014). This system has been tested as an alternate to the EM61 for both terrestrial and marine surveys. It was specifically designed for detection and classification of UXO in challenging environments where ruggedization and mobility are key requirements.

The sensor tow package is comprised of two marinized transmitters and six small high-resolution marinized 3D EMI receivers mounted on a non-metallic sled riding on three ultra-high molecular weight (UHMW) skids. The sensor head features a form factor that is comparable to that of the EM61 coil and comprises base units with 1.0 m x 0.5 m transmitter coils that encompass 6 small (8x8x8 cm) 3-axis receiver cubes (see Figure 4). In its current configuration, the two transmitters are excited in series to form an effective single 2m by 0.5m loop. They are protected by a fiberglass and epoxy housing with wet-mateable marine connector and coil interconnects. Each receiver is also housed in custom PVC or delrin housings machined from monolithic blocks and fitted with o-ring seals and wet-mateable connectors. The enclosures were designed for and rated to seawater depths of up to 100 m. These receiver enclosures were previously tested in SERDP project MR-1714.

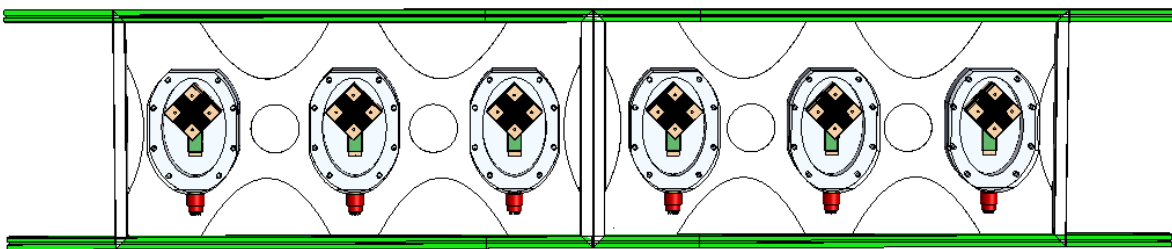


**Figure 4. Top: Plan view drawing of the Flex-EM array layout with 6 triaxial receivers mounted in pressure vessels and surrounded by 2 transmitter coils that operate in series. Bottom: Photograph of half of the FlexEM array including the transmitter and receivers.**

The system driver and data acquisition electronics are housed in a 9-inch outer-diameter cylindrical pressure vessel. The pressure vessel has been verified to accommodate other electronics modules such as an EM-61 console or MetalMapper 2x2 electronics. For the EM-61S marine coil, the sensor array mounting is very similar to the Flex-EM and readily accommodated through simple bracketry and fixturing. The electronics requires only internal jumper cables to the marine connectors on the pressure vessel (RS232 signals are readily handled by our existing wet-mateable connectors) and incorporation of a data consolidation and power supply circuit boards. Both PCBs have been developed, tested, and used with other systems. The data consolidation PCB has been validated to receive and converts EM-61 serial data to Ethernet format that transmits up the tow cable and/or written to local data storage devices.

The tow system with Flex-EM array weighs approximately 280 lbs in air and runs on 3 skids that exert a maximum static bearing pressure of 2 PSI on land and as low as 0.06 PSI in seawater. The tow sled also has a pair of low-profile foam-filled non-metal wheels that attach directly to the skids. These are primarily used for transit to and from the site location and surveys on dry beach or solid ground. Figure 5 and Figure 6 show the tow sled with and without the Flex-EM sensor mounted.

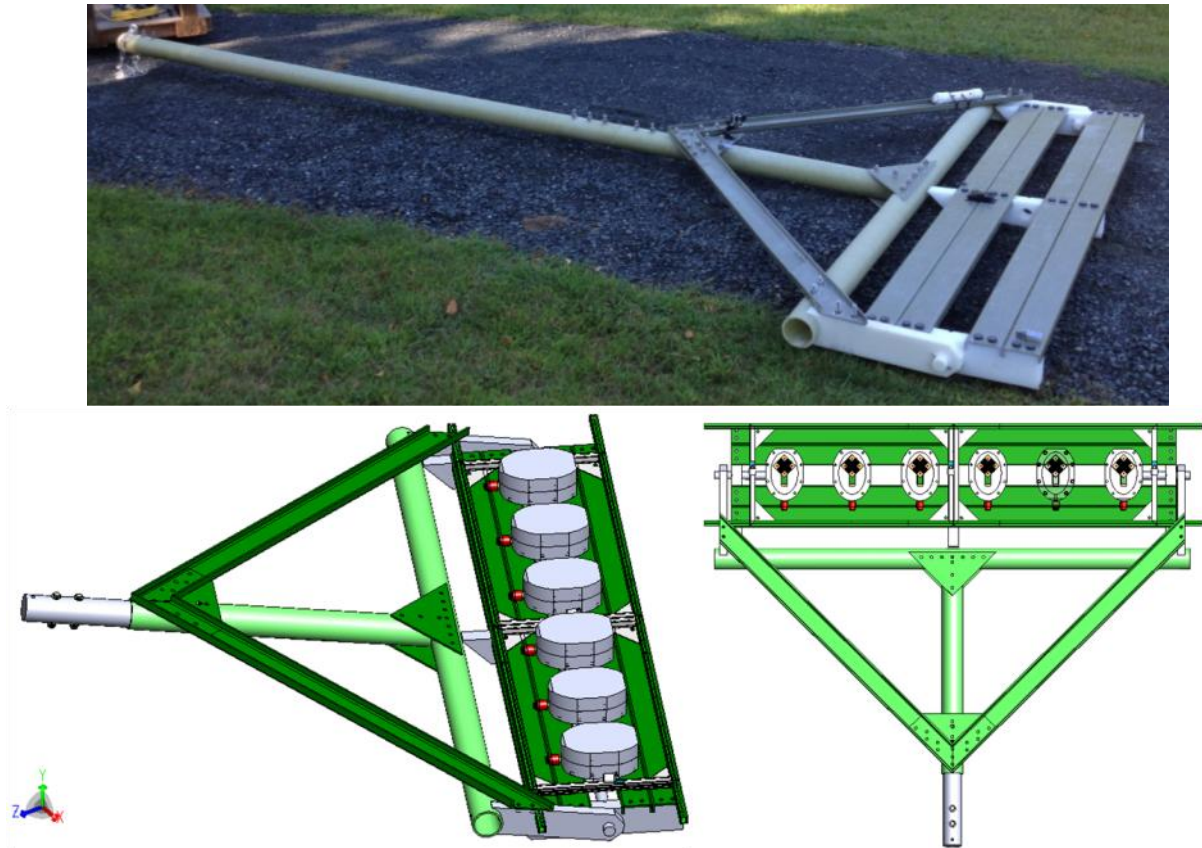


**Figure 5. Photograph (top) and solid models (bottom) of the sensor tow sled. All non-metallic materials are used including the 6-meter long tow boom and delrin inserts.**



**Figure 6. Photograph of the FlexEM array including the transmitter (foreground, right side) and receiver (foreground, left side) electronics pressure vessels, the sled attachment, and transmitter and receiver components mounted to the FRP sled system.**

The overall system components, developed in conjunction with previous DOD-funded efforts (i.e., Army SBIR A12-040), were completed in 2014 and implemented for terrestrial UXO surveys. This version of the system (the EMPACT Dynamic Discriminator Cart) underwent terrestrial verification testing and evaluations at the Fort A.P. Hill (APH) and Aberdeen Proving Ground (APG) UXO test sites in 2014 and 2015. Independent scoring of the Flex-EM array during these tests yielded unmatched performance relative to all previous man-portable systems at APG’s blind UXO grid and achieved >50% clutter rejection and >88% background false alarm rejection while retaining a 99% detection probability. Localization accuracy is within 3 cm in lateral and 2.5 cm in depth (Figure 7). Subsequent dynamic classification testing at the Army’s UXO site at APH has yielded 100% detection probability against small submunitions with 89% clutter rejection.

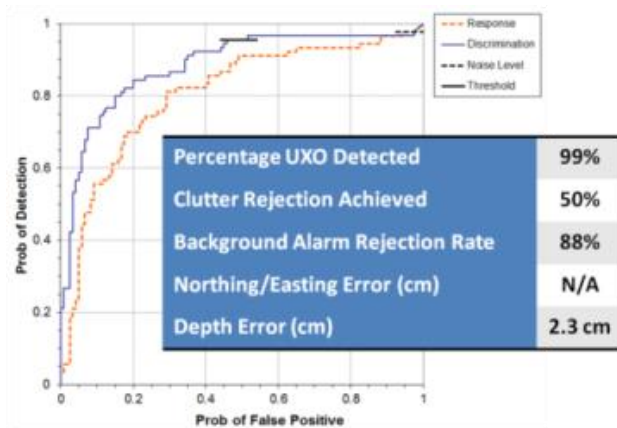


**Figure 7. In April 2014, the prototype EMPACT system conducted data collections at the Aberdeen Proving Ground (APG) Standardized UXO Test Sites. Excellent signal-to-noise was attained over small targets and deeply buried larger munitions. ROC and associated analyses were performed by independent DOD analysts that support the Army’s Standardized UXO Test Site.**

Because this sensor has only one effective transmitter coil, data aggregation of consecutive soundings along the transect line (i.e., line methodology) ensures the target receives required multi-axis illumination from the transmitter to produce useful polarizabilities for classification analysis. As the transmitter passes over the target, any offset of the sensor from directly over the target produces a different angle of incidence between the impinging transmitter field and the target. Raw decay transients received during transmitter off times are stacked (averaged) with appropriate sign changes for positive and negative half cycles. The resultant data are saved as a single scan consisting of 16 or 32 time gate values between 50 us and 15 ms for each of the 3 triaxial components on all receivers. This yields 288 individual data channels on each scan (18 receiver channels times 16 time gate values), which is repeated at a rate of 10 Hz.

This data has been shown to produce adequate angular illumination and data quality so that dipole inversion methods can be applied for generating axial magnetic polarizability response curves. We acquired data with the Flex-EM system over canonical test targets such as steel spheres, plates, 60mm and 81mm mortars and industry standard objects. Some examples of polarizabilities from these objects are shown in Figure 8.

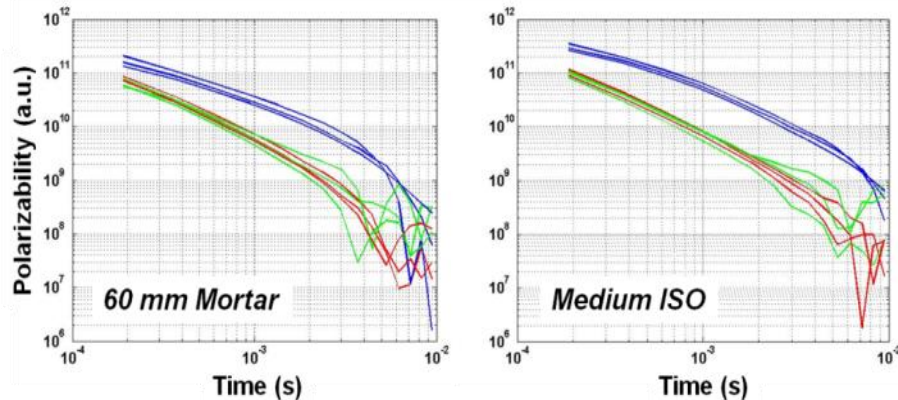


**Figure 8. Example triaxial magnetic polarizability response curves inverted from Flex-EM data over a 60mm UXO and medium schedule 40 ISO oriented in all three primary directions. The blue curves show the primary polarizabilities with red and green illustrating the secondary and tertiary polarizabilities.**

### 2.1.3 Positioning and Vehicle Control

Positioning and navigation options for the crawler-towed system include both GPS-based and underwater positioning technologies such inertial navigation and ultra-short baseline (USBL) or long baseline (LBL) systems. Positional accuracy varies depending on the method used and can be dependent on site and deployment conditions. Practical experience with USBL positioning of ROV systems in a number of environments has yielded accuracies of approximately 1 m in less than 25 m water depths but larger positioning errors are typical. Although USBL is relatively simple to operate, bearing accuracies exceeding ~3 degrees lead to unsuitable positional errors for UXO detection operations that increase with range from the USBL transducer.

Our positioning problem is exacerbated by the fact that we have a two-body system comprised of the crawler itself and the tow platform. Although the tow platform is coupled to the crawler through a rigid tow bar, the tow point has 3 rotational degrees of freedom to allow motion over

roll, pitch, and yaw angles (Figure 9). This means that the tow platform is not necessarily following directly in-line with the crawler trajectory. Therefore, we need to provide instantaneous relative position and orientation estimates of the tow platform relative to the crawler. This is accomplished through an incremental angle encoder at the tow point to measure the yaw (azimuth) and an inertial measurement unit on the tow bar that provides roll and pitch angles. These measurements can be combined with those measured on the crawler platform itself to generate relative orientation between the two bodies.



**Figure 9. Photograph of the 3 DOF tow point hitch and incremental angle encoder on the aft portion of the crawler. The marine-grade encoder supplies serial data to the multiplexer and fiber optic tether modem for topside data logging and integration with other navigation and positioning information.**

Mounted on the crawler platform itself are sensors for positioning and orientation when the crawler is in sufficiently shallow water (<4m) and when it is in relatively deep water (>4m). In shore-based and shallow water operations, a rigid GPS mast provides a mounting point for a RTK-DGPS antenna at 6 meters above the base of the tracks (i.e., the seafloor in no sinkage/scour conditions). The mast extends down to a base point in the center of the crawler body as shown in Figure 11. Mounted to the mast is a Hemisphere V320 dual heading marine-grade RTK DGPS system. This system allows acquisition of GNSS-enabled RTK-DGPS data. The Hemisphere V320 is based on the Eclipse Vector GNSS technology utilizing the all-in-one GNSS Eclipse vector-based receiver and two integrally separated rover antennas with a baseline of 50 cm. The V320 specifications indicate a heading accuracy of up to 0.17 degrees RMS and positioning accuracy down to 2 cm RMS depending on survey conditions. Precise RTK positioning is achieved through the Athena L1/L2 technology which is capable of integrated SBAS, beacon, and Atlas L-band. It also supports GLONASS, BeiDou, and GNSS augmentation automatically.

The rover antenna is 629mm long and 208mm wide, make it a bit larger than conventional single antennal RTK DPGS rovers. Once installed, the system has three serial ports for receiving

differential corrections via full-duplex RS232 or RS422 connections. This is handled through a serial-to-NMEA 2000 port that contains both signal and power conductors through a single waterproof connector. A photograph and drawing of the V320 rover antenna are shown in Figure 10.

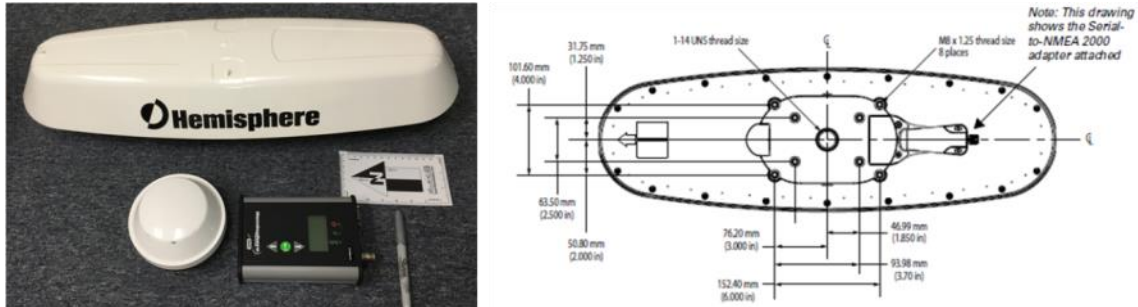


**Figure 10. Photograph of the Hemisphere V320 GNSS Smart Antenna RTK DPGS system (Left) and drawing of the plan view aspect of the rover antenna (Right).**

The rover antenna is mounted to the GPS mast through a flush mounting template to ensure alignment relative to the tow point encoder and vehicle. The mast is comprised of multiple sections of schedule 40 fiber-reinforced plastic (FRP) and aluminum jointing fixtures. Two 10-foot long sections can be coupled to create a total mast height of 655 cm above the receiver base on the crawler, which is approximately 35cm above the track base. For the extended 6.5 meter mast, a series of spreader booms and Dyneema rope stays are used to stabilize the mast under water. Photographs of the V320 GPS rover mounted on the mast are shown in Figure 10.



**Figure 11. Photograph of the crawler system with dual heading RTK DGPS rover attached to its mast (Left). The extended GPS mast and tensioned stays are shown with antenna 6.5 meters above the ground (Right).**

## 2.2 TECHNOLOGY DEVELOPMENT

### 2.2.1 Trafficability Assessment and Crawler Pull-Force Optimization

As described in Section 2.1.1., the SurfROver utilizes four rubber track drive systems. The configuration of these tracks in combination with vehicle parameters such as thrust capacity, torque, drawbar pull force, gross weight and weight distribution, and buoyancy constrain the mobility, stability, and overall trafficability of the system. *Mobility* assessments consider the entire effects of the terrain on platform operations, including obstacles and bathymetry/topography. The ability of terrain to support and provide traction for vehicle platform operations is termed *trafficability*. Similarly, the study of vehicle performance in relation to its operating environment is often referred to as *terramechanics*.

To maximize tractive performance and minimize soil disturbance, the pressure distribution on a rubber track should be uniform and the dynamic weight distribution between fore and aft bogie wheels should be equivalent. The dynamic weight distribution on rubber tracks depends on factors such as static weight, tractor dimensions, center of gravity location, and the magnitude and angle of the pull force. Unlike platforms with tires, both the magnitude and uniformity of the dynamic load distribution are important during test of these systems.

Several theoretical, empirical, and experimental studies have been conducted to better understand the traction behavior of tracked crawler systems on the seafloor. Shoop [1993] provides a comprehensive overview of terramechanics and trafficability that assesses terrain or substrate characterization methods for a wide variety of vehicle traction studies. Jenkins [1986] describes methods for determining beach trafficability based on soil mechanics and available observations. Grisso [2006] developed mathematical models for describing the interaction of rubber-track systems and sediments they are in contact with for predicting crawler traction performance. In addition, Katusui et al. [2012 and 2014] and Waldman and Richter [2007] developed detailed numerical investigations of dynamic motion of crawler systems on the seafloor. These studies combine computational fluid dynamics models with dynamic mechanical analyses to better understand the "running" conditions of the platforms with various contact and propulsion mechanisms.

In our work for this project, we investigated simple pressure-sinkage relationships using the fundamental empirical relationships of Bekker and Wong (generally known as Bekker's Derived Terramechanics Model or BDTM). To the extent possible, we apply data from motion of the platform over varying substrates using the NATO and/or US Army empirical equations for computing the mobility (MI) and vehicle cone indices (VCI). The MI and VCI metrics relate the vehicle parameters to the cone index for fine grained substrates (such as sand and silt). This provides the most straightforward method to relate data we obtain from the vehicle mobility and those that may be available from geotechnical investigations of substrates in our test areas (e.g., cone penetrometer measurements).

Using Bekker's pressure sinkage relationship for a rigid (relatively smooth), uniformly loaded track, we can determine the track sinkage  $z_t$  as a function of the static weight  $W$  or average ground pressure  $p$ :

$$z_t = \left[ \frac{p}{(k_c/b) + k_\phi} \right]^{1/n} = \left[ \frac{W/bL}{(k_c/b) + k_\phi} \right]^{1/n},$$

where  $k_c$ ,  $k_\phi$ , and  $n$  are Bekker pressure-sinkage parameters (empirically determined) and  $b$  is the track width and  $L$  is the track length. The motion resistance of the track due to soil compaction  $R_c$  is:

$$R_c = \frac{1}{(n+1)(k_c/b + k_\phi)^{1/n}} \left[ \frac{W}{L} \right]^{(n+1)/n}.$$

If the contact pressure is uniformly distributed (Figure 12) and the shear displacement can be approximated by a simple exponential relationship (as is conventional in simple BDTM), then the tractive effort of track with contact area  $A$  can be determined from:

$$F_t = b \int_0^L \left( c + \frac{W}{bL} \tan \phi \right) (1 - e^{-ix/K}) dx = (Ac + W \tan \phi) \left[ 1 - \frac{K}{iL} (1 - e^{-iL/K}) \right],$$

where  $i$  is the slip,  $K$  is the shear modulus,  $c$  is the soil cohesion and  $\phi$  is the soil angle of internal friction. If we assume the maximum shear strength  $\tau_{max}$ , the maximum tractive effort  $F_{tMAX}$  is

$$F_{tMAX} = Ac + W \tan \phi.$$

With the tractive effort and compaction resistance in hand, we can determined the available drawbar pull  $F_{DP} = F_t - R_c$ .

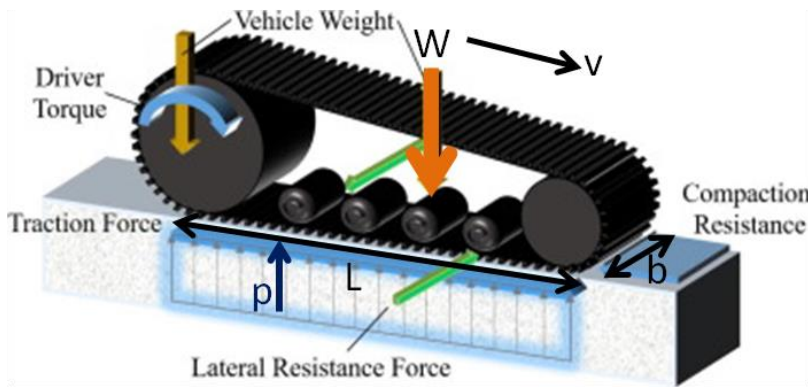


**Figure 12.** Schematic diagram of a crawler track showing torque generated by a drive wheel and transferred to bogie wheels via a rubber track. The forces acting on the system and primary dimensions are shown.

One of the most straightforward considerations is the trackwidth affect on tractive efficiency of the crawler vehicle. Grisso [2006] utilized the Brixius formulations for interaction of traction devices and soils to predict rubber track performance. We used this generalized modified formulation to understand the relationship between tractive efficiency, track parameters, dynamic load, and sediment cohesion. Tractive efficiency is the ratio of drawbar power to axle power, or otherwise and more generally the ratio of the output to input power of the track:

$$\eta = \frac{F_{DP}v}{T} = \frac{GTR - MR}{GTR} (1 - slip),$$

where  $F_{DP}$  is total drawbar pull [N],  $v$  is travel velocity [m/s],  $T$  is input torque [Nm],  $GTR$  is the gross traction ratio, and  $MR$  is the motion resistance ratio.  $GTR$  is generally derived empirically by assessing the relationship between soil cohesion, track length and width, system wieght, and the mobility number. Although the surfROVER crawler was designed to accomodate the Mattrack-EZ rubber track systems, we compare the performance of other commercially available

tracks in Table 1. These bolt-on track systems range from 25 cm (11 inches) to 43 cm (15 inches) wide and from 1.2 m to 2.4 m long.

**Table 1. Comparison of commercial rubber track systems.**

	Mattrack EZ	Mattrack XT	Mattrack M3	Mattrack 65M1-A1	KIMPEX WSS4	CAMOS R4S
Track Width (cm)	33.0	27.9	33.0	38.1	33.7	20.32
Track Length (cm)	114.3	99.1	106.7	114.3	246.4	243.8
Grouser Height (cm)	3.56	2.54	4.45	2.54	3.30	2.79
GCSA* (m <sup>2</sup> )	1.52	1.10	1.41	Unknown	1.57	1.29

\* GCSA=Ground Contact Surface Area

Using the range of track parameters represented by commercially available systems and the specifications of the SurfROVer crawler, we show the tractive efficiency for varying track width over different soil strengths in Figure 13. For nominal sediment cohesion conditions of 30-70 kPa, this trafficability simulation yields very little variation for different track widths. Although, these are accentuated for very low cohesive strength sediment (10 kPa), the tractive efficiency is not significantly improved by changing the track width.

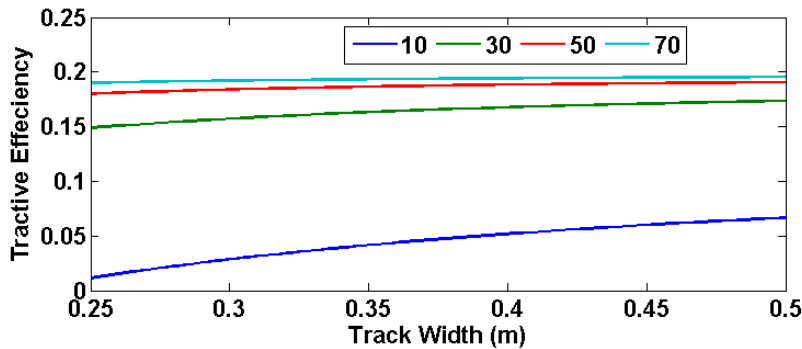


**Figure 13. The effect of varying track width on tractive efficiency in different soil types represented by cohesive strengths of 10, 30, 50, and 70 kPa.**

The variability in tractive force and normalized maximum force versus system weight for variable soil types (characterized by cohesive strength) is shown in Figure 14. Here we see that the system weight plays a greater role in the overall tractive efficiency.

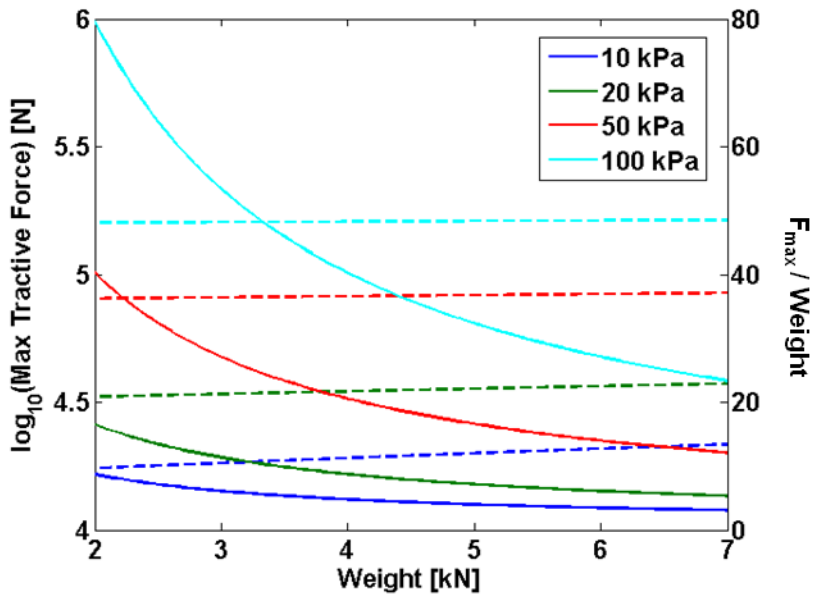


Figure 14. Estimated tractive force as a function of total system weight on various soils. The ratio of maximum tractive force to weight is also shown by the dashed curves relative to the values on the righthand side axis.

The effect of slip on tractive efficiency for variable track widths is generally insignificant given the range of tracks we considered. This is shown in Figure 15 for tracks ranging from 20 to 50 cm wide and assuming a cone index for nominal sandy beach. Several empirical models have been developed using the cone index, where it is assumed that the soil strength is only proportional to the cone index value. In this case, drawbar pull increases and motion resistance decreases as the cone index increases. This type of model was originally utilized by the US Army Waterways Experiment Station (WES) for military prediction of cross-country ground vehicle performance including the concepts of mobility index and go/no-go conditions.

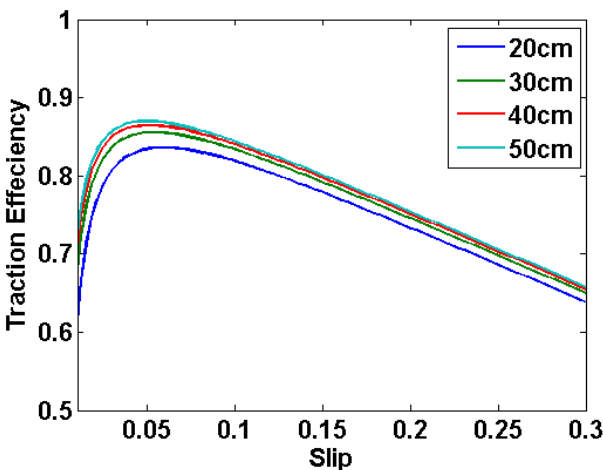
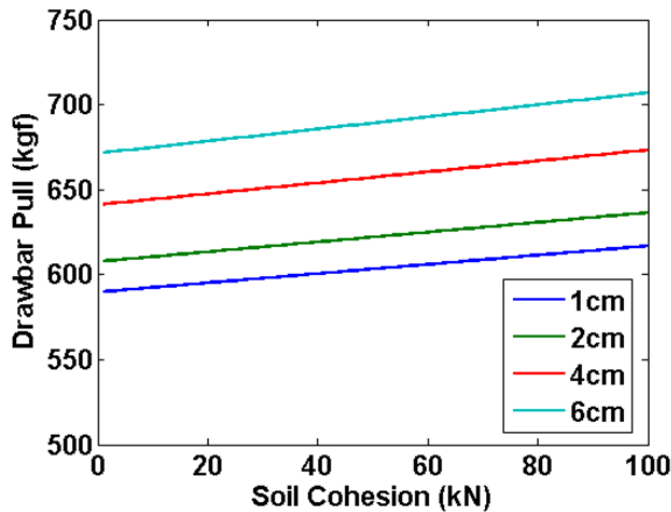


Figure 15. The relationship between traction efficiency and slip is shown for varying track widths. Simulations were conducted assuming a nominal beach sand substrate of 30 kPa cohesive strength.

Using the simplified model of Grisso [2006], we can also simulate and evaluate the relationship between soil properties and drawbar pull force. In particular, we analyzed the impact of varying the grouser height on drawbar pull over a range of expected soil cohesion for soft sediment such as dry or saturated sand. Figure 16 shows that as the grouser height is increased drawbar pull

force is also increased as expected. The SurfROVER Mattrack EZ grousers are approximately 3.5 cm tall and thus should provide ~600-650 kgf of drawbar pull.



**Figure 16. Drawbar pull force across varying soil cohesive strengths using tracks with different grouser heights. As expected, larger grousers increase the drawbar pull capacity by about the same ratio regardless of the soil cohesion.**

To compare simulated drawbar pull to measurements and to ensure sufficient thrust force, we performed bollard pull force tests on the SurfROVER. The original georotor hydraulic driver motors that we tested during initial integrated system trials proved to limit our top-end velocity to ~2-3 kph. Since our goal was closer to 10 kph on land, we investigated a set of larger hydraulic drive motors that would increase our speed while retaining an acceptable bollard pull force and related low-speed torque. After retrofitting the SurfROVER with the new motors, we performed a series of bollard pull force tests. These tests were conducted by attaching the crawler frame to the tow point on a 2-ton pickup truck. A load cell was integrated into the tow line to measure the maximum force attained by the crawler. The motors were engaged and driven to their high-end limit. At the limit, the pull force measured by a digital force gauge was 1264 lbs (573 kgf) of force. A photograph of the bollard force test set up is shown in Figure 17.



**Figure 17. Photographs of the bollard pull force test set up and configuration.**

### **2.2.2 Towed Sled Configuration**

The tow sled configuration was first designed using computer aided design and solid modeling in SolidWorks. The sled, tow bar, and crawler models were integrated in SolidWorks and assessed to estimate the submerged weights, forces, and geometry. Figure 18 shows the design drawings prior to fabrication of the tow sled. The design was intended to produce a sled capable of integrating two 1.0 x 0.5 m EMI units (e.g., 2 EM61-S units) on low-pressure sled runners and be adaptable to run on a set of wheels or tracks. The construction was primarily fiber-reinforced plastic so that the integrated system was sufficiently negative with respect to buoyancy. This presents a trade-off between weight required to resist heave motions, stability and strength to withstand slamming forces of breaking waves and have low pressure so it does not scour the runners into the seabed. The tow system was also designed with a configurable tow boom that can readily adjust to longer or shorter lengths.

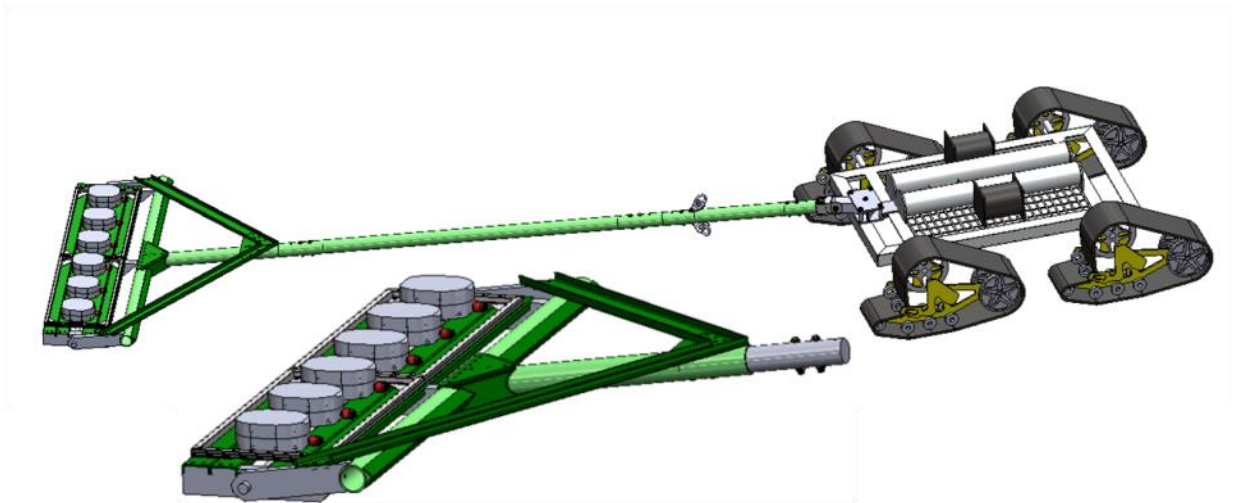


Figure 18. Solid model design showing the sled mount and tow boom configuration attached to the crawler.

Once assembled, the tow sled was fit up with a set of instruments and demonstrated on grass, gravel, and pavement. Accelerometers were rigidly mounted to the port and starboard rear edges on the sled mount surface as well as on the tow bar as shown in Figure 19. A self-contained logging inertial measurement unit (IMU) was mounted to the center of the sled mount surface. A S-type strain gauge load cell was installed at the end of the tow bar and self-logging GoPro cameras were mounted on the sled.

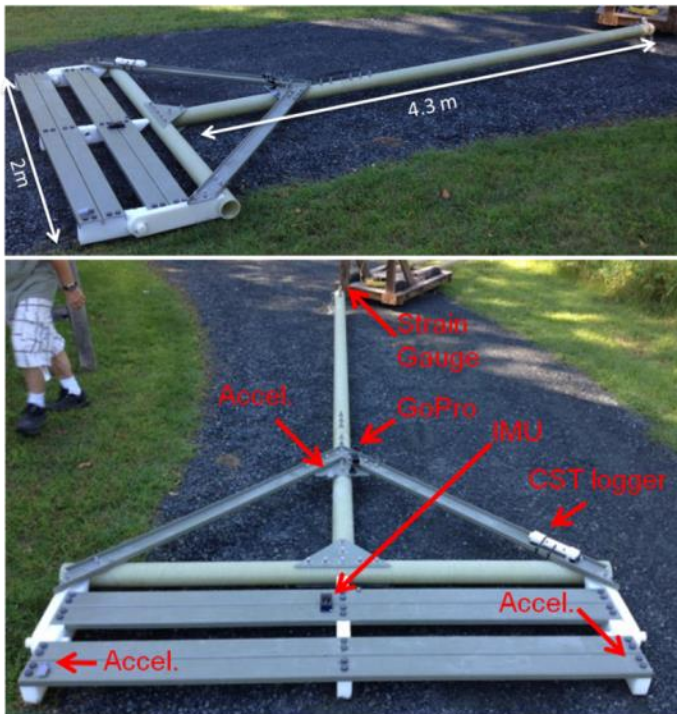


Figure 19.

A. Photograph of the array sled prior to installation of the Flex-EM transmitter coils and receivers.

B. Photograph showing the location of test instrumentation used to assess the sled stability and mobility during initial shakedown tests. Accelerometers (3) were utilized on each side of the sled as well as at the apex of sled tow mount. A force strain gauge was used at the tow point to measure dynamic loads and pull forces. A self-logging IMU and high-definition camera were used to log system motions and accelerations during tests.

To better understand the tow sled dynamics and assess the overall towing strategy (e.g., bridle configuration, downward forces, control, turning radius), we performed a series of tests at the

USACE Field Research Facility in Duck, North Carolina. These tow sled shakedown tests consisted of tow sled stability and geotechnical properties measurements. During these preliminary tests, we acquired data from sensors on the sled to quantify its dynamics when towed over dry sand on the beach, in the surf zone, and in deeper water. Geotechnical and oceanographic data were acquired using a dynamic bottom penetrator and a single beam full-waveform sonar system. Both shore parallel and shore perpendicular transects were acquired. Sled measurements comprised global position, translational and inertial measurements, and pull forces. We also conducted limited studies of the effects of towing and EM system. Both frequency-domain and time-domain EM systems were tested on the tow sled. The tow sled was pulled from a All-Terrain Utility Vehicle (UTV) on the beach and by the USACE CRAB (Coastal Research Amphibious Buggy) for off-shore/on-shore surveys (Figure 20).

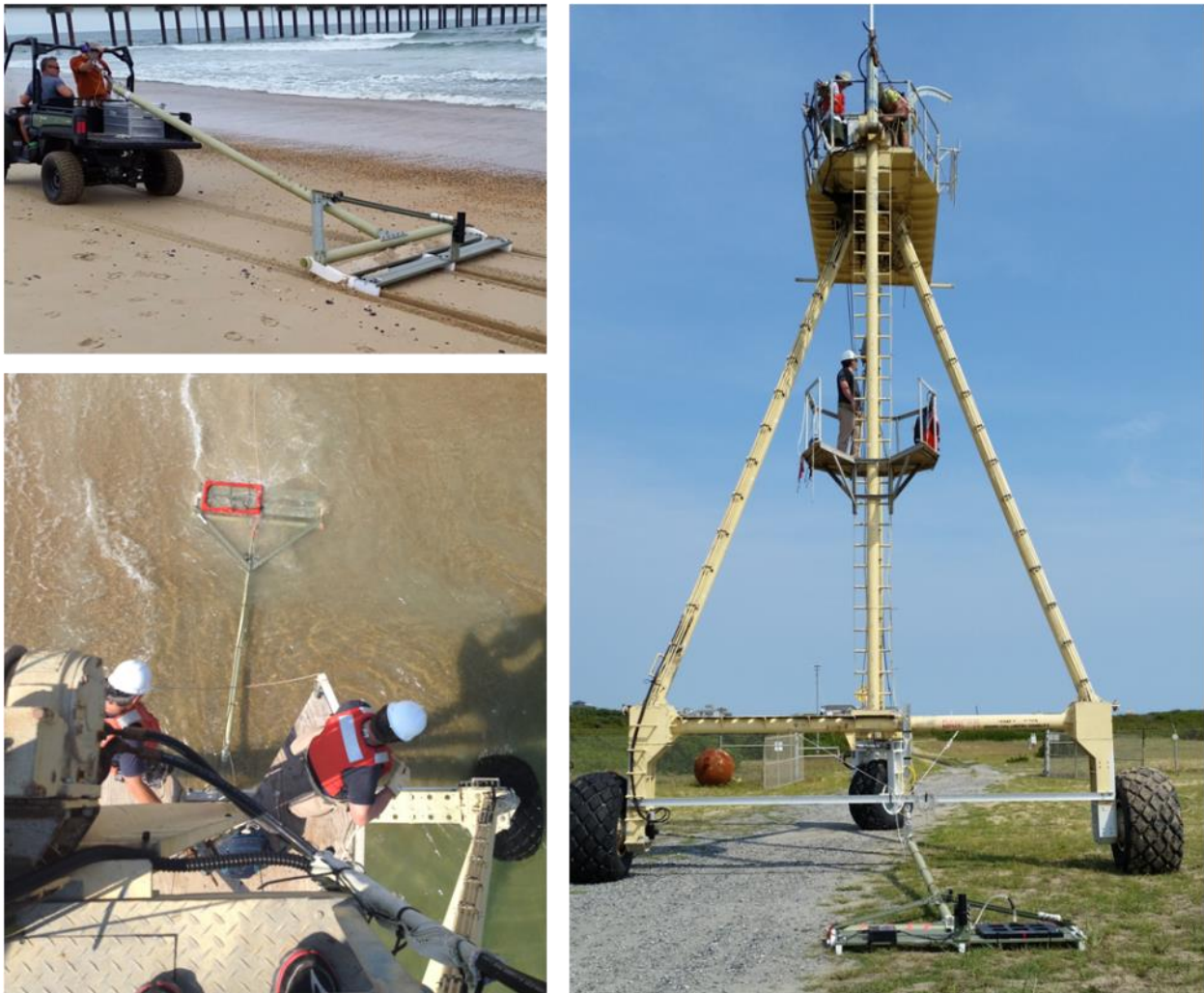


**Figure 20. Photographs of the preliminary tow sled configuration tests performed at the FRF Duck, NC site.**

Among the primary goals of these tests was quantification of the sled load forces while being pulled from offshore to onshore through the surf and swash zones. This presents the most challenging conditions in terms of required pull force to tow the sled since both gravity forces and hydrodynamic forces are acting against the system. The instrumented sled attached to the CRAB, we acquired data along a transect of approximately 350 meters long extending from the

backside of the primary beach sand dune along the lower beach and through the surf zone to an offshore sand bar 105 meters offshore. The profile of this transect is shown in Figure 21. Load forces on the tow point are also shown (Figure 22) for a sled with a single EM-61S coil mounted. Load forces varied quite a bit between maximum values of 60-70 kg force on the lower beach to average values of 15-35 kg force when submerged. Load forces in the swash and surf zones varied  $\pm 6-14$  kgf with mean values during dynamic towing of approximately 20 kgf.

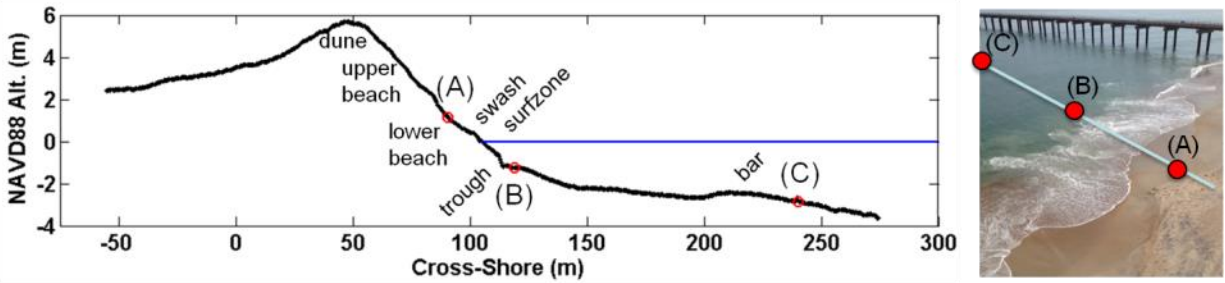


Figure 21. Profile of the topography across the CRAB transects extending from shore through the surf zone just north of the FRF pier. Depicted are the locations of lower beach, surf zone (near wave trough), and sand bar along the profile where both static and dynamic measurements were taken.

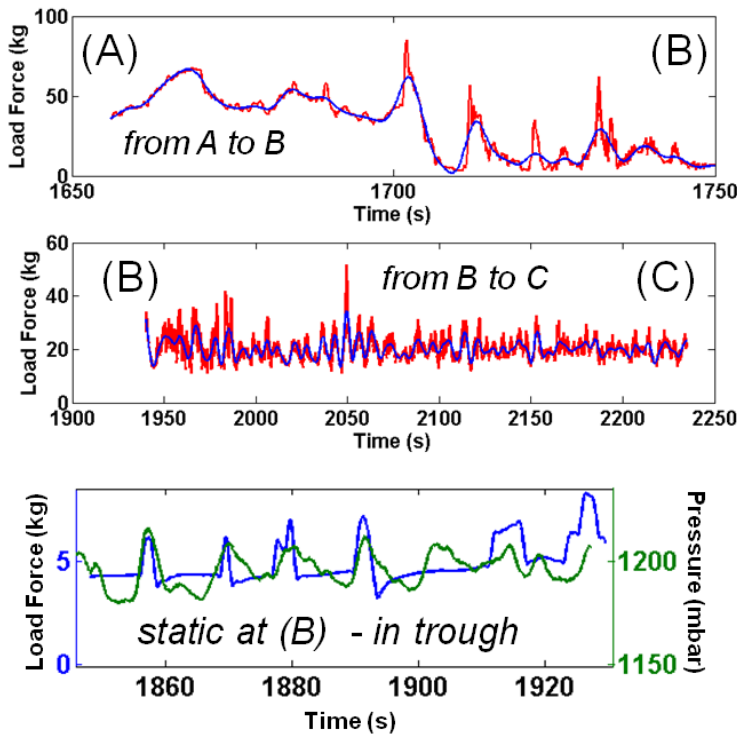
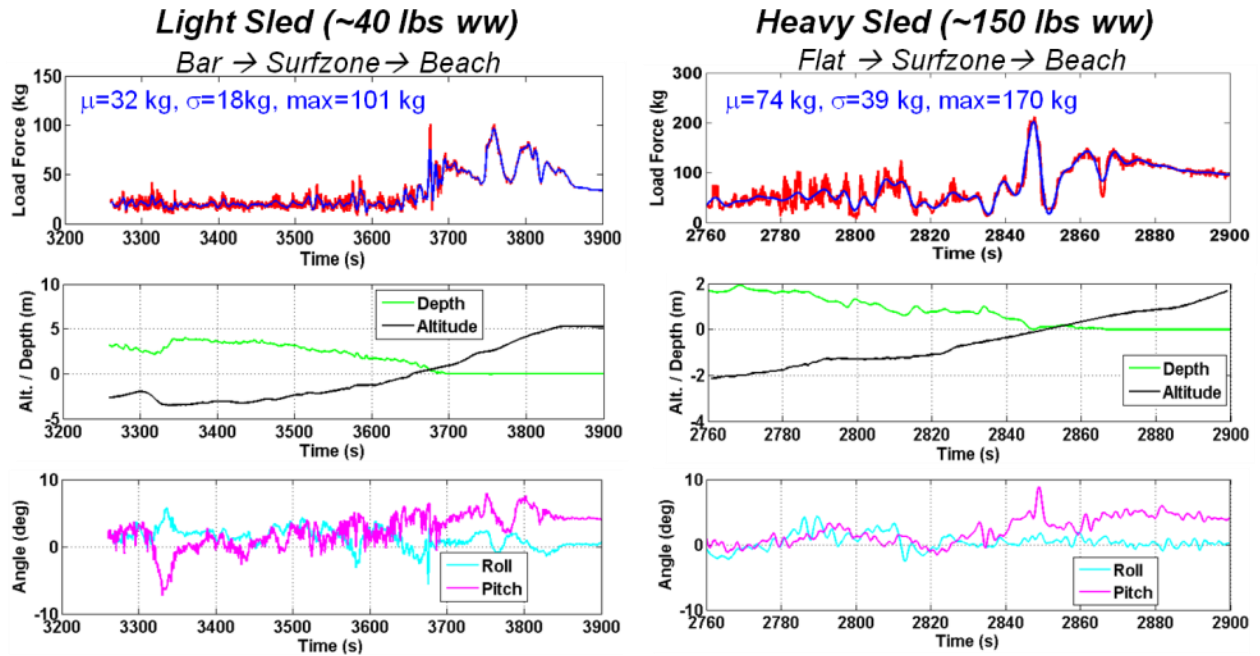


Figure 22. Load force data along various parts of the shore normal transect. The top two plots show both the raw (red trace) and filtered (blue trace) load force as measured at the tow point of the sled (by a strain gauge). The top plot shows the shore to surf zone portion of the profile and the middle plot shows the profile extending from trough out through the surf and onto the sand bar offshore. The bottom plot shows the time evolution of the load forces while the sled sat in the trough and was repeatedly forced by waves. The local pressure is also plotted showing a strong correlation between wave pressure and load force as expected.

Transects from off-shore to on-shore were compared for both a relatively light sled (~20 kg static weight in seawater) and a weighted-down "heavy" sled (~68 kg static weight in seawater). Lead weights were distributed along the sled width to produce the heavy configuration. The transects began on a submerged sandbar and shoaled toward surf and swash and then onto the lower beach once out of the water. Although the greatest variability occurred while submerged, the

maximum load forces correlated with pulling the tow sled up the relatively steep incline at the transition from lower beach to upper beach and dune. The light sled experienced a maximum pull force of 101 kgf while the heavy sled experienced a maximum pull force of 170 kgf. Roll and pitch measurements reveal increased variability on the lighter sled as expected. Roll and pitch deviations remained within  $\pm 5$  degrees as shown in Figure 23.



**Figure 23. Comparisons of the light and heavy versions of the sled. The top plots show the load force for the light (approximately 40 lbs weight in saltwater) and heavy (approximately 150 lbs weight in saltwater) sled pulls from offshore to onshore. Although it was not possible to traverse the exact same offshore-to-onshore transect for both experiments, similar vertical relief and wave conditions were experienced by both. The roll and pitch angles were slightly more exaggerated for the light sled.**

During assessment of the light sled configuration, we also acquired single beam sonar data using the Echologger EA400 self-logging backscatter instrument shown in Figure 23. This system operates at 450 kHz with a 5-degree beam width to acquire acoustic backscatter waveforms at 10 Hz. Figure 24 shows variation in backscattered acoustic intensity from the bottom during survey transects offshore to onshore. Bubble in the swash zone are also evident at early time (shorter ranges).

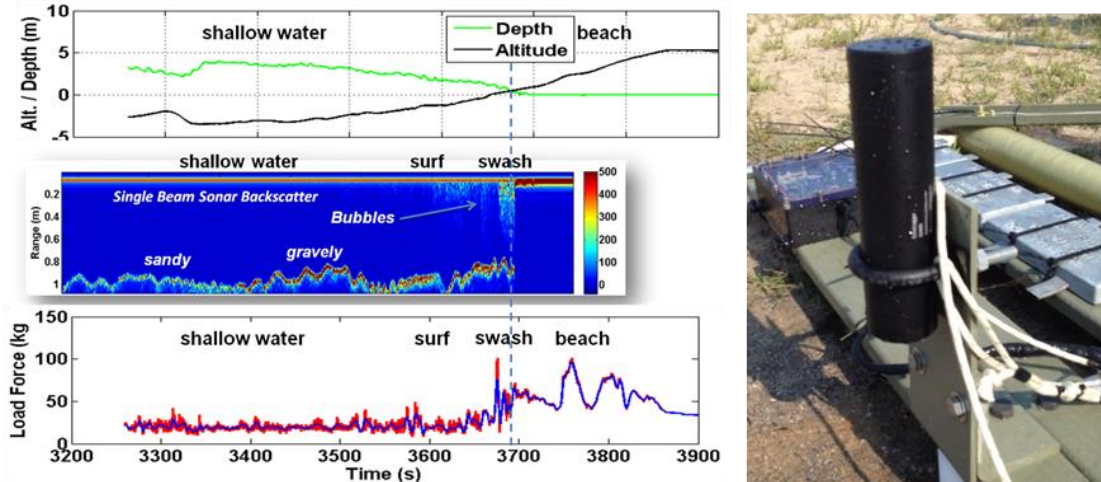


Figure 24. Left: Load force (bottom) and water depth / altitude off bottom (top) are correlated with single beam acoustic backscatter intensity (middle). Transition from offshore sandy substrates to larger grain size gravely material in the surf and swash zone are evident in the backscatter range versus distance profile. Right: Echologger EA400 sonar mounted on the test sled during FRF data collection.

### 2.2.3 FlexEM Array Characterization

Characterization of the FlexEM crawler-array configuration was conducted over a series of tests that extended from benchtop proveouts to fully-integrated data collections. Preliminary verification tests were conducted with the array configured for the 2-meter wide sled array consisting of two 1.0-meter-wide transmitters arranged side-by-side and six 3-axis cube receivers. After benchtop proveouts, we acquired data on a test stand to better understand the angular illumination of the transmitters. Two types of experiments were conducted: 1) controlled testing with targets placed at multiple relative positions under the array and 2) "pull-through" tests, where targets are pulled under the array in either the along-track or across-track direction. The latter pull-through tests are meant to mimic motion of the sensor array over targets along various approaches. Lastly, the array was towed from a proxy mobile vehicle (e.g., ATV or UTV) over a target field at the WRT facility in New Hampshire and at the Blossom Point UXO test range in Maryland.

In addition to noise characterization of the SurfROVer crawler platform, we also performed separate measurements to characterize the Flex-EM array independently. This included both in-air dry and submerged test stand data collection and analysis. In-air test stand measurements were conducted to assess the baseline sensitivity to different targets as well as the multi-angle illumination and associated sensitivity to target magnetic polarizabilities. For these tests, the Flex-EM array was placed on a non-metallic test stand and targets were positioned at various lateral and vertical offsets from the array.

Figure 25 depicts the test set up and configuration. Targets tested include: medium ISO and similar sized aluminum pipe section, a 2.5-inch solid steel sphere, 81mm mortar, 60mm mortar, and 37mm projectile. Targets were oriented in both the longitudinal and transverse directions relative to the array transmitter.

Follow-on dynamic testing was conducted at the WRT facility in New Hampshire over our emplaced target lanes. The system was mounted on a set of wheels and towed from a law tractor as shown in Figure 25.



**Figure 25. Photographs of the experimental test stand and dynamic test area for dry characterization tests. A select set of targets were used to characterize the array performance in both the test stand and buried in the test field.**



**For dynamic survey tests, the system was mounted on a set of wheels and towed from a lawn tractor.**

#### **2.2.4 Topside Operator Interface**

The topside interface for the crawler-EM system is focused around the operator workspace and user interface. This contains a graphical user interface (GUI) and a joystick control box. The GUI is based on a software environment that provides correlation of navigation, control, and EM sensor data on multiple screens. Data is distributed and shared over an ethernet-based network via the topside de-multiplexer and ethernet switch. This provides a common network such that all subsea and topside networked devices can communicate, synchronize, share resources, and access common data. A schematic diagram of the subsea and topside components is shown in Figure 26.

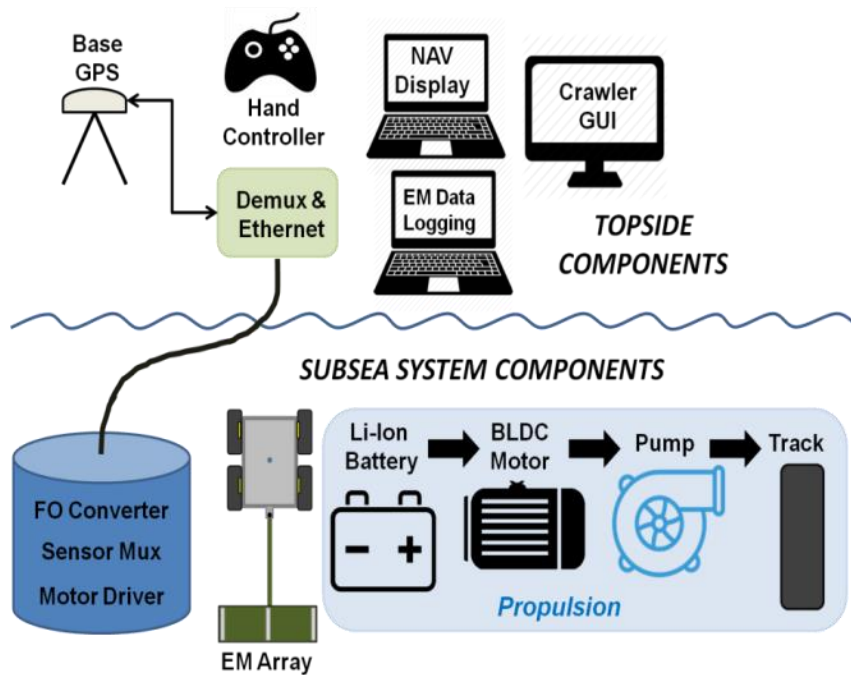


**Figure 26. Block diagram of the overall system configuration split between topside and subsea components. Subsea systems that travel with the crawler include the bottomside motor drive and multiplexer unit, the FlexEM array, and the power and mobility subsystem. Topside comprises the demultiplexer, handheld operator controller, GPS base station, and data processing and visualization computers and monitors.**

An overview of the operator workspace is shown in Figure 27. The operator uses the joystick controller to guide the crawler based on the navigation display and 3-4 camera views placed on and around the crawler. We utilized: 1) mast camera, 2) forward-looking camera, 3) backward looking camera, and 4) downward looking camera views for the operator. The operator may also view real-time updated sonar image views from the sector scanning sonar display as well as real-time feedback from the battery management system.



**Figure 27. The topside operator control station with multiple operator displays. These include (from left to right) the navigation and mission control user interface, 3 crawler-based cameras, the FlexEM array data acquisition and real-time display, the power management system interface and scanning sonar display.**

The workspace environment enables real-time data acquisition and logging and mission pre-planning. The workspace also supports navigation with left/right indicators to keep the operator tracking the current profile line plan and waypoints. The navigation display also marks areas to avoid or site boundaries and alarms the user when the system is coming close to these areas. Global position and inertial data are updated on the display including RTK northing and easting updates, roll, pitch, and heading updates, as well as GPS UTC time and data quality indicator. Photographs of select camera views, the navigation software display, and the sonar and battery management GUI are shown in Figure 28.

**Figure 28. Close-up views of some of the operator displays. The top two monitors show camera views from the crawler, while the bottom two monitors display the navigation and control interface software and the battery management and scanning sonar information to the operator.**



For our demonstration, we added the Flex-EM data logging and real-time display on a separate laptop computer. The data logger GUI displays both GPS data information as well as waterfall trace profiles from each channel component of the array (6 tri-axial receiver channels). The GPS information displayed includes UTC time, latitude, longitude, northing, easting, number of satellites, signal quality type indicator, and the UTM zone used for UTM northing and easting values. The logger portion of the display includes the elapsed sortie time, EM time gates to display, axial component selection, display gain, and logging toggle buttons and filename entry as shown in Figure 29.

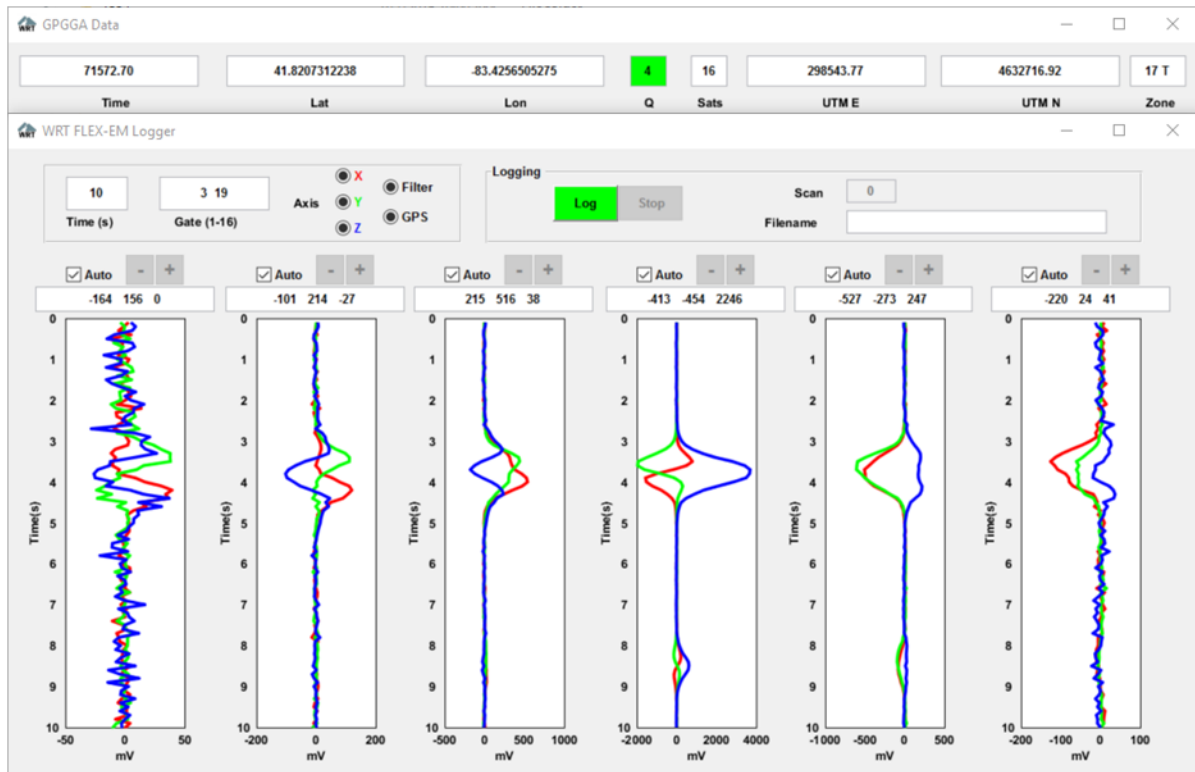


Figure 29. The standalone FlexEM data UI showing navigation information panel on top and real-time waterfall display on the bottom. Additional configuration and diagnostic feedback from the sensor system are displayed to the analyst. In this example, a clear anomaly is displayed (centered) for all axial components for the 6 receiver units across the array.

### 2.2.5 Launch and Recovery System

Launch and recovery of the system is relatively straightforward. The SurfROver crawler system has been configured such that it can be hauled in a standard US DOT trailer that does not exceed the maximum of 102 inches (259 cm). We utilized two different trailers for the system during shakedown testing. The first trailer was a standard open deck car trailer as shown in Figure 30. The system is simply remotely driven on and off the trailer and tied down for transport. The second trailer used was SeaView's customized enclosed trailer that has been outfitted for marine/ROV operator workspace with up to 8 different monitors, power receptacles throughout, integrated tool chests, sink, and lighting. For transport, all workspace control station components are stowed and the SurfROver crawler is driven into the trailer and tied down for transport. To deploy the system, the tether and operator control station is powered from ship, shore or generator and the crawler is driven from the trailer and connected to the EM array tow system.



**Figure 30. Photographs of the open and closed trailer launching of the crawler system. The operators are able to launch and operate the crawler within minutes of arriving on site. The enclosed trailer system houses the crawler for transport and is converted into a fully functioning operator control station once launched. The OCS is completely outfitted for operations included all data displays, rack-mounted computers and data interface modules, dry and wet lab benches, and crawler control systems.**

### **2.2.6 Preliminary Shakedown Tests: Blossom Point, Maryland & Toledo Beach, Michigan**

Prior to our demonstration at the USACE FRF site in North Carolina, we performed a series of engineering shakedown tests at the UXO test field at Blossom Point, Maryland and at a nearshore site on Lake Erie near Toledo Beach, Michigan. Shakedown testing was utilized to validate end-to-end functionality and crawler-sensor interoperability.

Tests at Blossom Point were specifically focused on exercising the system over emplaced targets on dry land before conducting submerged tests of the system. We conducted tests to test and calibrate the tow point encoder as well as the RTK dual-heading GPS system. Navigation verification tests were completed on the UXO grid area following pre-loaded waypoints. We followed lines in the east-west and north-south directions to ensure proper function of the navigation systems. We also conducted a limited set of noise tests with the EM array positioned at different standoff distances behind the crawler (5-10 meters behind crawler). The background noise was monitored in all receiver channels. Although we did not observe any temporal or distinct spectral noise, we did observe higher background noise in the Z-oriented receivers relative to the X- and Y-oriented receivers. A series of tests were conducted to better understand the potential source of this noise. Most of the noise appears to be directly correlated with power supplied to the BLDC motors, but did not appear to be directly coupled into the EM array. Isolated power to the EM array reduced the noise to some extent, but the Z-oriented receivers remained noisier than the X- or Y-receivers. In-line power filtering and standard analog noise cancellation techniques were used to further reduce the noise. This is exemplified in the power spectral density estimate shown in Figure 31.

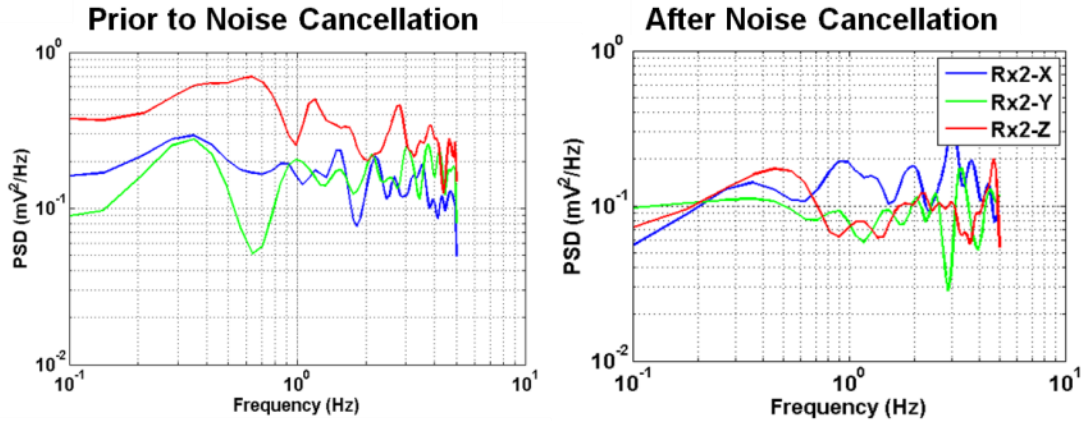


**Figure 31. Power spectral density plots of the estimated noise from measurements during shakedown tests. The plot on the left shows the PSD for all axial components of one receiver channel (Rx-2) on the array prior to noise cancellation while the plot on the right shows the results of noise mitigation methods described. Note the higher than expected noise in the Z-oriented receiver prior to noise cancellation. Noise across the band is similar for all axial components and reduced after application of noise cancellation methods.**

Coincident with engineering integration at Seaview's facility in Michigan, we mobilized the integrated system (SurfROver and Flex-EM array) to a small sandy peninsula approximately 18 km north of Toledo, Ohio on the far western shore of Lake Erie. The Toledo Beach site is adjacent to the Toledo Beach Marina, whom granted us access to the uninhabited peninsula for testing. The site is on approximately 1.5 hectares of sandy and grass or shell covered berm that protects Allen Cove from Lake Erie. We utilized the beach and nearshore areas for on-shore/off-shore shakedown testing. Figure 32 shows the location of the site in context of the great lakes region and an aerial view of the peninsula with one of our navigation tracks overlain.

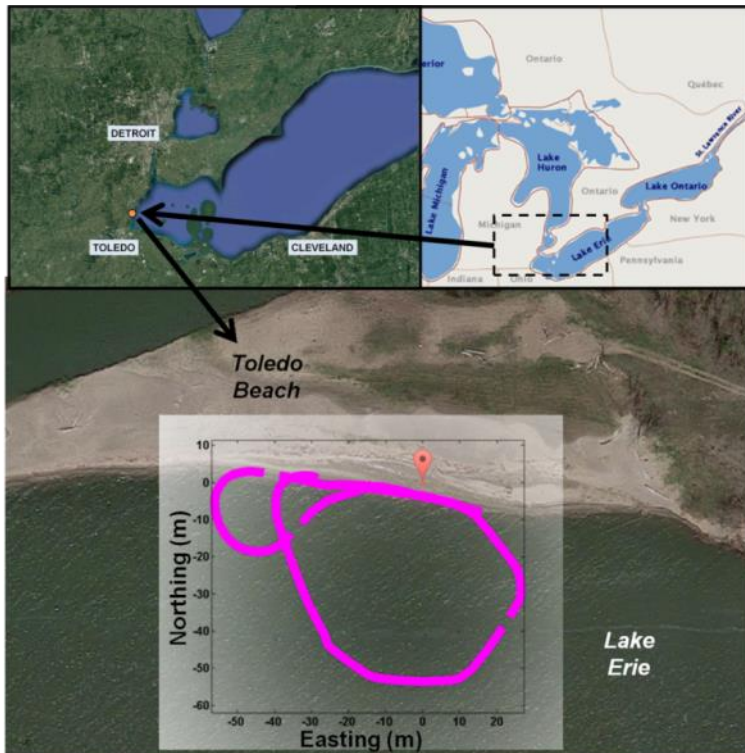


Figure 32. Maps depicting the area on the far western shore of Lake Erie where we conducted shakedown tests with the integrated system. Testing was conducted at Toledo Beach, Michigan on a rocky, sandy shoreline adjacent to shallow waters of Lake Erie.

To facilitate testing, we laid out an instrument verification survey strip parallel to the shoreline very close to the mean waterline of the Lake Erie. Six simulant targets we buried about 2.5 m apart. Targets included a 3" solid steel sphere, large and medium ISO's, 60mm, 81mm and 105 mm inert projectiles. Each target was buried approximately 30 cm below the ground surface. Figure 33 shows photographs of the IVS layout and targets used.



Figure 33. The shakedown test area including target strip at the initial water line (the water line shifted or receding during our tests). The locations of the 5 targets we used are shown in the photograph parallel to the shoreline.

The integrated crawler-based EM system was then operated on the sand shoreline, along the water line over the IVS, and into Lake Erie until it was fully submerged. Photographs of the system during testing operations are shown in Figure 34.



**Figure 34. Photographs of the integrated system in operation during shakedown tests in Lake Erie.**

Among the primary objectives of these shakedown tests was a functional assessment of the dual-heading GPS rover system, and in particular its heading precision. During testing, we acquired positional and heading estimates from the Hemisphere V320 dual heading rover antenna. These were integrated in our data stream and saved on a topside computer. Figure 35 shows a comparison of the heading metrics reported from the GPS system and an on-board IMU. Location-based estimates of heading require multiple estimates of position that are averaged and then a heading vector is computed. The IMU compass-based solutions for true-track and magnetic heading track contained a great deal of short-run variability that must be filtered out. The heading made true (HDT) estimated from the dual heading V320 GPS system provides a smoother solution that tracks the averaged location-based heading relatively closely (i.e., within a few degrees).

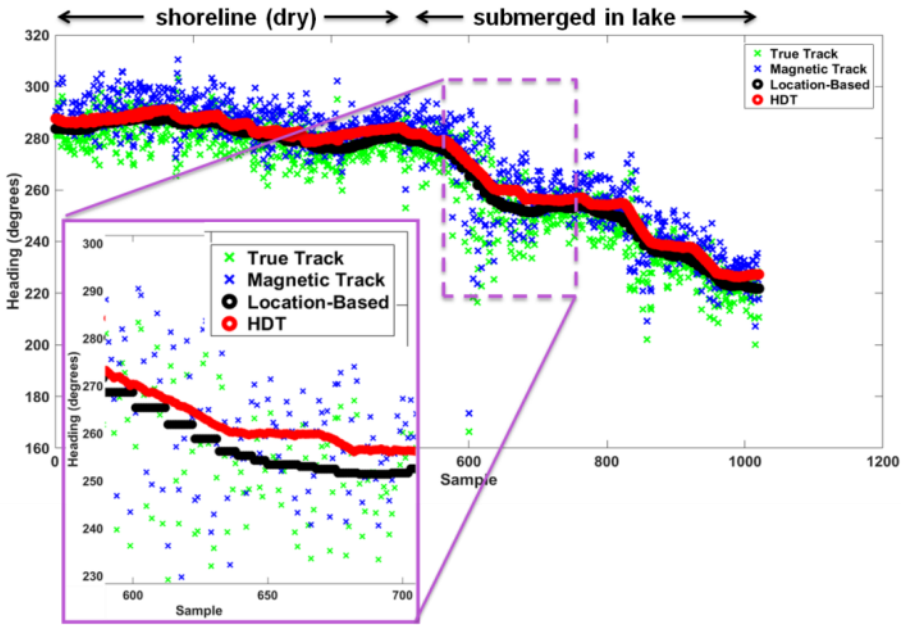


Figure 35. Example GPS heading track data from a shore-normal transect. The profile extends from the shoreline beach area into the water until fully submerged. The dual heading GPS system provides a true-track and magnetic track from the magnetic compass and IMU as well as an independent location-based track from point-to-point GPS motion (course over ground). The best track is the heading based on calculated true vessel heading (HDT) from the dual antenna system.

Global position estimates were calibrated and verified by traversing the system over the IVS and comparing the target pick locations to previously surveyed ground truth locations (acquired during installation of the targets by averaging static position estimates over  $N > 40$  samples). EM array anomalies during traverses over the IVS target profile are shown in Figure 36. Multiple traverses were conducted using different approach angles relative to the general north-south orientation of the IVS. In every case (i.e., for every axial receiver component), the signal-to-noise ratio (SNR) over each target exceeded 15 dB. Single profiles were processed using Geosoft UX Detect software to produce gridded maps and target pick locations as shown in Figure 37.

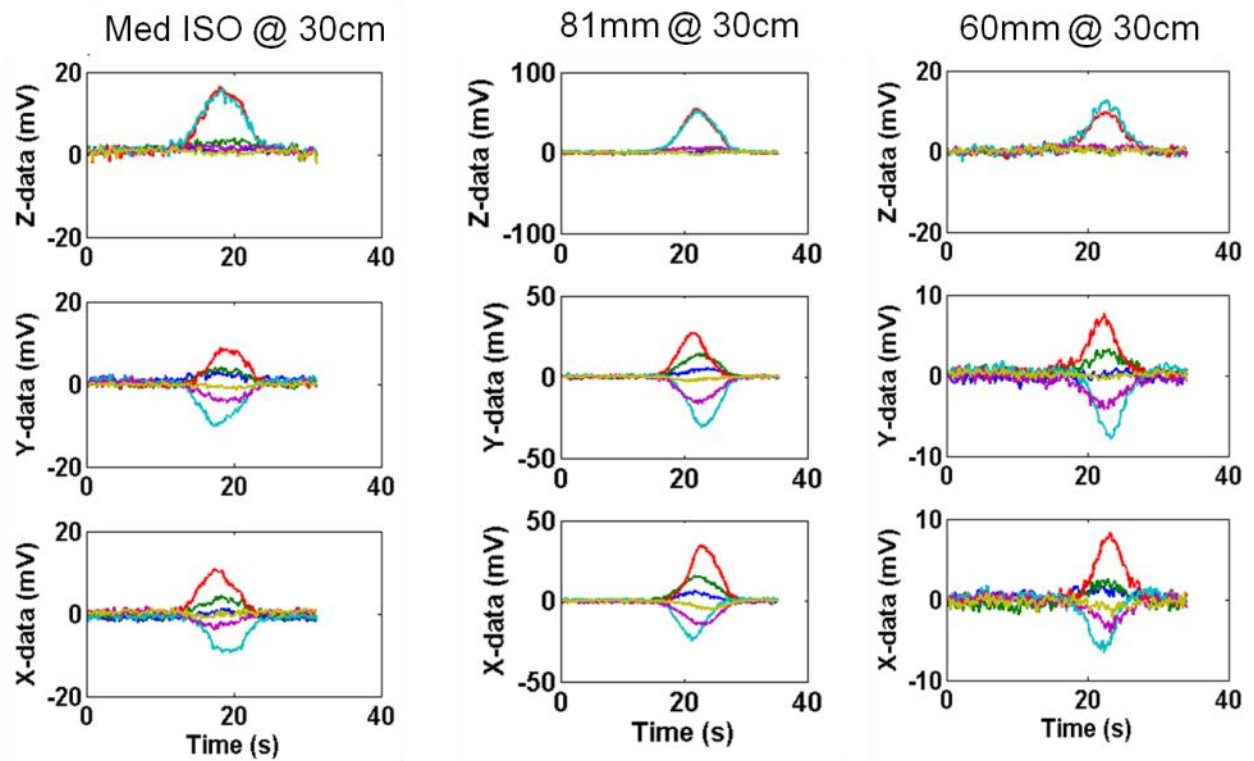
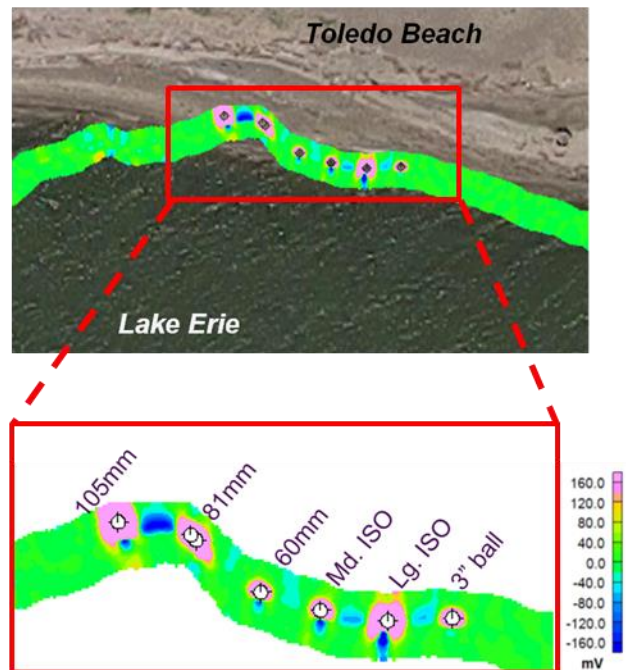
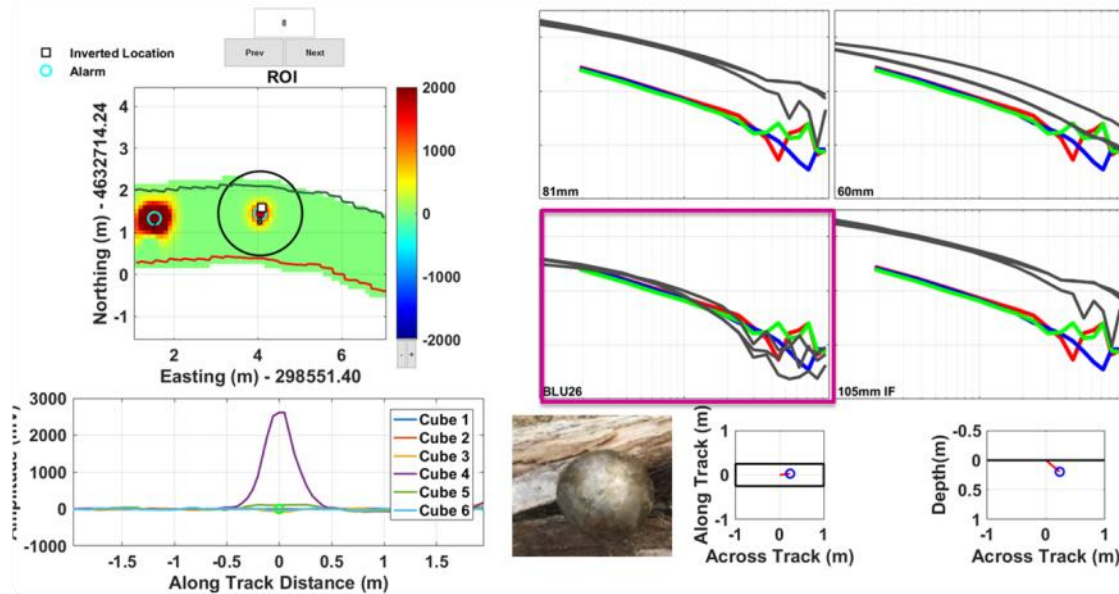


Figure 36. Example of raw three component (X, Y, Z) receiver signals for nominal target buried during shakedown tests.

Figure 37. Example array signature maps showing the integrated Z-axis response for early-to-intermediate time gates over the test string along Lake Erie. Data were processed using the Geosoft Oasis Montaj UX-Detect modules and overlain on a Google Earth image of the site. The bottom plot shows more detail of the target responses - all of which had excess signal-to-noise for detection and mapping.



Limited space and time at the site prevented opportunities to acquire the multiple overlapping profiles needed to adequately produce inverted magnetic polarizabilities from the dynamic Flex-EM data. However, in some cases, single pass data produced polarizability inversions that were of classification quality. Figure 38 shows an example of inverted polarizabilities generated from a single pass of the array over the 3-inch steel sphere. The inversions yielded polarizabilities for the sphere that are indicative of an axially symmetric object such that all primary, secondary, and tertiary polarizabilities are generally equal over the entire time window sampled. The analyst display (Figure 38) also provides map-view information of the array data, profile data, polarizability matches to libraries, and inverted locations relative to the array in both depth and map view.



**Figure 38. Example analyst display of selected target magnetic polarizability classification. The selected target was a 3" diameter steel sphere exhibiting good triaxial symmetry in the polarizabilities. The BLU-26 target match is expected due to the spherical nature of that submunitions target, which is also similar in size to our test sphere.**

### 2.3 ADVANTAGES AND LIMITATIONS OF THE TECHNOLOGY

The crawler-based EMI technology has particular advantages over surface-towed or ROV-based deployment methods in challenging nearshore areas such as surfzones and strong tidal channels.

Divers are highly constrained in terms of the mobility, depth and duration during dives due to strict health and safety regulations as well as physics. Surface towed systems as well as fully autonomous unmanned undersea vehicles (UUVs) place sensors 2-5 m above the sea floor, and thus restrict detection capabilities to large UXO only. The crawler-based EMI technology to be demonstrated has particular advantages that can be leveraged for marine UXO operations:

- Stability and mobility in challenging high-energy nearshore environments
- On-shore / off-shore capability
- Integrated crawler and high resolution active-source EMI array.
- Tele-operation

- Tightly integrated vehicle position and control with high resolution active source EMI data. This will lead to improved detection and a reduction in false alarm rate through improved classification resulting from high resolution EM sensor data collected synchronously with high resolution position data.
- Real-time operator situational awareness and dynamic repositioning capability. This affords the operator both dynamic mapping mode and detailed reacquisition or static characterization data collection over suspected targets.
- Precise navigation and positioning of the sensor array in close proximity to the seafloor. This provides accurate positioning, tracking, and bottom following, which leads to improved survey efficacy and efficiency. Because signal levels drop off quickly with range from a target, it is critical to accurately and precisely position the sensor in varying conditions.
- Tele-operation removes the operator from the water column and allows for accurate operations in both shallow (<3m) and deep water (>10 m).

Limitations of the technology to be demonstrated include:

- limited high-end speed (<5 kph)
- loss of positional accuracy in water depths greater than the height of the GPS mast
- transportability
- tether system
- seafloor obstructions and tight area investigations (due to turning radius required)

### **3.0 PERFORMANCE OBJECTIVES**

The performance objectives focused on demonstration of integrated system (crawler and EMI array tow platform) mobility, stability, and precise system positioning and control required for execution of UXO detection and characterization missions. The functions demonstrated include stability in surf zone conditions, mobility and area coverage, on-shore / off-shore traverse over varying bottom substrates, EMI array positioning, UXO detection performance, and clutter rejection capability. These objectives are summarized along with their respective success criteria in Table 2.

**Table 2. Performance Objectives**

Performance Objective	Metric	Data Required	Objective Criteria
<b>Quantitative Performance Objectives</b>			
Surfzone Stability	Average error between desired and true roll, pitch, yaw, horizontal position, and altitude of system, standard deviations during 10 m long shore-parallel and shore-normal traverses in water depths of approximately 0 m, 1 m, and 2 m below MSL	<ul style="list-style-type: none"> <li>Desired tolerances on orientation and translation of the sensor array</li> <li>Current velocity data from an ADCP array</li> <li>Orientation and translation position data from the navigation and control system</li> </ul>	$\Delta R < \pm 6^\circ$ , $\sigma R < 3^\circ$ $\Delta P < \pm 6^\circ$ , $\sigma P < 3^\circ$ $\Delta Y < \pm 4^\circ$ , $\sigma Y < 2^\circ$ $\Delta X < 0.20$ m, $\sigma X < 0.15$ $\Delta Y < 0.10$ m, $\sigma Y < 0.07$ $\Delta A < 0.10$ m, $\sigma A < 0.15$
Area Coverage	Average forward advance rate over 5 adjacent (100% coverage) shore-parallel traverses in water depths between 1 and 3 meters	<ul style="list-style-type: none"> <li>Position, time, and orientation reports from the navigation and control system</li> </ul>	Shore-Parallel Adv. Rate $\geq$ 0.42 m/s
On-shore / off-shore Mobility	Average forward advance rate over 5 adjacent (100% coverage) shore-normal traverses in water depths between 0 and 2 meters	<ul style="list-style-type: none"> <li>Position, time, and orientation reports from the navigation and control system</li> </ul>	Shore-Perpendicular Adv. Rate $\geq$ 0.28 m/s
Detection of all munitions greater than 60 mm	Signal to Noise Ratio (SNR) of signal produced by munition in EMI sensor to noise in EMI sensor	<ul style="list-style-type: none"> <li>Signal received during anomaly interrogation</li> <li>Noise estimate during anomaly interrogation</li> <li>Position reports from the navigation and control system</li> </ul>	SNR > 9 dB
Detection Location Accuracy	Average error in northing and easting between true position and estimated target position	<ul style="list-style-type: none"> <li>EM array data</li> <li>Navigation data</li> <li>True Target Locations</li> </ul>	$\Delta TN$ and $\Delta TE < 1.0$ m $\sigma TN$ and $\sigma TE < 0.35$ m
Classification of all munitions $\geq 60$ mm	Number of munitions ( $\geq 60$ mm) identified as such out of total number of TOIs detected (Pclass)	<ul style="list-style-type: none"> <li>Signal received during anomaly interrogation and resulting inverted polarizabilities</li> <li>Ranked anomaly list</li> <li>Ground truth target positions</li> </ul>	Probability of Classification, Pclass > 0.75 with at least 50% of clutter ranked below the UXO
<b>Qualitative Performance Objectives</b>			
Ease of use	Operator observations	<ul style="list-style-type: none"> <li>Field notes recorded during setup and testing</li> </ul>	Ease of use compared to alternate standard marine surveying procedures
Launch and recovery	Operator observations	<ul style="list-style-type: none"> <li>Time to launch/recover</li> <li>Observational notes</li> </ul>	Time to launch, time to recover, mean down time

### **3.1 OBJECTIVE: SURFZONE STABILITY**

The ability of the system (crawler with the EMI sensor attached) to maintain stable operation with respect to surge, heave, and impact from plunging or breaking waves directly affects the motion control of the sensor and thus SNR and detectability of metallic objects on, or below, the seafloor.

#### **3.1.1 Metric**

Compare the measured roll, pitch, yaw, and translational motion of the crawler and the sensor tow sled over time periods consistent with the relevant sensor measurement bandwidth (approximately 0.3 to 3 Hz). Changes in roll, pitch, yaw, longitudinal, transverse and vertical motions over measurement intervals between 300ms and 3s will be averaged over 1-2 minute periods and the standard deviation will be calculated.

#### **3.1.2 Data Requirements**

Orientation data will be derived from the crawler's IMU and those for the sled will be derived from a self-logging IMU mounted on the front of the sled. We also acquire pressure depth and acoustic altimeter data for the crawler platform. We calculate the stability metrics for experiments in which the system is traveling parallel to the shore in water depths of 0.1, 1, and 2 meters. The 0.1 m water depth test will be in the swash zone where water periodically floods and drains from under the system. The 1 m water depth test exemplifies conditions in the surf and/or wave breaking zone where hydrodynamic forces are extreme. The 2 m water depth test is intended to test the stability of the system in shallow water outside of the breaker zone and where the system is fully submerged. We record roll, pitch, and yaw directly from the IMUs and estimated translational motion will be derived from double integration of measured accelerations. All data will be acquired at 10 Hz or faster rate. Each test was repeated to estimate variability.

#### **3.1.3 Success Criteria**

Our objective is to achieve roll and pitch stability to within  $\pm 6^\circ$  and yaw stability within  $\pm 4^\circ$  for both the crawler platform and tow sled platform over the frequency range relevant to EM array sensor measurements. Translation motion should remain within the tolerance envelopes specified over the duration of each test: less than 20 cm of sway motion; 10 cm of surge motion, and 10 cm of heave motion.

### **3.2 OBJECTIVE: AREA COVERAGE RATE**

In our demonstration, area coverage refers to the system's ability to maintain an adequate advance rate for efficient surveying while operating parallel to the shoreline. The ability of a crawler-based system to cover a nearshore area is an important criterion in determining its survey efficiency relative to comparable methods. This is a function of the advance rate, maneuverability, and stability. These tests will be conducted in shallow water areas in water depths averaging between 1 and 3 meters.

### **3.2.1 Metric**

Compare the measured average forward velocity of the platform to the success criteria. The key metric is the forward advance rate averaged over 5 adjacent passes with as close to 100% coverage as possible. The resolved forward motion of the sensor sled will be determined by combining information from the GPS position, orientation, and velocity measurements with relative yaw measurements of the tow sled given by the tow point encoder. The average advance rate will be calculated as the average over 5 adjacent traverses of at least 15 meters in length. The total coverage area should be approximately 150 m<sup>2</sup> if 100% coverage is possible and average production rate would then be the total coverage area divided by the total time including turn-arounds.

### **3.2.2 Data Requirements**

To demonstrate the area coverage or advance rate parallel to the shore, we require data from the GPS and the tow point encoder. We also record pressure, depth, and altimeter height of the crawler platform. Data will be recorded at a rate of 1 Hz or higher.

### **3.2.3 Success Criteria**

Our objective is to achieve an average forward advance rate of the system of at least 42 cm/s (1.5 kph or 0.8 knots).

## **3.3 OBJECTIVE: ON- AND OFF-SHORE MOBILITY**

The system's ability to operate in survey mode while traversing on-shore to off-shore and vice versa is an important mission feature. Effective operations perpendicular to the shoreline requires stability of both the crawler and sensor platform to maintain a suitable advance rate. This allows for continuous surveying in an out of the water and over areas of very shallow water such as the swash zone.

### **3.3.1 Metric**

Compare the measured average forward velocity of the platform moving from dry land to submergence under 2 meters of water to the success criteria. The resolved forward motion of the sensor sled will be determined by combining information from the GPS position, orientation, and velocity measurements with relative yaw measurements of the tow sled given by the tow point encoder. The average advance rate will be calculated for at least 3 traverses extending from on-shore to off-shore and 3 traverses extending from off-shore to on-shore in approximately the opposite direction. Multiple traverses in the same direction will be averaged and advance rates will be computed separately for shoreward and seaward directions.

### **3.3.2 Data Requirements**

To demonstrate the area coverage or advance rate perpendicular to the shore, we require data from the GPS and the tow point encoder. We will also record pressure, depth, and altimeter height of the crawler platform. Data will be recorded at a rate of 1 Hz or higher.

### **3.3.3 Success Criteria**

Our objective is to achieve an average forward advance rate of the system for shore-perpendicular traverses of at least 28 cm/s (1 kph or 0.54 knots).

## **3.4 OBJECTIVE: UXO DETECTION PERFORMANCE**

The ability of the crawler-based EM system to detect relevant UXO simulant objects yields quantification of a key system metric. To produce detections the EMI array must be functioning properly, data must be processed to improve signal-to-noise characteristics, and positioning of receivers must provide the resolution required to delineate individual targets of 60 mm diameter or larger.

### **3.4.1 Metric**

Compare the total number of target encounters to the actual number of targets detected. A target encounter is determined by any part of the EMI sensor have an easting and northing coordinate within 0.5 m of the recorded position of a seeded test item while at a reported altitude less than 0.5 m. The metric that we will measure will be the Signal to Noise Ratio (SNR) of signal produced by a munition in EMI sensor to noise in EMI sensor.

### **3.4.2 Data Requirements**

Georeferenced EMI sensor and navigation data correlated in time are required for input into custom detection algorithms.

### **3.4.3 Success Criteria**

Our objective is to achieve an average SNR of 9 dB or greater over all target encounters against targets that are 60 mm in diameter or larger at CPA ranges of 10 times or less the diameter of each object (e.g., 60cm for a 60mm projectile).

## **3.5 OBJECTIVE: UXO DETECTION LOCATION ACCURACY**

The ability of a crawler-based EM array to produce accurate anomaly locations is critical to UXO survey and detection missions. To produce accurate detection locations, the estimated position of the EMI sensor must be accurate during target investigations.

### **3.5.1 Metric**

Compare the estimated position (northing, easting) of each target detected by the EM sensor to the true position of each target. Average northing and easting error, defined as the mean of reported position minus the true position, will be calculated. Separate metrics will be reported for detection surveys along shore-parallel and shore-perpendicular transects to segment any potential directional biases.

### **3.5.2 Data Requirements**

Georeferenced EMI sensor and navigation data correlated in time are required for input into detection algorithms.

### **3.5.3 Success Criteria**

Our objective is to achieve an average northing and easting error less than 100 cm and standard deviation of less than 35 cm.

## **3.6 OBJECTIVE: UXO CLASSIFICATION**

Our objective is to successfully classify emplaced UXO as such.

### **3.6.1 Metric**

We apply a Probability of Classification (Pclass) metric. Pclass is determined from the ration of the number of UXO correctly identified as such to the number of UXO detected.

### **3.6.2 Data Requirements**

We apply classification to all regions-of-interest (ROIs) generated from the detections identified in the dynamic survey data. Each ROI contains a subset of soundings from the dynamic data that correspond to an anomaly. Base on the results of inverting these data, we generate a ranked list of likely UXO. This list should be scored based on the emplaced target ground truth list. The scoring results quantify the classification performance.

### **3.6.3 Success Criteria**

$P_{class} > 0.75$  with at least 50% of clutter ranked below the UXO will indicate success.

## **3.7 OBJECTIVE: EASE OF USE AND OPERATOR INTERFACE**

The ease of use of the integrated system including control of the crawler system, EMI sensor, topside control system, and navigation and mission planning/lane following is important to determine the level of training required for use of this equipment in a production environment. Ease of setup, calibration, and operation will be determined.

### **3.7.1 Metric**

There is no specific quantitative metric for this objective. The qualitative metric is determined based on notes and observations from operators and crew.

### **3.7.2 Data Requirements**

Observations and field notes taken by test personnel will be reviewed to determine the qualitative ease of use of each component in the system and identify any shortcomings of each component's operation.

### **3.7.3 Success Criteria**

Success should be relative to other similar survey systems in the experience portfolio of the operators. If the system is considered significantly more complex, difficult, or unwieldy relative to similar or comparable marine survey systems, it will not be considered successful.

## **3.8 OBJECTIVE: LAUNCH AND RECOVERY**

Launch and recovery encompasses all resources and processes required to mobilize and deploy the integrated system to and from the survey area. We also include required maintenance or other standard procedures for keeping the system operating efficiently during operations. For example, we assess the time and effort required to stabilize the system using ballast, if needed. This may be necessary when moving from one operating area (e.g., freshwater to saltwater; or high to low energy hydrodynamic environment) to another.

### **3.8.1 Metric**

There are no specific quantitative metric for this objective. The qualitative metric is determined based on notes and observations from operators and crew.

### **3.8.2 Data Requirements**

Observations and field notes taken by test personnel are to be reviewed to determine the effectiveness of launch and recovery (e.g., shore- versus ship-based), battery charging and endurance, tether management, system stowage, and required maintenance of mechanical components such the hydraulics system.

### **3.8.3 Success Criteria**

Success shall be evaluated relative to nominal remotely operated marine systems. An evaluation of shore and (hypothetical) ship launch and recovery and general system maintenance shall be conducted and reported on.

## **4.0 SITE DESCRIPTION**

The primary site for this demonstration comprises beach and nearshore areas at the USACE Field Research Facility (FRF) in Duck, North Carolina. This site provides a mix of conditions and excellent support infrastructure for engineering evaluations with thorough testing under representative conditions. The following sections describe the site selection and site areas in more detail.

### **4.1 SITE SELECTION**

This demonstration is the first field data collection of the combined crawler-based EMI technology. This data collection was intended as a thorough shakedown and evaluation in preparation for follow-on demonstrations. As such, the site should contain a wide range of features and conditions to provide the most thorough assessment as possible. The test-site preferably has: (i) hydrodynamic challenges such as currents of 1 to 3 knots and surf/breaking wave conditions, (ii) a range of different water depths; (iii) variable bottom type and topography; and (iv) both large (155mm) and smaller simulant munitions (60mm) or munitions surrogates (ISOs). This demonstration was also intended to test extended capability from beach and shorelines areas to deeper water (>2m) coupled with challenging hydrodynamic environments. Amongst the most difficult and potentially interesting nearshore environments are those with high energy surf encompassing a range of wave heights and types, substrates, and water depths (from dry to 2-3 meters submergence).

Given the range of conditions desired and support infrastructure available, we propose the nearshore areas at the USACE FRF for both engineering tests and more comprehensive site demonstrations. This is managed by the USACE Environmental Research and Development Center (ERDC) and houses an on-site permanent staff of about 13-15 scientists, engineering, and technicians. It resides in the northern portion of the outer banks barrier island chain near the North Carolina - Virginia border. An overview map of the outer banks and general site location are shown in Figure 39. The FRF site also provides water conditions and support logistics that are supportive for the timeframe and desired operations for demonstrations.

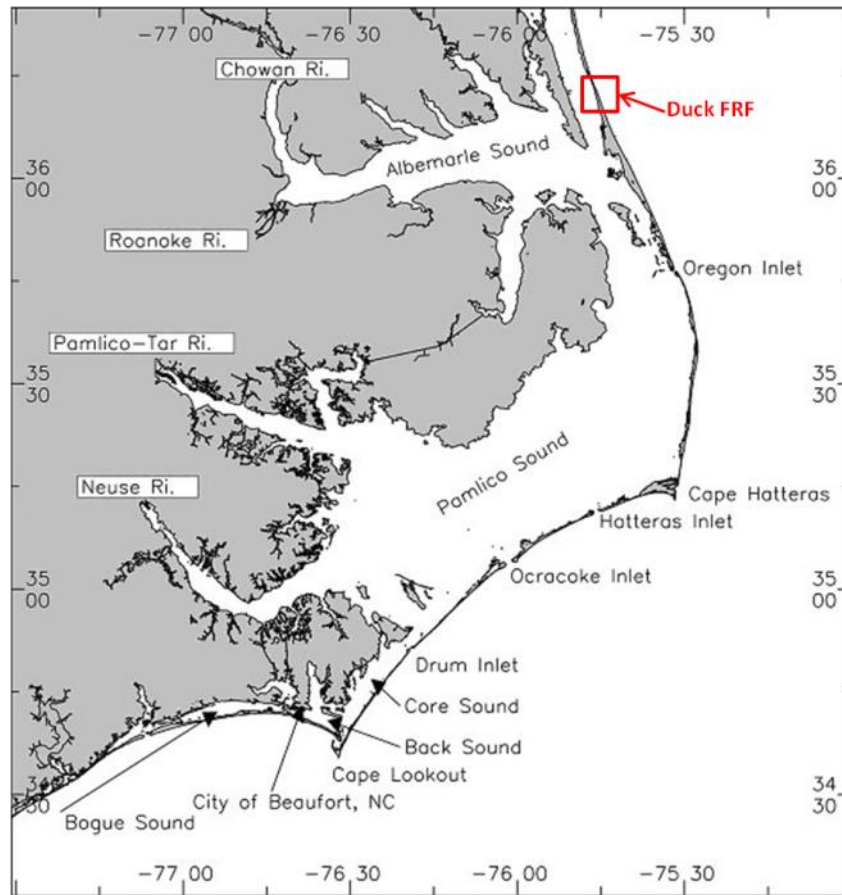


**Figure 39. Regional map of the North Carolina Outer Banks and general site area location at the US Army Corps of Engineers (USACE) Environmental Research and Developmental Center (ERDC) Field Research Facility in Duck. The demonstration is along the beach and seaward shore of the barrier island adjacent to the FRF pier.**

The general test area is located within the USACE FRF site approximately 100 km south-southeast of Norfolk, Virginia. The FRF was established by the USACE in 1977 to support coastal engineering research. The facility consists of a 560-meter-long research pier (see Figure 40), a main office building, large high-bay field support building, and a 40 meter high observation tower. Since its creation, the FRF has maintained long-term monitoring records of coastal oceanographic information including waves, tides, local meteorology, and concomitant beach response. The USACE monitoring program is supported by a field staff and several unique vehicle platforms that permit successful operation in the turbulent surf zone and adjacent nearshore environments.



**Figure 40. Photograph of the FRF pier extending 560 meters into the Atlantic Ocean. Not also the extensive surf zone at the site.**

The selection of the particular survey areas will be determined in conjunction with FRF staff. The area just south of the FRF pier has been well studied and is the area we selected for conducted on-shore and off-shore data collection. The criteria for selecting data collection areas represent a tradeoff between desired site conditions and access and availability. Preferred site conditions contain a range of water depths and variety of bottom types and current conditions. The site should be amenable to access by USACE vessels such as the CRAB to support seeding of surrogate targets and standard test objects (e.g., ISO's). This part of the site has had extensive prior marine surveying conducted to help pre-characterize site conditions and survey areas.

Shallow water areas of interest are 0-3 meters deep with seafloor conditions that ranges from relatively flat sandy bottom to gravely sand to more complex bottom types and hydrodynamics. The use of these sites allowed us to configure, test, and assess system validation results from realistic conditions without incurring logistics and DoD intrusive site investigation expenses that would be required for demonstration at a live site during this stage. An example bathymetric profile acquired just north of the FRF pier during preliminary testing at the site is shown in Figure 41.

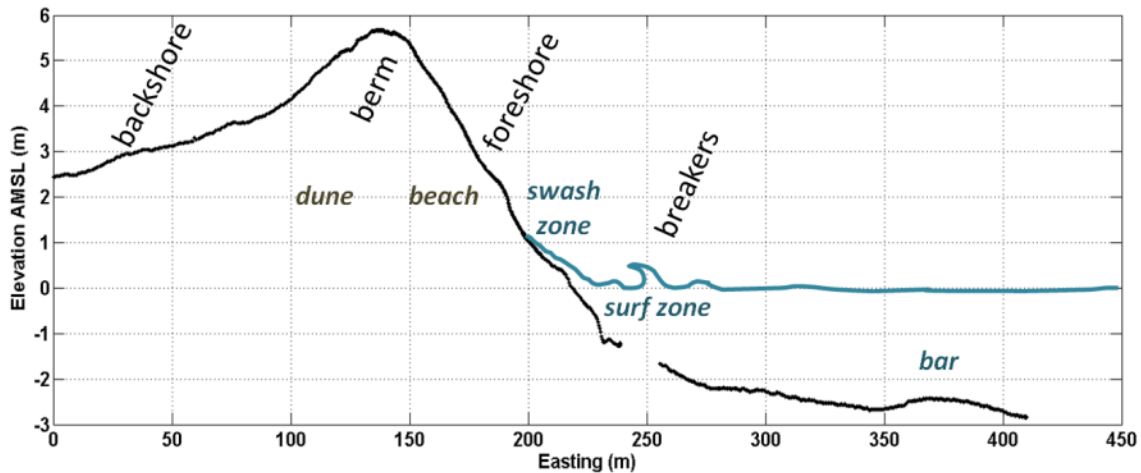


Figure 41. Annotated bathymetric profile in 2015 during preliminary testing at the site. This profile was acquired along a shore-perpendicular transect from the CRAB platform approximately 75 meters north of the FRF pier.



Figure 42. Left: Location of the FRF site and pier annotated over the NOAA nautical chart for this part of the Outer Banks. Right: An aerial photograph looking west over the FRF site with pier in the foreground and facility buildings beyond the dune ridge. The Currituck Sound is the background part of the photo. The general site area is outlined in red.

At FRF there is an array of permanently installed instruments to measure wave heights, currents, and water conditions at the site. There is also an extensive historical database that is continuously being updated with meteorological and oceanographic information. Near real-time data from on-site instruments are made available through the site data portal ([navigation.usace.army.mil/CHL\\_Viewer/FRF](http://navigation.usace.army.mil/CHL_Viewer/FRF)).

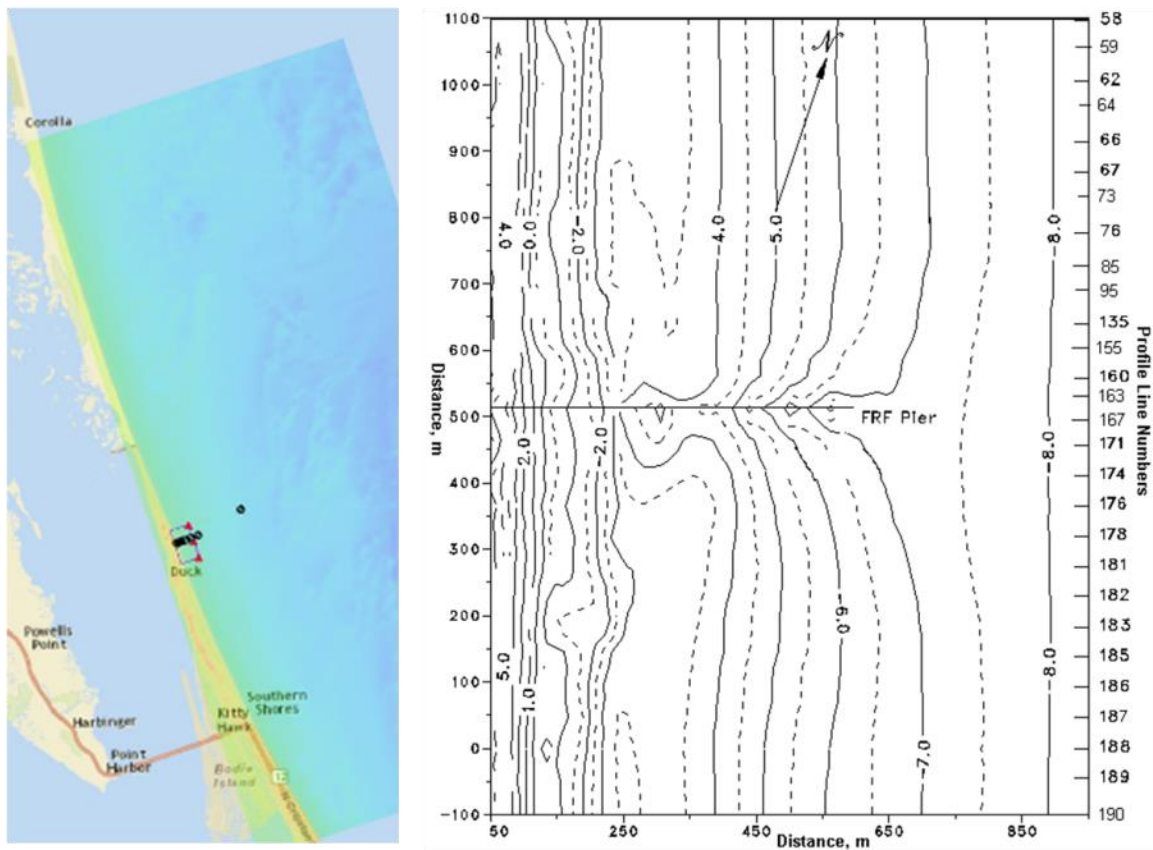


Figure 43. FRF site data showing detailed very near-shore bathymetry maps for the general area offshore of Duck (Left) and areas directly north and south of the FRF pier (Right).

We have identified both NOAA tidal water level stations and National Geodetic Survey benchmarks in the area that may be used for baseline information (Figure 44 and Figure 45). Confirmation of the existence of geodetic benchmark stations is needed since they may have been overcome by storm activity on the barrier island. In addition, it is known that the fishing pier that used to house the NOAA tide station no longer exists, so the location of the station also needs to be confirmed.

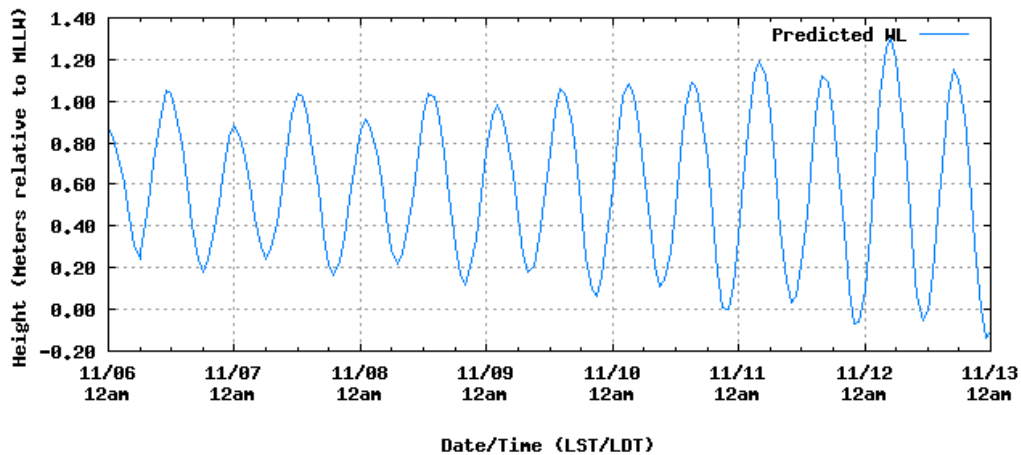


Figure 44. Tidal water level predictions for the Duck FRF Pier (Station ID: 8651370) for early November 2016.

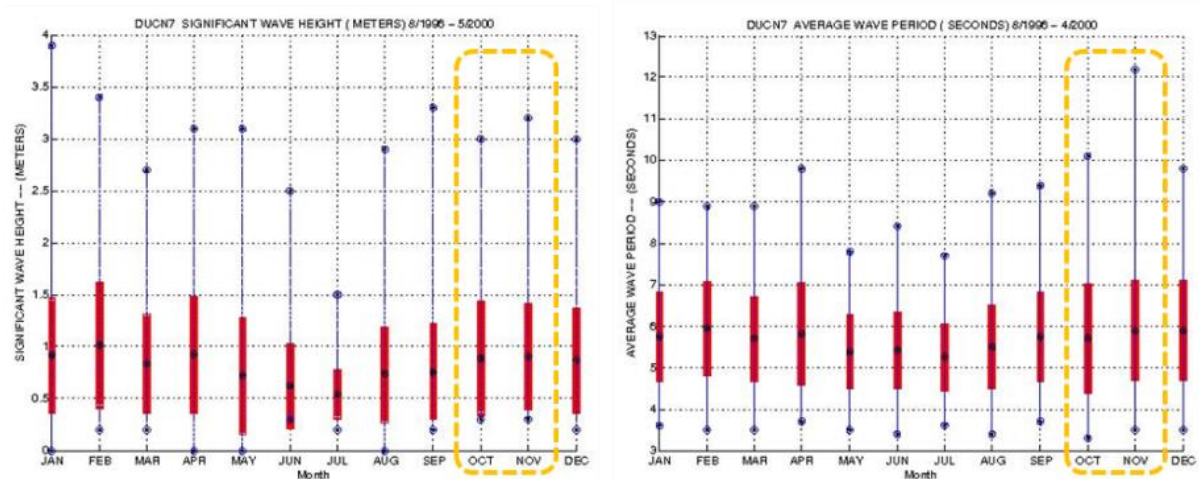


Figure 45. Significant wave height statistical data compiled over the period from June 1995 to April 2000 at the FRF site. Wave heights for October and November are highlighted.

## 4.2 SITE HISTORY

Duck, North Carolina is the northernmost incorporated town within Dare County and previous to 2002, was unincorporated. Duck is located at approximately at 36 ° 10' N, 75° 45' W with a maximum elevation of 45 feet above sea level. The town is situated between Corolla at its northern boundary, Southern Shores at its southern boundary and by the Currituck Sound to the west. The FRF site is located approximately 1 mile north of the current town of Duck. Prior to the establishment of the Army Corps of Engineers FRF in 1977, the area was used as a naval training range.

During and subsequent to World War II, squadrons of pilots from the Norfolk Naval Yard utilized the area to conduct bombing and rocket practice launch sorties. The entire area of the bombing target range was transferred in 1973 to the Department of the Army Civil Works Division by the General Services Administration. Soon after, the Army Corps of Engineers established the FRF on the target range to conduct marine research. They constructed the 600-

foot long pier on concrete pilings to extend out into the Atlantic Ocean to water depths of 20 feet or more. Present operations at the site are under the purview of the US Army Corps of Engineers Environmental Research and Development Center in Vicksburg, Mississippi.

### **4.3 SITE GEOLOGY**

The general study area encompasses onshore and offshore areas of the northern Outer Banks. The Outer Banks are a chain of transgressive barrier and spit island features that span approximately 250 km from the Virginia-North Carolina border south to Shackleford Banks. The FRF site is located on a relatively narrow part of the sandy barrier between the Atlantic Ocean and the Currituck Sound, which separates the barrier beach from the mainland.

Coastal areas, such as those around the Outer Banks, are significantly influenced by the surficial geologic framework that exists beneath and seaward of the shoreline. In areas such as these with limited sand supplies, any accretion is derived from erosion and transport of sediment from adjacent coastal areas. This also leads to relatively thin and dynamic accretion zones of sand perched upon pre-existing geology. Current features on the Outer Banks are beaches, dunes, and marsh landforms, typical of Holocene and Pleistocene barrier island complexes. On the nearshore seafloor there are submarine scarps, shoals, and bars.

A number of studies have been undertaken to evaluate offshore sand barrow resources for beach nourishment (Dolan and Lins, 2000; Coastal Planning and Engineering of North Carolina, 2014; 2015). These studies highlight that the inshore zone along this part of the Outer Banks has free circulation of oceanic waters with little direct input of fine-grained material from inlets or estuaries. The surf zone is devoid of fines because of relatively high, wave-energy characteristics of the beach environment. The combination of low amounts of fine-grained sediments and frequent, high-wave energy off the coast tends to inhibit the accumulation of silts and clays (USACE, 2014). As part of some recent beach nourishment studies geophysical and geotechnical surveys have been conducted over approximately 230 miles in the summer of 2014. An example of high resolution bathymetry is shown in Figure 46.

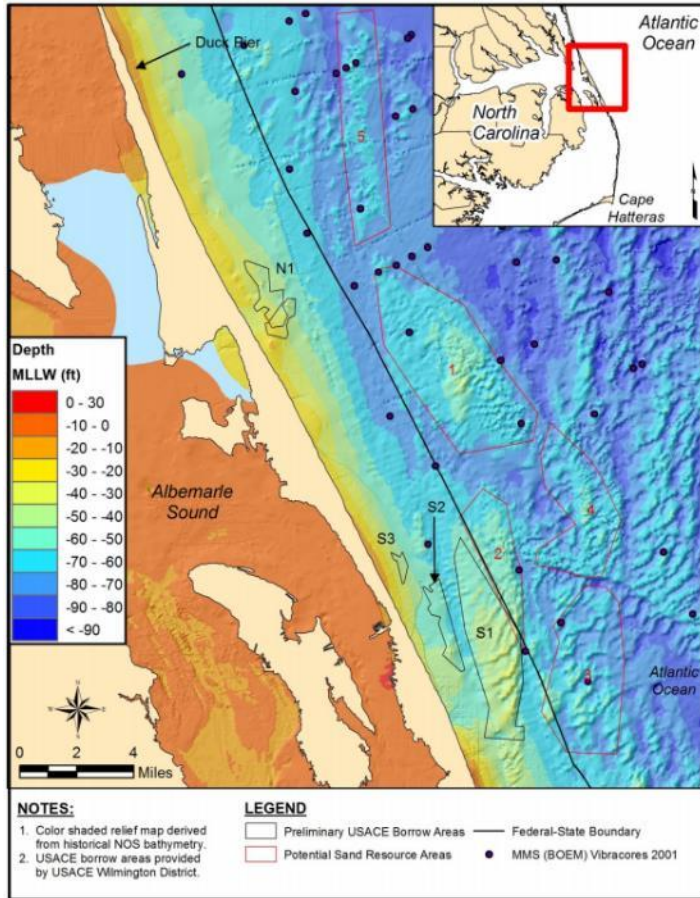


Figure 46. Bathymetry focus map near the study area (from USACE, 2000). The Town of Kitty Hawk in cooperation with the state of North Carolina, USACE, and BOEM conducted studies on sand barrow areas and beach renourishment in 2005 and a comprehensive study was undertaken in 2014 by the towns of Duck, Kitty Hawk, and Kill Devil Hills.

The general northeastern North Carolina coastal system is within the Albemarle Embayment complex and contains a 90 m thin Quaternary stratigraphy. The structural basin it forms is bounded to the east by a relict inter-stream divide (at the location where the current Outer Banks barrier islands reside) with Pliocene and Quaternary sequences dipping and thickening toward the center of the seaward basin (Mallinson et al., 2005). The barrier islands are constructed from sediment sourced from paleofluvial channels, shoal complexes, and sand-rich Pleistocene sedimentary deposits. Most of the region is characterized by overwash barriers while less area is covered by wider segments.

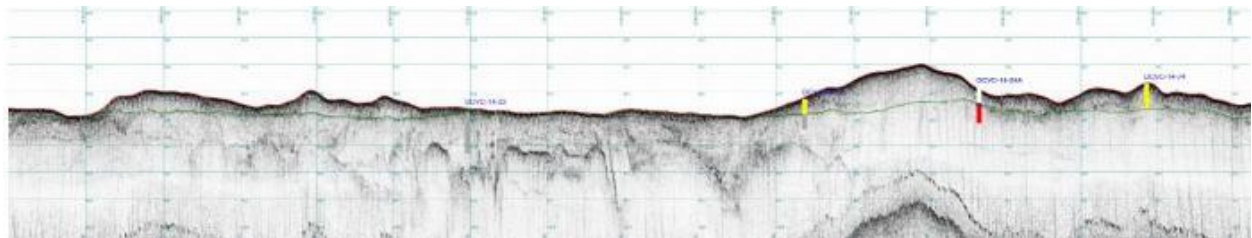
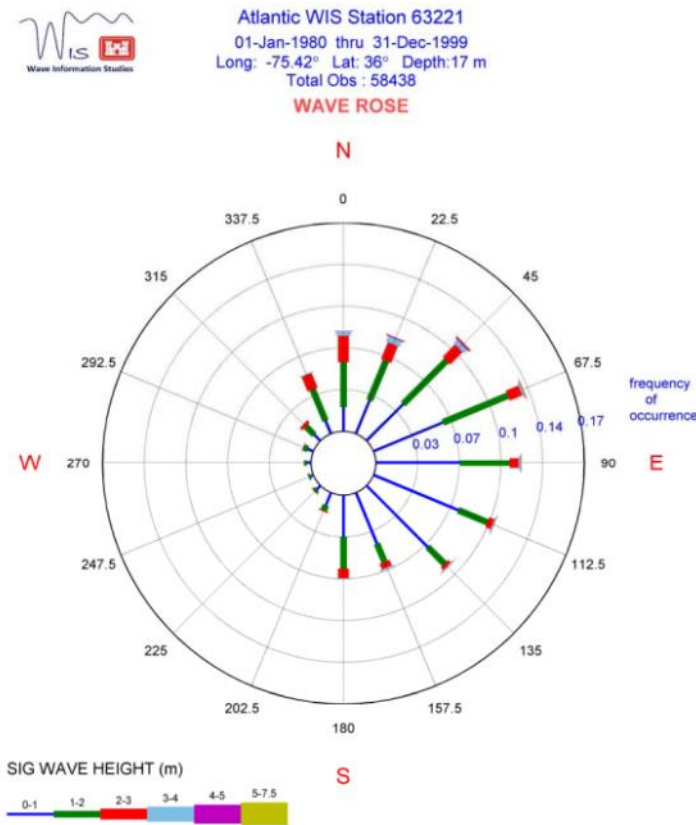


Figure 47. Shallow chirp seismic cross-section acquired approximately 3 km offshore from the FRF pier and extending to 5.5 km (from Walsh and Piatkowski, 2014).

The physical processes that drive the morphology of the general study area are well known and expected in this type of nearshore environment: tides, waves, currents, and storms. Tides are semidiurnal with a mean range of approximately 1m. Mean significant wave height over the period from 1997 to 2012 was  $1.0 \pm 0.6$  m with mean periodicity of  $8.7 \pm 2.8$  seconds (<http://www.frf.usace.army.mil>). The predominant wave direction is from the south to southeast in the spring and summer and from the north to northeast in the fall and winter.

**Figure 48. Wave direction rose diagram from the Wave Information System (WIS) Station 63221 aggregating offshore winds between 1980 and 1999.**

Figure 48 presents a wave rose from Wave Information System (WIS) station 63221 located offshore and near Duck in 17 m of water. Examination of hindcast data shows the majority of waves higher than 0.5 m come from the northeast and the east northeast. Currents and mean flows form an important part of the shelf circulation including those from the Gulf Stream. Storms prevail in the fall, winter, and early spring (Birkemeier et al., 1985) with tropical and extratropical storms mobilizing the most significant portions of shelf sediment.



**Figure 48. Wave direction rose diagram from the Wave Information System (WIS) Station 63221 aggregating offshore winds between 1980 and 1999.**

Extensive geophysical surveying and coastal geologic characterization have been conducted in this area. A great deal of work reported appears to have been conducted by Stanley Riggs of East Carolina University, his collaborators and students over the past 3-4 decades (Riggs, 1996; Riggs et al., 1995; Riggs et al., 1992; Schlee et al., 1988; Riggs and Belknap, 1988; Eames, 1983; Bellis et al., 1975; Riggs and O'Connor, 1974; O'Connor et al., 1973).

The beach and nearshore sediments around the FRF pier have been characterized on several occasions since the early 1980's via grab samples, box cores, vibracores, and side-scan sonar (Byrnes, 1989; Haines et al., 1995; Drake, 1997). Previous long-term studies at FRF along shore-normal profiles (e.g., Duck94 and SuperDuck, 1986 studies) have characterized cross-shore grain size variability. In 2002, researchers from FRF also studied beach and nearshore morphology using repeated sub-bottom chirp and swath bathymetry surveys. The surficial sediment in this area is predominantly a bimodal mix of medium quartz sand and small pebbles. Sediment size becomes progressively fine in the offshore direction, grading to very fine and fine sands with less than 10% silt (McNinch, 2004). Sediments become finer offshore to 13 m water depth and are well sorted fine to very fine sands (0.21 to 0.07 mm). Five non-opaque heavy minerals (garnet, staurolite, edpidote, amphiboles, and tourmaline) occur with regularity and a frequency of 2% or higher (Meisburger and Judge, 1989). The dominant foraminifera found in sediment samples are *Elphidium excavatum*.

Dunes are dynamic geologic features that continually accrete and erode from factors such as seasonal fluctuations in wave height and storm activity (Rogers and Nash, 2003). Dune vegetation is essential to maintaining dune structure, and generally consists of hearty plants tolerant of extreme conditions such as sea oats, beach elder, and beach grasses. Other vegetation typical along the uppermost dry beach of Duck includes beach spurge (*Euphorbia polygonifolia*), sea rocket (*Cakile edentula*) and pennywort (*Hydrocotyle bonariensis*). The foredune includes American beach grass (*Ammophila breviligulata*), panic grass (*Panicum amarum*), sea oats (*Uniola paniculata*), broom strae (*Andropogon virginicus*) and salt meadow hay (*Spartina patens*) (USACE, 2000). The beach and dune community within the demonstration area is limited in extent due to development and a coastline that is receding due to storm events and beach erosion (Leatherman et al., 2000).

#### **4.4 MUNITIONS CONTAMINATION**

Although our test area was not specifically selected based on proximity to known munitions areas, the FRF is a former bombing target range. In fact, the northern part of the Outer Banks has a history of use of military munitions including the Corolla Naval Target, Buxton Naval Facility, and our study site, the former Duck Naval Target (all in congressional district NC-3; see Figure 49). The USACE Savannah District is the Program Manager for the DERP/FUDS program in this part of North Carolina with the USACE, Wilmington District acting as project manager.

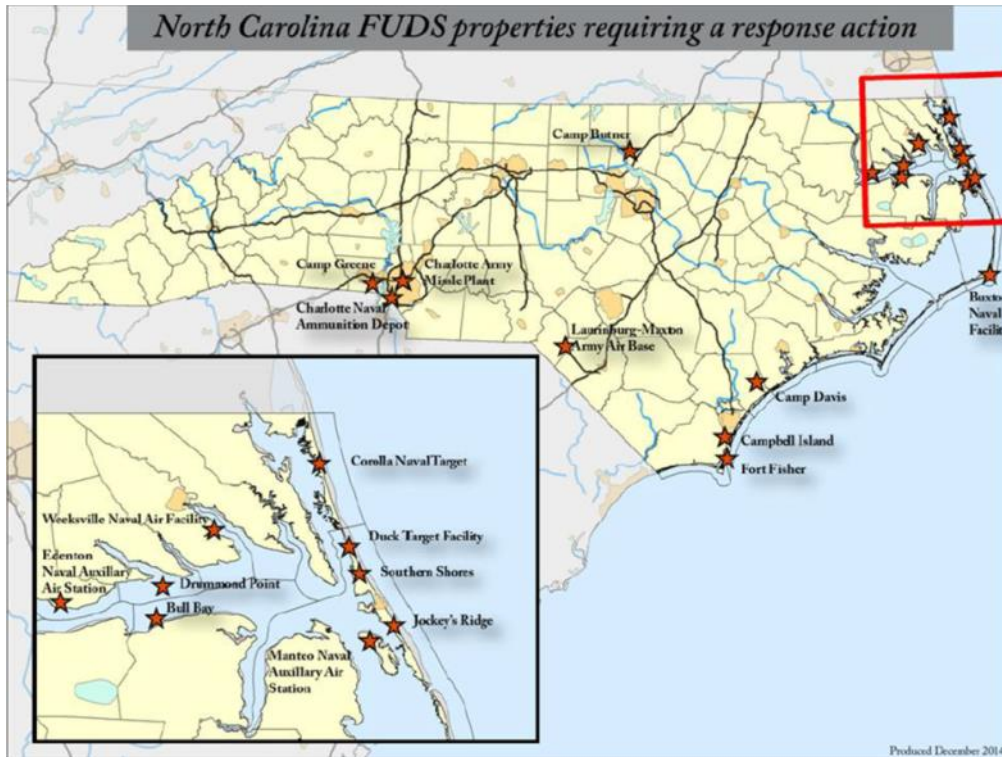


Figure 49. Map highlighting the locations of Formerly Used Defense Sites (FUDS) in North Carolina with inset showing those in the far northeast part of the site and along the northern Outer Banks.

The former Duck Naval Target range site was established as a Naval training area in 1941 and constitutes approximately 175 acres. It was used extensively during the period between 1941 and 1965 by aircraft from the Norfolk Naval Yard for practicing aerial bombardments. It appears that the majority of practice runs started with pilots entering from the west and firing munitions eastward at land-based stationary targets (Figure 50 and Figure 51). The primary objective was accuracy and precision training. Spotting charges have been reported to have been used for observations. Practice munitions used included practice rockets (2.25-11.75 inches), practice bombs (miniature - 250 lbs), and MK4 spotting charges, based on USACE historical records.

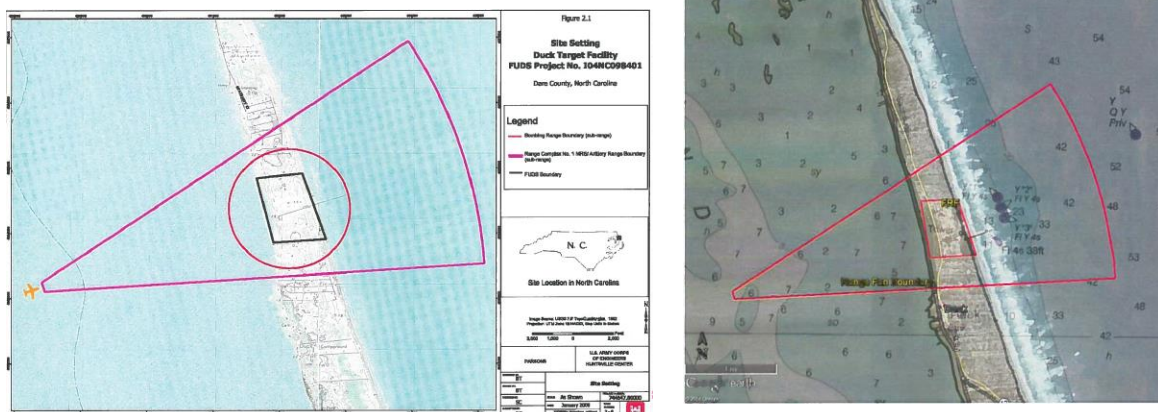
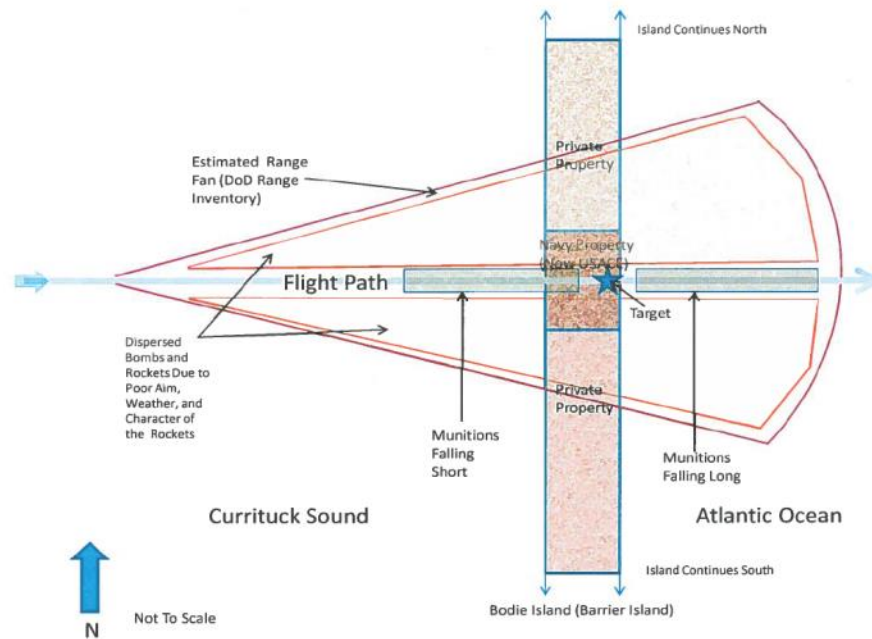


Figure 50. Maps and overlay diagrams depicting the former Duck Target Facility range fan and munitions response site.



**Figure 51. Overview conception site model diagram developed by USACE.**

UXO investigations and remedial actions on the site date back to 1971. Among the most significant actions are a 1972 clearance conducted before the property passed control from the Navy to the Army. An Engineering Evaluation and Cost Analysis (EE/CA) investigation was also conducted by Parsons Engineering Science and USACE in 1996 following a limited Removal Action (RA) and Archive Search Report in 1994. These activities also followed a 1993 Time Critical Removal Action (TCRA) that removed 821 total Material Potentially Presenting an Explosive Hazard (MPPEH). The 1996 EE/CA report described UXO surveys conducted using EM61 sensors that covered nearly 30 acres and identified 3,757 buried anomalies that were potentially UXO. Between 1996 and 2000 remediation activities led to the removal of over 3,500 MPPEH items. A summary of these are listed in Table 3.

**Table 3. Summary of MPPEH items removed from the Duck munitions response site.**

ITEM	MODEL/TYPE	BODY	PROPELLANT	WARHEAD/FILL
2.25" Rocket (SCAR)	MK16 Mod 4, 5, 6	Steel	Ballistite (NC and NG)	No fill -Hollow or solid steel
Miniature Practice Bomb	MK5	Zinc	NA	No HE – Spotting charge
	MK23	Iron		
	MK43	Lead		
5 lb Practice Bomb	MK106	Steel	NA	No HE – Spotting charge
25 lb Practice Bomb	MK76	Iron	NA	No HE – Spotting charge
100 lb Practice Bomb	MK15, Mod 2	Steel	NA	Water or sand Spotting charge
50 lb Practice Bomb	MK89	Iron	NA	No HE – Spotting charge
250 lb Practice Bomb	MK86	Steel	NA	No HE – Spotting charge
2.75" Practice Rocket	MK2, MK3, MK4, MK5, MK6, MK7	Steel	Ballistite	No fill-hollow
3.5" Practice Aircraft Rocket	MK3	steel	Ballistite	Solid steel
5" Practice Rocket	MK28, MK32, MK34, MK35	Steel	Ballistite	No fill-hollow
11.75" Practice Rocket	MK4	Steel	Ballistite	No fill-hollow

In 2008, USACE conducted a Site Inspection (SI) to evaluate the former Duck Target Facility munitions response site for potential release of munitions and explosives of concern (MEC). During this activity a qualitative reconnaissance was conducted, surface soil samples were analyzed, and few munitions debris items were found (some small arms cartridges, practice rocket pieces, and inert practice bombs). USACE concluded in their 2009 SI report that no MEC had ever been confirmed at the site and that the potential for unspent spotting charges is extremely unlikely. Figure 52.

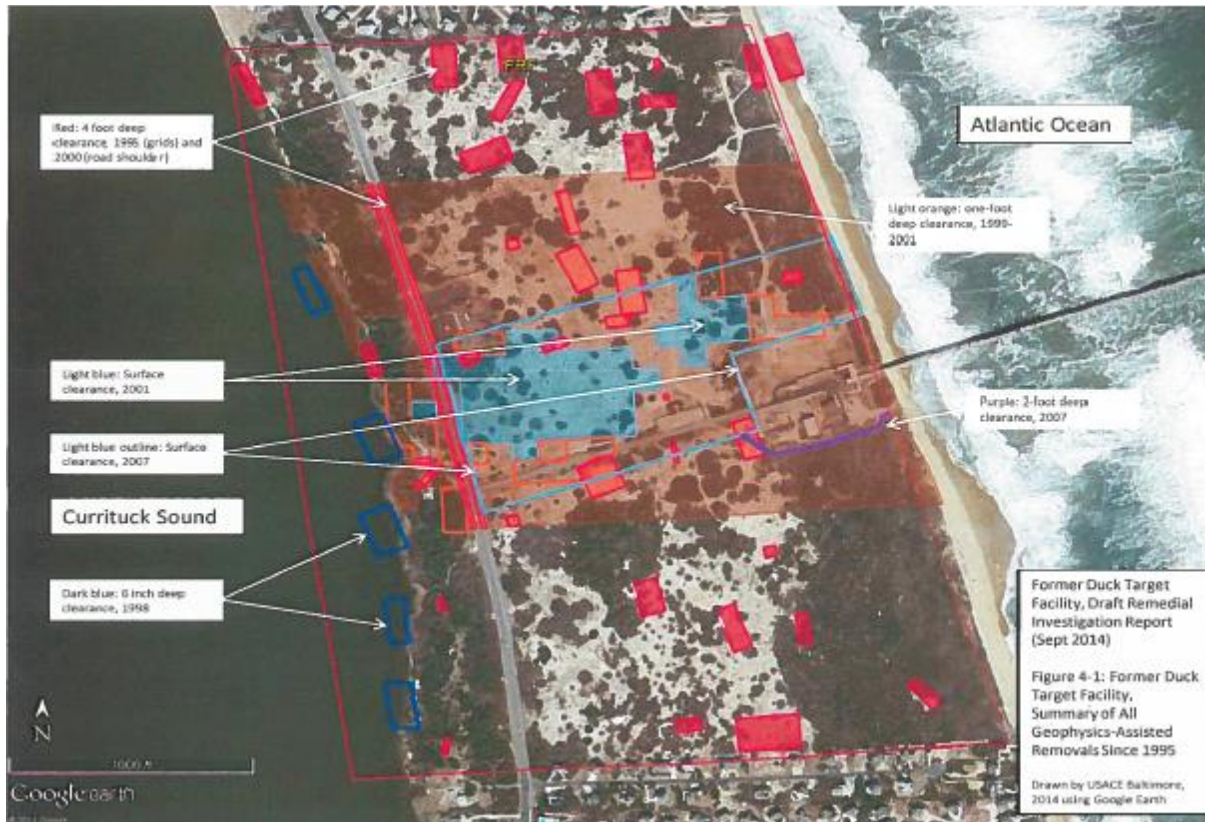


Figure 52. Previous UXO and site characterization investigations at the FRF.

## 5.0 TEST DESIGN

### 5.1 CONCEPTUAL EXPERIMENTAL DESIGN

The Duck FRF site encompasses both surf zone and intertidal sites that are appropriate for demonstrating the crawler towed sensor array implementation. For this first demonstration, we utilized both surf zone areas just south of the Duck FRF Pier and nearshore intertidal areas in the adjacent Currituck Sound. Recently acquired high-precision bathymetric data at FRF as well as historical data were used to plan survey profiles and select specific test areas. An example of recent beach profiles acquired from the USACE data portal along two transects in the area near our test site are shown in Figure 53. Shoreline and beach profiles can vary depending on seasonal weather and storm influence, especially during the transition between summer and winter.

Hydrodynamic measurements provided at FRF include water and wave height monitoring data, directional spectra of incident waves, offshore current profiles, tidal elevations, wind speeds/direction, and atmospheric pressure. The FRF Data Portal ([navigation.usace.army.mil/CHL\\_Viewer/FRF](http://navigation.usace.army.mil/CHL_Viewer/FRF)) provides access to near real-time and archived observations from the site. This includes point observations from beach, ocean bottom, or buoy-based measurement stations as well as geomorphology GIS layers (point, raster and vector data) and some limited analysis tools and raw data download capability.

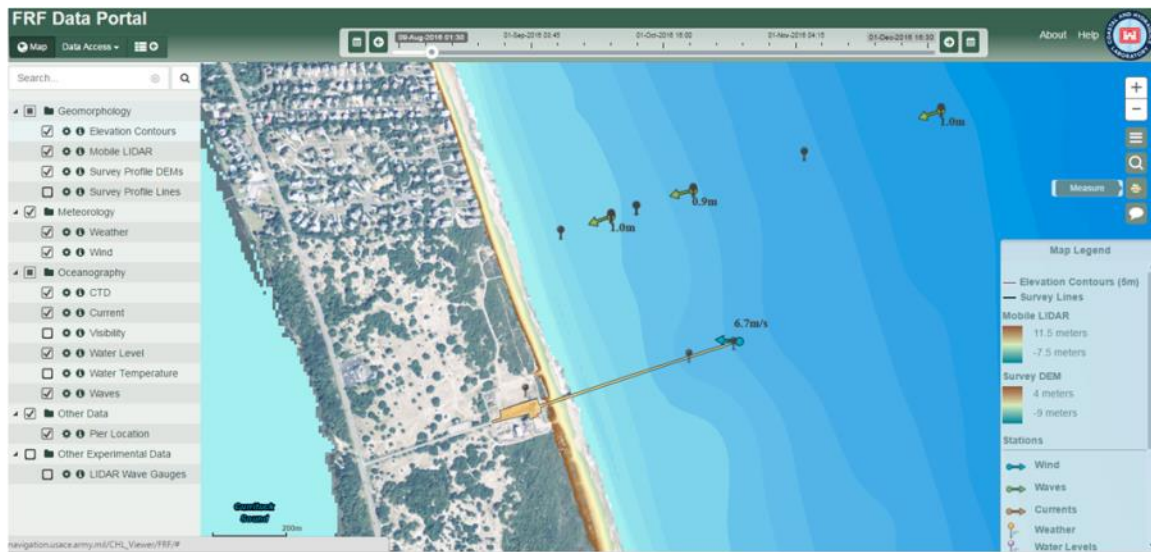


Figure 53. Top: GIS layer map showing recently acquired (August 2016) LiDAR nearshore bathymetry at the FRF site along with wind and wave vector information from the in-shore array. Two high-resolution bathymetric profiles sampled from ~50 and ~100 meters south of the FRF pier are shown in the bottom. Note the beach slope extending toward a trough and bar sequence before shoaling more gradually seaward. The area 100 to 300 meters along the shore-normal baseline (x-axis) is the area targeted for our demonstration.

Demonstrations were conducted first on the beach and swash/surf zone, and then in the shallow sound adjacent to the FRF site. The general set up comprised the integrated crawler and sensor tow system connected to a shore-based operator control station (OCS) via a fiber optic tether. The system was controlled from the OCS. The crawler tether was managed on the FRF pier, which also provided an excellent vantage point for observation of operations on the beach and in the surf zone. An instrument verification survey (IVS) strip was established on the upper beach for daily quality assurance checks. Survey areas included transects from the lower beach area perpendicular to the shoreline through the surf zone and wave break area to shallow water (~2-2.5 m deep). Figure 54 shows the basic set up including relative locations a primary test resources. Further detail on the site preparation, system specifications, and test procedures is provided below.

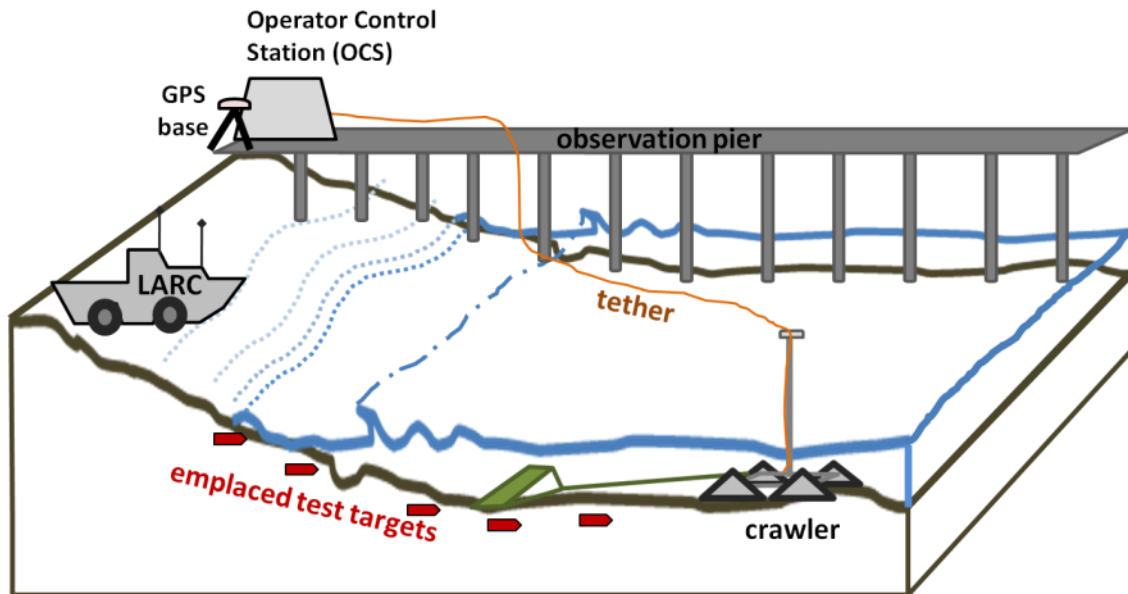
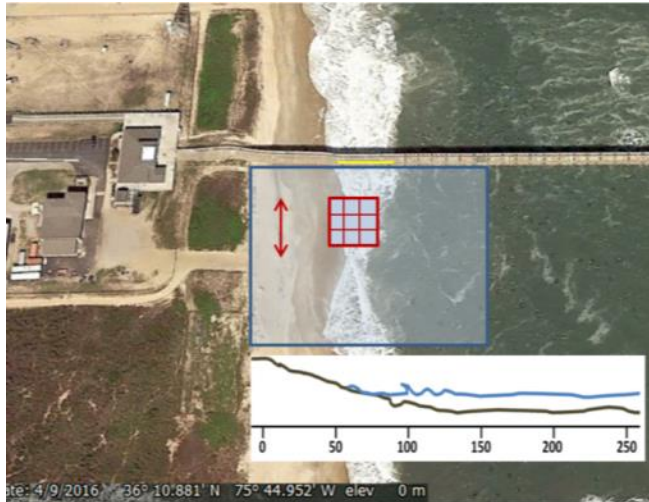


Figure 54. Conceptual overview schematic of the crawler-EM demonstration.

Our demonstration began with a day of site reconnaissance and setup including setup of auxiliary equipment such real-time kinematic (RTK)-GPS and operator control station, preparation of the crawler to be used during testing, and assembly of the tow system including mounting the EMI array and GPS rover antenna onto the crawler. This was followed by preliminary integrated system deployment and data collection by the crawler system operator/pilot. Data collections on the upper beach were used to test the functionality of all subsystems, calibrate GPS and two-point encoder, and to characterize the data collection area in terms background conditions, and location of EM clutter.

Following setup activities, we emplaced and surveyed inert UXO targets in the swash and surf zones. Targets used for testing included 22 different items: 14 UXO simulants and 8 ISO objects. Figure 55 shows an overview of the surfzone target emplacement areas relative to the shoreline and approximate wave break zone. Note that the swash and wave break zone varied considerably with weather patterns.



**Figure 55.** Google Earth image showing the location of target emplacement areas across the surf zone. Site areas are outlined in blue with target emplacement transects indicated in red. The inset shows the shore-perpendicular bathymetric profile scaled to the image easting. A 50 m transect from the shoreline to past the wave breaking zone will be established with UXO targets buried along it. In addition, a small target grid will be set up just seaward from the shore-perpendicular transect.

## 5.2 SITE PREPARATION

The primary tasks associated with site preparation were survey control, target emplacement, and monitoring of environmental parameters such as weather, waves, and currents. Horizontal and vertical control and datums are necessary for accurate RTK-DGPS surveys. Survey control was established through FRF's geodesy control system and used the NAD83 datum adjusted to the 2001 North Carolina State Plane for horizontal and NAVD88 vertical datum using the 2003 Geoid for elevation. We located the FRF calibrated monument points that are also frequently used for bathymetric surveys (from both the LARC and CRAB platforms). These control points have been cross-checked against the National Geodetic Survey monuments around the northern part of the Outer Banks. Crawler support equipment was located on the FRF pier to minimize the length of the support-tether and to reduce wave and current loading on the tether.

Placement of munition surrogates (aka, UXO targets) was focused on the most challenging regions of the nearshore – depths of 0.1 to 1.2m - where waves shoal and break and where the seabed is most dynamic. We surveyed and emplaced targets just to south of the Field Research Facility (FRF) pier between the lower beach (mean high tide water line) and the wave break zone seaward of the swash area. Unfortunately, we experienced particularly challenging surf zone weather conditions at the scheduled time for target emplacement. Winds persisted at 20-25 mph for extended durations with gusts up to 40 mph at times. These conditions, surf in excess of 5 feet and difficult currents, conspired against our target emplacement objectives. This is shown in the wind and wave height profiles in Figure 56.

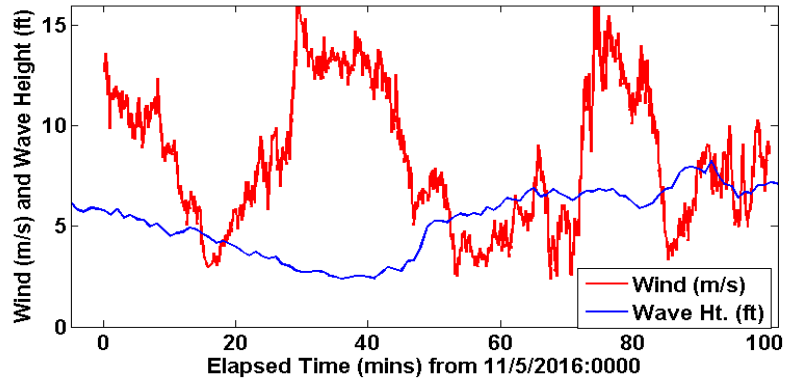


**Figure 56. Surf weather during our demonstration presented significantly challenges for target emplacement and safe operations. Surf waves were typically greater than 5 feet tall and in some cases were 8 or more feet. Strong winds persisted during most of our available testing window.**

Due to the challenging weather conditions, we adjusted our original plan that involved water jet emplacement and utilized manual digging and covering of UXO. At low tide, we utilized prepared target strings (UXO objects tied to sinking line) along 4 shore-normal lines. The shore-normal lines extended from the lower beach, through the swash zone, and into the surf zone. Each target was installed in the seabed by a two-man team. Targets were installed in an approximately 30 cm deep hole and then connected to the sinking line via a non-metallic (hard plastic) carabiner. The most seaward target along each of the four shore-normal lines had small surface float tied using 500lb test monofilament line attached to a clump weight. The targets themselves were tethered together with leaded-line that was buried between each target. This is shown in Figure 57.



**Figure 57. Annotated photograph from the upper beach looking seaward at the 4x4 target grid extending from the water line to the surf zone. The IVS strip is also shown in the foreground on the left side.**

A separate team followed along and performed geodetic surveying of each target just prior to burial. The CRAB was used as a stable, mobile platform following wading personnel to provide proximal RTK-GPS equipment, a jetting wand, and distributing individual targets. The CRAB geodetic survey system consists of a Trimble 4000 SSE RTK-DGPS system. This system is a

dual-band L1/L2 capable receiver with very low noise C/A code processing for cm-level accuracy. Independent field tests of this system have resulted in demonstrated RMS errors of  $\pm 12.2\text{mm}$  and  $\pm 22.6\text{mm}$  for the respective horizontal and vertical errors. This CRAB-based GPS system is the primary survey control for the CorpNet station at the FRF facility and thus mandates high quality assurance and accuracy for geodetics.

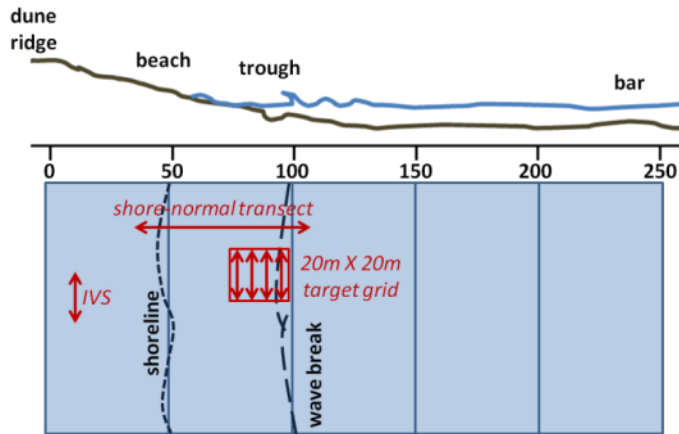


Figure 58. Schematic diagrams of the target emplacement areas at the FRF demonstration site: Instrument Verification Strip (IVS), shore-normal transect, and 20x20 m target grid area.

Seeded items included both ferrous and non-ferrous ordnance simulants (Figure 59) of different sizes (60 mm to 155 mm). A ground truth target spreadsheet was created containing the target's type, latitude (northing), longitude (easting), orientation, and burial depth.



Figure 59. Photographs of the simulant targets used in the demonstration. These include ISO's, simulant UXO from the Aberdeen Test Center (ATC) test set, clutter objects, and other canonical metal objects for assessing the performance of the overall system.

An instrument verification survey strip (IVS) was also established along the upper beach directly adjacent to the offshore survey areas. IVS seed items consisted of schedule-40 small Industry Standard Objects (large or medium ISO40) buried along the IVS line. Each of the items was placed in hand-dug holes, surveyed in using RTK-DGPS, and covered and marked with a plastic or wooden stake and labeled (Figure 60).

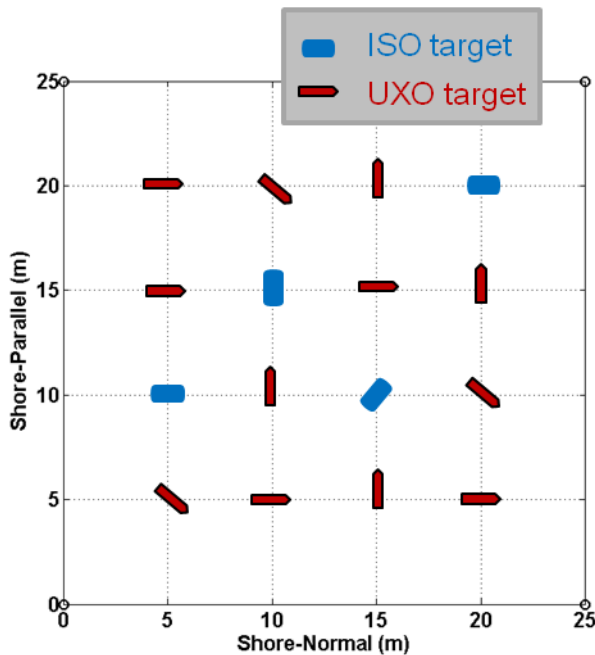


**Figure 60. Left: Diagram of the 4x4 offshore target grid used for area coverage and UXO target detection and localization testing. The site consisted of 20 by 20 meter grid with 4 target lines buried below the seafloor at nominal depths of 15-45 cm. Sixteen items were emplaced including 12 UXO simulants and 4 ISO objects.**

We also utilized data from the FRF surf zone instruments to determine the relevant water characteristic parameters during our test. A CTD instrument installed at the end of the pier provided measurements of water visibility, temperature, density, salinity, and sound speed. The average conditions over the test period of 6-10 November were as follows:

- Visibility: 1.1 meters
- Temperature: 16.7 degrees Celsius
- Density: 0.0015 g/cc
- Salinity: 28.75 psu
- Sound speed: 1506 m/s

The temperature and salinity measurements are used to compute an average water conductivity of 4.45 S/m.

Mobility assessments consider the entire effects of the terrain on platform operations, including grain size, internal friction, cohesion, bearing strength and bathymetry or topography. Therefore, during preliminary site assessment activities we acquired some basic sediment properties data including dynamic cone penetrometer (CPT) instrumented "drop logs" and sediment samples. The dynamic CPT instrument we used was the portable free fall penetrometer called BlueDrop ([www.bluecdesigns.com/blueDrop.aspx](http://www.bluecdesigns.com/blueDrop.aspx)). It is a small and lightweight penetrometer (88mm diameter at widest) developed for rapid in-situ geotechnical characterization of nearshore coastal sediments. It has five on-board microelectromechanical systems (MEMS) accelerometers measuring up to 250 g of gravitational acceleration with an accuracy of up to  $\pm 15.6 \mu\text{g}$ . A pressure transducer located behind the sensor tip can measure up to 2 MPa with accuracy of  $\pm 4.67 \times 10^{-4}$  kPa. A photograph and basic specifications of the BlueDrop are shown in Figure 61 along with examples of processed bearing capacity, deceleration, and velocity penetration curves.

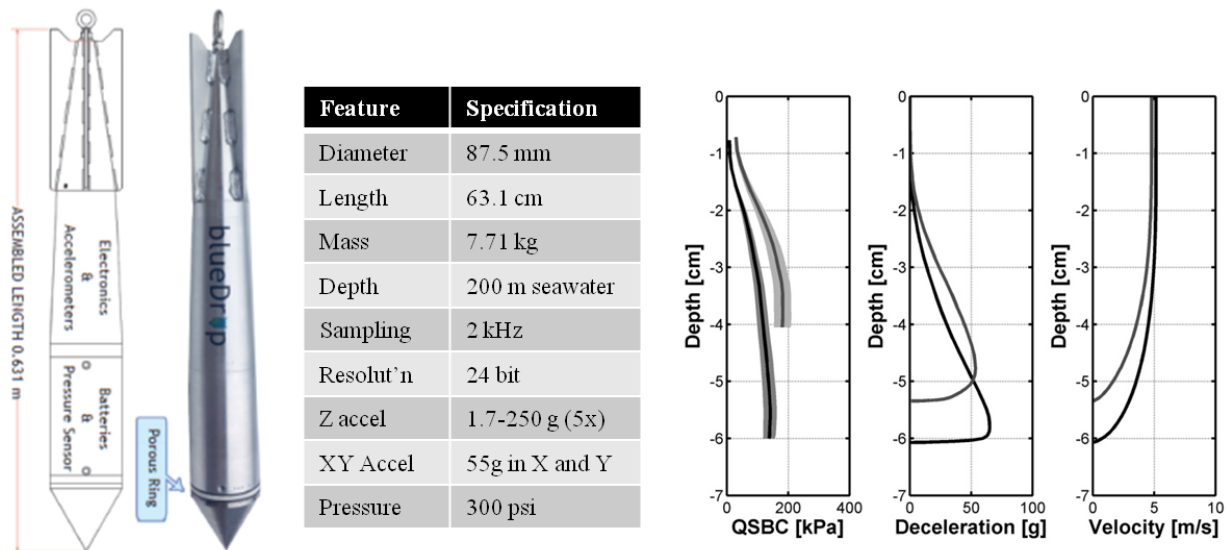


**Figure 61. Left: Photograph and dimensions of the BlueDrop free-fall penetrometer. Middle: Summary of BlueDrop specifications. Right: Example of processed data estimated from raw BlueDrop deceleration and pressure distributions with penetration depth. The instrument produces the velocity and deceleration data needed to estimate the quasi-static bearing capacity (QSBC) profile as a function of probe penetration depth.**

The BlueDrop penetrometer was dropped from the CRAB at select locations along survey transects in order estimate the quasi-static bearing capacity (QSBC) over the penetration depth of each drop sounding. The evolution of velocity and penetration are derived from recorded accelerations and processed to estimate QSBC. In addition, in areas where corresponding sediments were accessible, we acquired disturbed sediment grab samples for follow-on grain size analysis. Figure 62.



**Figure 62. Photographs of BlueDrop free fall data collection and associated sediment sampling during preliminary site assessment work.**

Additional BlueDrop data collection and analysis was conducted by Albatal et al (2017) as part of a corresponding study to monitor spatial and short-term temporal variations of seabed geotechnical properties in the nearshore zone at the USACE FRF site. During the combined

studies, over 32 penetrometer drop soundings were conducted south of the FRF pier. Figure 63 shows the locations of 27 of the survey stations parallel to pier.



**Figure 63.** Aerial view of the BlueDrop sounding locations along the Duck FRF pier. Additional sounds were acquired on the beach and in the swash zone adjacent to the pier.

Grain size analyses for samples acquired at select stations the shore-normal transect are shown in Figure 64.  $D_{50}$  grain sizes were finer in the surf zone and coarser in the swash and lower beach areas with a relatively large degree of variability. The largest  $D_{50}$  size was approximately 5mm recovered from the outer swash near the wave break trough where we might expect larger sediment sizes to accumulate. The smallest  $D_{50}$  grain size was found at the deepest water location sampled and was 0.3 mm.

The bathymetric profile along the ~50 meter transect shows that all but two of the sample locations were submerged or partially submerged. Bathymetry data were determined using the CRAB positioning system during surveys in 2016. We also estimated the slope along the transect as the sediment side and corresponding cone index can be inferred from slope along the transect. Jenkins [1985] developed a regression equation for calculating cone index values for saturated samples given field values for average grain size  $D$  and beach slope  $m$ :

$$CI = \frac{2 \sin(\phi - m)}{\tan \phi (1 + \cos \phi)} \left[ 10240D + \frac{0.0024}{D^2} - \frac{0.158}{D} \right].$$

We applied this empirical relationship to the locations where we had both sediment grain size estimates and slope from bathymetry and beach slope. The grain sizes, slope calculations, and estimates of cone index for stations along the shore normal transect are shown in Figure 64. An alternative method described by Mulhearn [2001] is to estimate cone index from surf hydrodynamic observations. This method assumes an equilibrium beach profile and assigns the smallest grain size to be just under the wave break point. The threshold drag velocity is related to grain size and from the grain size the cone index value. Since the foreshore zone and beach are not always in equilibrium, the underlying assumptions used in this method can lead to inaccurate estimations and were not used here. More recent research has worked to develop bearing strength estimates from hyperspectral imagery (Smith et al., 2007; Bachman et al., 2016). These methods generally employ a spectral look-up table for bearing strength based on visible and near-infrared wavelength where forward radiative transfer models are calibrated by in suite geotechnical measurements.

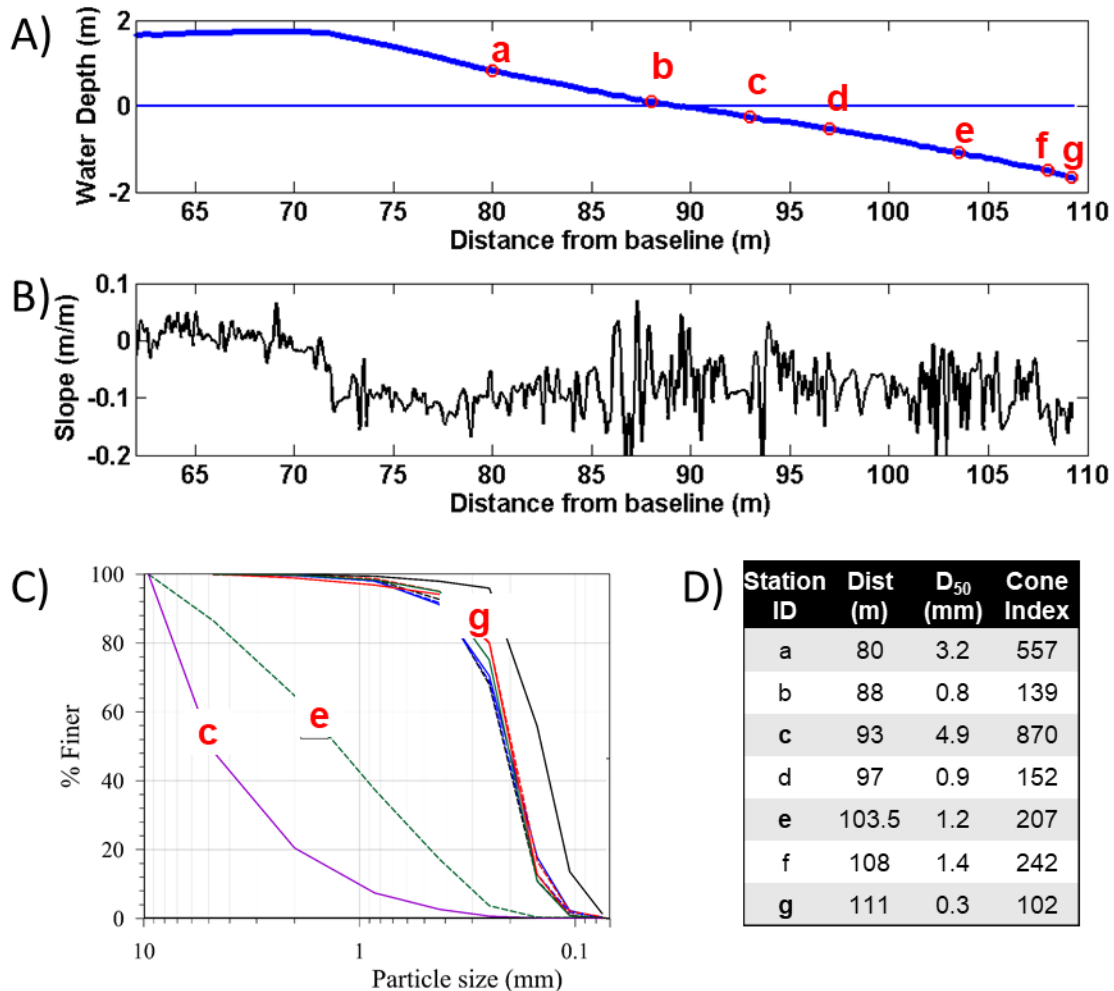


**Figure 64.** Data acquired from foreshore and beach geotechnical sampling and surveying during preliminary site assessment. A) Beach and surf zone bathymetric profile relative to the mean water level across shore-normal transect. Data were acquired from the CRAB bathymetric survey platform. Select penetrometer and sediment grab sample locations are indicated by a-g. B) Average slope computed across the profile showing variability of ~0-10cm/m. Slopes at select locations were used to estimate cone index using the method of Jenkins [1985]. C) Grain size distribution estimates from sediment samples at select locations along the shore-normal transect. Coarsest sediments (1-5mm) were found in the shallow swash and surf zone areas, with largest grain sizes accumulating in the wave break trough in approximately 0.3-1.3 meters water depth. D) Table of average grain size (D<sub>50</sub>) and estimated cone index for select locations along the shore-normal transect.

Figure 65 shows estimates of QSBC at three locations across the transect. Repeated surveys were conducted and used for estimating bearing strength. Estimated bearing strengths varied between approximately 20-90 kPa over the 0-25 cm penetration ranges sampled. The shallowest station, corresponding to the coarsest grain size material, yielded the largest QSBC. Bearing capacity estimates decreased with increasing water depth and decreasing grain size with the lowest QSBC estimates at station “g” where bearing strengths were as low as 19.8 kPa.

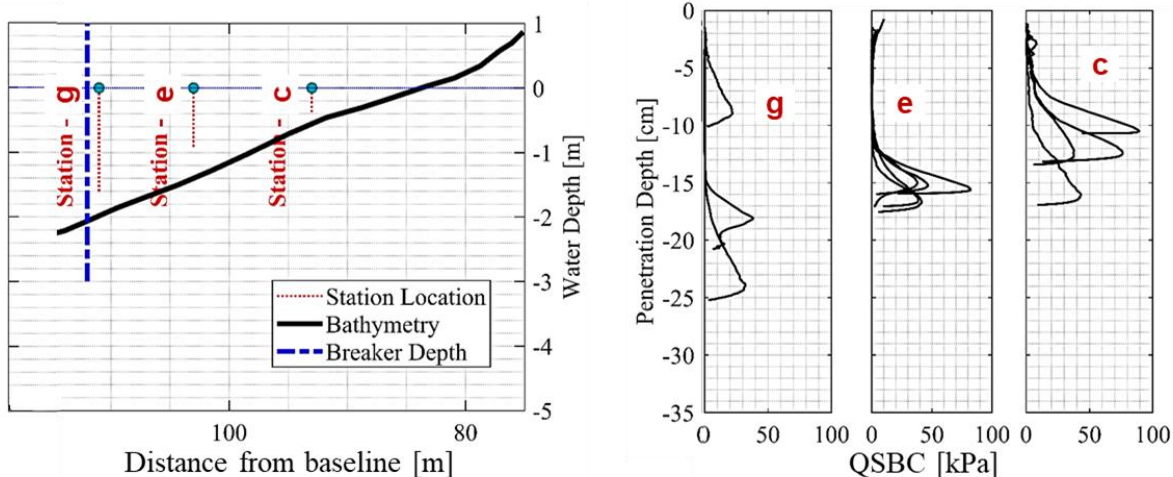


**Figure 65. Data acquired from foreshore and beach geotechnical sampling and surveying during preliminary site assessment. A) Beach and surf zone bathymetric profile relative to the mean water level across shore-normal transect.**

We note that the utility of the QSBC measurements in defining trafficability parameters such as traction efficiency rely upon the translation of QSBC to the more functional cone index. In general, if the bearing capacity is low, the crawler vehicles tracks will sink and increase the motion resistance. The cone index is the resistance to penetration developed a cone penetrometer and is equal to the vertical force applied the cone tip divided by its projected surface area. Some field tests have shown a linear or relatively linear relationship between cone index and bearing capacity. However, we were unable to find sufficiently rigorous research that established robust relationships for saturated sands that we might expect in nearshore UXO environments such as the FRF test site.

### 5.3 SYSTEM SPECIFICATION

The system for demonstration includes the SurfROver crawler platform, inertial navigation and control system, integrated Hemisphere V320 dual-antenna rover and GPS mast, the Flex-EM time-domain array, and the sensor array tow sled system. Each system will be described in detail in the following section.

#### 5.3.1 SurfROVer Crawler System

The crawler used for this demonstration is the SeaView SurfROVer crawler system designed and manufactured by SeaView Systems Inc. (Dexter, MI). The SurfROVer is a purpose-built crawler developed for shallow-water operations such as pipe and cable tracking, UXO detection surveys, and bathymetric or hydrographic surveying. It was previously demonstrated at Toledo Beach, Michigan. This system has four crawler tracks on independent suspensions, integrated drive propulsion and control, subsea lithium-ion battery power supply subunit, subsea lighting, a 1000-foot long fiber-optic tether, and topside operator control station. The vehicle also provides a mechanically-scanned forward looking sonar as well as a payload capacity supporting up to three additional serial sensors and three additional Ethernet sensors. The specifications for the demonstration-ready version of the crawler are shown in Table 4.

**Table 4. SurfROver System Specifications**

<b>GENERAL</b>	
Max Operating Depth	150msw
Overall Dimensions (LxWxH)	2.6m x 2.0m x 0.9m
Composition	Low Magnetic / Corrosion Resistant / low EMI & low EMC
Weight (in air)	390kg (860 lbs) (estimated)
Weight (submerged)	Negatively buoyant: 222 kg (490 lbs) (estimated)
Ground Pressure (submerged)	0.2 PSI
Pull Force	400 kgf (estimated)
Range	4000ft from control trailer
Speed (Ground)	0.83 m/s (3 kph, 1.6 knts)
Speed (Submerged)	0.45 m/s (1.6 kph, 0.86 knts)
Propulsion	Ge-roller based Hydraulic Power Units
Turning Radius	Approx. 11 m diameter
<b>OPERATING CONDITIONS</b>	
Current Conditions	3 knt current regardless of incident angle
Bottom Type Environments	Range of soil types (sands, muds) up to 80 kPa
Wave Action / Sea States	Up to 2 m plunging waves; Sea State 3
Traverse Capability / Obstructions	Traverse capability for obstructions 0-20 cm above flat seafloor; barriers, troughs, macro-ripples, shell reefs; etc.
<b>PAYLOAD CAPABILITY</b>	
Payload Allocation	150 kg; 100 L (e.g., three 20cm OD x 30 cm long pressure vessels)
Payload Power	5/12/15/24/48Vdc up to 200 W each; Capable of 5 Amp Min in-rush current per channel.
Payload Data Interface	Ethernet 10/100 (Gbit available)
<b>TOPSIDE INTERFACE</b>	
PC Interface	Windows or Linux User Interface for Control/Display
Motion Command	Motor % Power; Direction; Counter-rotate; Joystick or PC
Data Interface	3ch SD Video, 10/100 Ethernet, 4 x RS232, 2 x RS 485, 2 x RS485/232 onboard conversion, 2 high speed TTL.
Platform Data	10 Hz: camera awareness, direction, velocity, roll/pitch/yaw, pressure depth, altimetry, health status
Positioning	RTK-DGPS; allocation for IMU and USBL
<b>MECHANICAL INTERFACE</b>	
Winch Tow Anchor	Four padeyes
Launch & Recovery (LAR)	2 ton winch recovery (Dyneema rope)
Tow Bridle	3DOF tow point interface
Soft Buoyancy System	Optional (desired for emergency lift to sea surface)
<b>AUXILLARY SENSING</b>	
Cameras	Two (Min) RGB or Greyscale Fixed View Cameras (e.g., 1 forward looking and 1 downward looking)
Lamps	Three sets of 10k lumen LED lights
Depth Sensor	Pressure
Sonar	Imagenex 881a imaging scanning sonar.

### 5.3.2 Flex-EM Sensor Array and Tow Platform

The crawler will be configured to tow the 2-meter wide sensor sled and a dual-heading RTK-based DGPS system. The Flex-EM sensor electronics housing will be in pressure vessels attached directly to the tow platform. The tow platform will be deployed with sufficiently negative buoyancy for operation in seawater. A single cable connects the sensor head to the sensor electronics. The electronics receive power and an Ethernet connection to the vehicle data network through the central sensor manifold provided on the crawler. A topside computer running a software application interface communicates with the Flex-EM electronics through the vehicle network. The topside software application displays and logs Flex-EM sensor data and RTK-GPS data. Figure 66.

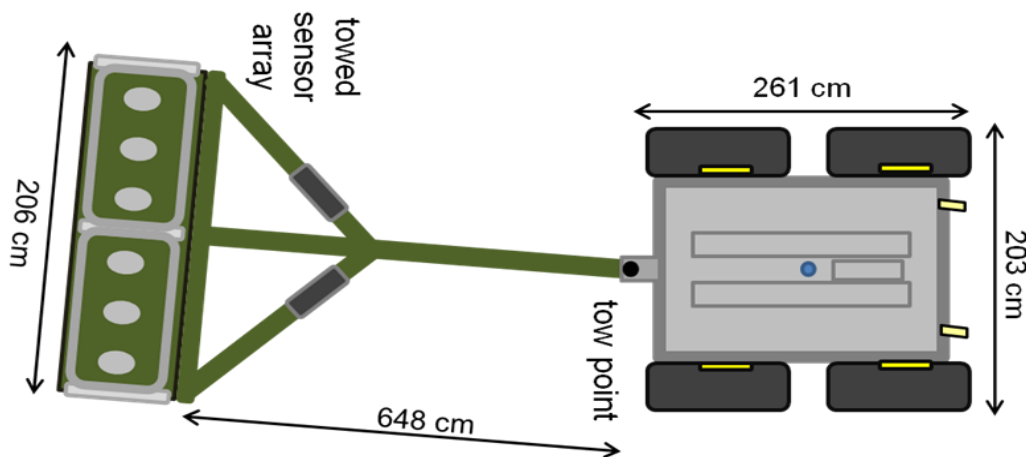


Figure 66. Configuration diagram of the crawler-based EM system used for the initial demonstrations. The bulk dimensions of the configuration are shown.

### 5.3.3 Dual-heading RTK-GPS and GPS Mast System

The RTK-GPS system consists of a Hemisphere V320 GNSS-enabled dual-heading smart antenna and a Hemisphere R320 GPS base station. The rover outputs NMEA GPGGA, GPVTG, GPGSV, and GPHDT data strings at a rate of 10 Hz via an RS232 serial cable connected to the crawler junction box and converted to RS422 for transmission via the crawler fiber optic tether to topside. The baud rate is set to 19.2 Kbps over the GPS serial port B. RTCM RTK DGPS corrections are sent via the crawler tethered modem directly from the GPS base station to the rover unit on the crawler.

### 5.3.4 Auxiliary Platform Characterization Sensors

A number of auxiliary sensors were used to help characterize the mobility, stability, and overall operating envelope of the integrated crawler-EM system. In our early trials, we utilized a load cell strain gauge with corresponding digitizer module to assess the pull forces on the crawler tow point. The S-type load cell we used was a model LCC-HRS 5K (5000 lb capacity) stainless steel gauge submersible to 95 PSI with a Matracourt DCS-USB digital signal conditioner. We also utilized a standalone self-logging inertial measurement (IMU) with integral 3D gyroscope, 3D

accelerometers and magnetometers, and pressure and temperature units (Loggerhead OpenTag Datalogger). In addition to the IMU, we used a set (4) Onset HOBO self-logging Pendant-G accelerometer/tilt-meters.

Environmental conditions associated with our test data were measured with a set of self-logging sensors. We mounted a single beam acoustic backscatter sonar for characterizing the seabottom and particular aspects of the water column (e.g., bubble cavitation). The single beam sonar used was the EoE Ultrasonics Echologger EA400 unit with integral power supply and data logging capability. This unit was attached directly to the crawler sled and when submerged produced full waveform acoustic backscatter data at a data rate of 1 Hz. Conductivity, salinity, and temperature of the water column were measured using an Onset HOBO U24-002 unit. In situ conditions were also observed after each mission from a set of GoPro progressive scan HERO 3+ cameras mounted on the crawler and tow sled boom.

### **5.3.5 Top-side Control and Display**

The OCS station was in a portable trailer and consisted of the complete operator control station, data interface and networking unit, multiple displays, and the Flex-EM data acquisition and user interface laptop. For our demonstration, the control station was manned by the crawler helmsman (remote operator) and an EM system analyst. The OCS crew has access to multiple monitor systems that display camera views on the crawler as well as real-time scanning sonar and feedback from the crawler battery management system, control system, and EM array.

The follow individual displays are available at the topside OCS (see Figures 9 and 10):

1. Camera View 1: mast-mounted forward-looking live RGB camera
2. Camera View 2: crawler-mounted rear-looking live RGB camera (pointed at array)
3. Camera View 3: crawler-mounted forward-looking live RGB camera
4. Crawler Diagnostic Feedback: real-time updates from the crawler battery management, control systems, and scanning sonar view (these constitute separate windows on a single monitor display, but could be split out over multiple monitors)
5. Navigation Display: integrated system navigation and mapping location display showing the real-time track of the crawler and sled along with waypoints and lines to follow and additional marker points or points of interest (e.g., obstacles or exclusions areas to avoid)
6. FlexEM Display: this display compiles navigation information from the GPS and IMU with real-time "waterfall" traces from the EM array receivers as well system configuration, data acquisition and file logging information.

## **5.4 CALIBRATION ACTIVITIES**

### **5.4.1 Encoder and GPS Calibration**

The tow point encoder requires calibration to ensure its zero position and any small changes in full range and angular resolution over the course of operations. Tow point encoder calibration involves zero point and full range calibration as well as correlation with the crawler GPS rover (Figure 67). The following outlines the encoder and GPS calibration.

Small yaw angles out of alignment with the crawler can cause a crabbing error effect on the heading measurements. These errors can be corrected by calibrating for the any angular bias between the in-line vehicle trajectory and the relative angle of the GPS rover antennae. The procedure is as follows:

1. Rigidly mount the GPS rover in the GPS mast receiver fixture.
2. Mount the GPS mast receiver fixture to the GPS mast using the index alignment marks and bolts.
3. Raise the GPS mast and index and bolt the fixture to the crawler.
4. Use the known towpoint fiducial mark as a reference between two know GPS survey control points. Note the deviation between true heading and measured heading from the Hemisphere V320 GPS rover. Use this heading offset as the bias correction in post-processing.

Encoder calibration:

1. With GPS antenna rigidly fixed and in-line with the crawler axis, align the towbar in-line with both GPS antennae with a long survey string.
2. Note the visual zero position.
3. Move the towbar (or towpoint) to the port side hardstop and note the positive encoder reading at hardstop.
4. Move the towbar (or towpoint) to the starboard side hardstop and note the positive encoder reading at hardstop.
5. Upon each power up, move the towbar to both hardstops and note readings.
6. Prior to each power down, move the towbar to both hardstops and note readings.
7. For each sortie, the zero position should be calculated from the hardstops using the original calibration numbers achieved from the string alignment procedure (steps 1-3).
8. Once the zero position is determined, offset the azimuth (positive or negative) should be applied to the positioning algorithm.

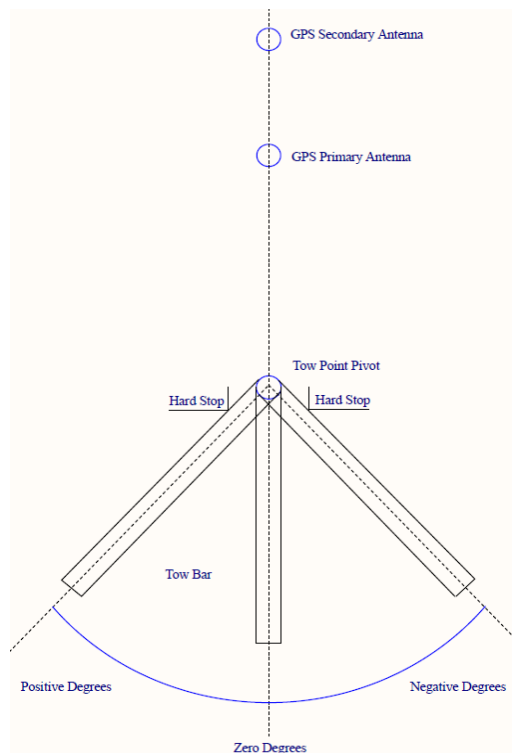


**Figure 67. Diagram of GPS rover and tow point encoder calibration.**

#### 5.4.2 IVS Surveys

Four ISOs, separated by 5 m and contained in a beach-based survey line, were used to calibrate the EM sensor and navigation and positioning system periodically throughout surveying; at minimum at the beginning and end of each data collection day.

Background surveys were performed with the system and using RTK GPS positions. The purpose of this step is to document the appropriateness of the location (e.g. few existing anomalies), and will verify that IVS targets are not seeded near existing anomalies. Once the IVS area is deemed suitable for use, (i.e. free of significant subsurface anomalies or containing anomalies that are clearly identified so that they can be avoided during seeding), ISO targets were buried horizontally at depths below ground surface of approximately 3 and 7 times their diameter. These depths are intended to provide adequate signal to noise ratio for detecting the targets. Measurements of the item depths were to the center of mass of each item. On-site personnel buried the IVS targets using shovels to dig the holes to the appropriate depths for burial of the seed items.

Prior to collecting production data and each morning before beginning field operations, data were collected with the EM system moving over the IVS including the background location (blank space). The SNR of EM sensor data collected over each target is compared to the SNR of data collected previously in a controlled setting. The EM sensor passed calibration if the SNR is within +/-15% of the controlled SNR. The distance traveled using the navigation solution was compared to the known separation (5 m) of the targets. The success criteria of the navigation system were if the distance traveled is within +/- 5% of the known separation of the targets (25 cm). Prior to any surveying RTK-GPS accuracy was verified by capturing GPS data and

confirming the rover is producing ‘RTK-fixed’ quality data indicative of cm-level accuracy. Standard pre-deployment functional checks of crawler motors, auxiliary sensors, and topside communication were performed prior to deployment of the crawler.

### **5.4.3 Flex-EM Calibration**

Static, or spike, tests were used to verify consistency in data channel output on a daily basis. Static tests are performed with the Flex-EM stationed in a clean area within the IVS. Spike tests were performed multiple times each day using 2.5-inch diameter steel sphere (aka, the calibration ball). Calibration consisted of placing one of these items on, or directly above, each receiver while collecting data. The proximity of these items to each receiver yields a response in each axis of the receiver (X, Y, Z). Following these data collections, the data were quickly post-processed to determine proper functionality of each receiver and each receiver axis. Any significant deviations in the calibration ball response may be indicative of hardware faults.

## **5.5 DATA COLLECTION**

The data required for creation of the metrics detailed in Section 3 are: (i) RTK-DGPS data from the crawler, (ii) raw inertial navigation sensor data from both the crawler and the tow sled, (iii) raw Flex-EM millivolt count data for each of the for 16 time gates in each of the 18 channels, and (iv) the process tow sled navigation solution including azimuth correction from the tow point encoder. These data types will be time-stamped and logged with the topside data acquisition computer during testing. Unless crawler speed is the variable being tested, the operator was instructed to maintain a speed of approximately 1 knot (~0.5 m/s) resulting in 5 cm sampling of the seafloor by the EM array operating at approximately 10 Hz. Data were stored locally on the topside operator computer.

### **5.5.1 Scale and Sampling**

The actual coverage rate and ground sampling distances varied during our demonstration depending on site area covered (surfzone or sound) and conditions. During the limited surveys we were able to conduct in the surfzone and lower beach/swash zone, we covered the small target grid with individual passes. Due to weather constraints, we were not able to complete full coverage surveys. An example of one our passes over the target area is shown in Figure 68. During this example, we mostly traversed parallel to the shore with an average advance rate of 3.8 line kilometers per hour. At 100% coverage, this would equate to approximately 2.1 hours to cover a hectare or 1.2 acres/hour. The average instantaneous speed was 1.01 m/s, which is faster than the objective of 0.42 m/s. However, a good portion of the time during these tests were spend traversing the lower beach during which time the crawler system was not submersed or only partially submersed. The average ground sampling distance was approximately 10.5 cm, although the mode value was approximately 4.1 cm with a standard deviation over the entire demonstration of 13.5 cm. The largest ground sampling distance was nearly 40 cm. Sampling distances larger than ~20 cm were uncommon and likely occurred due to acute motion of the GPS rover and/or sudden loss of accuracy in the GPS received signal.

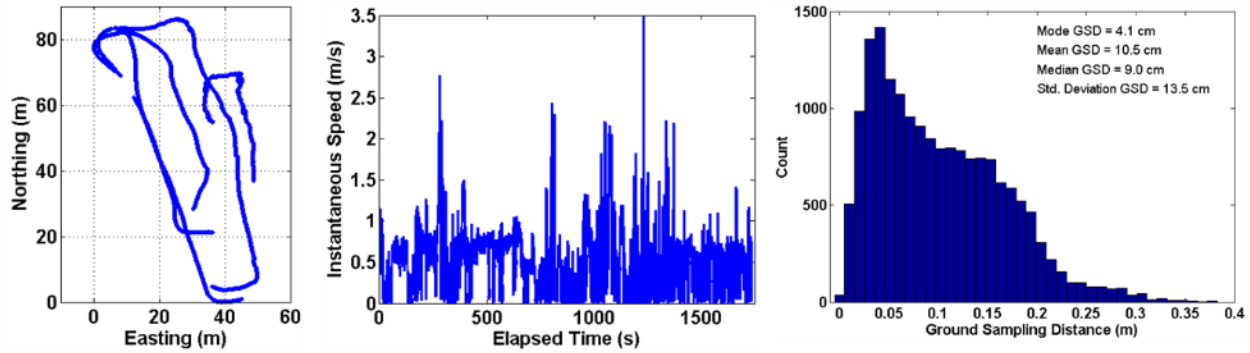


**Figure 68.** Scale and ground sampling metrics from demonstrated survey data collection in the surfzone. Left-to-Right: Overview map of the surfzone transects over which the statistics were calculated; instantaneous speed of the platform computed from GPS time and position; and histogram of the computed ground sampling distance of EMI data coverage.

A similar set of statistics were computed for the coverage and sampling for surveys conducted in the sound. These are shown in Figure 69. During surveys in the sound, we covered approximately 7.3 line kilometers over an area of 12,000 m<sup>2</sup>. The average instantaneous speed of the system was 1.45 m/s. At 100% coverage, this would equate to approximately 1.5 hours to cover a hectare or 1.7 acres/hour. For these surveys the average ground sampling distance was 14.9 cm with a standard deviation of 36 cm.

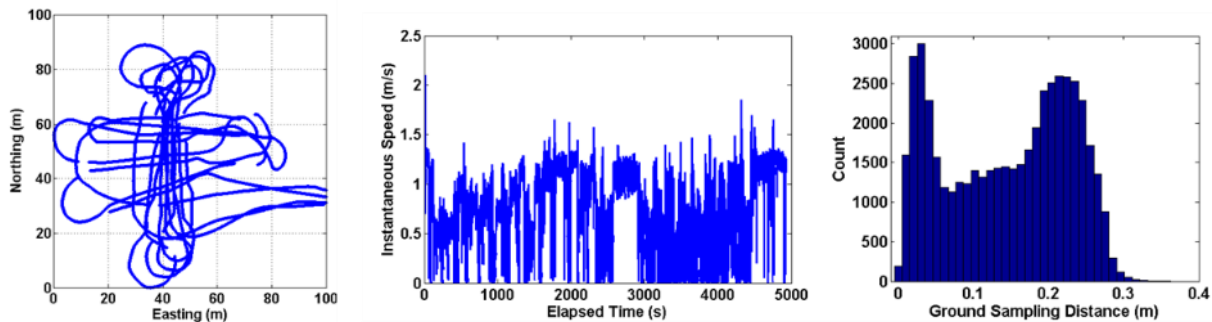


**Figure 69.** Scale and ground sampling metrics from demonstrated survey data collection in the sound. Left-to-Right: Overview map of the sound transects over which the statistics were calculated; instantaneous speed of the platform computed from GPS time and position; and histogram of the computed ground sampling distance of EMI data coverage.

### 5.5.2 Quality Checks

Periodically throughout each data collection day crawler navigation and EM data were processed to assure data quality. Quality control metrics produced include the standard deviation of each EM channel to illuminate noisy data channels. The sample time of each data collection was also reviewed to assure no gaps in sampling. The real-time navigation display flashes indicators if data quality of any sensor is not met including loss of RTK fix quality (e.g., Q=4 for the NMEA convention).

The Flex-EM data logging software displays the raw GPS and EM sensor data in real-time. These data are monitored by the data collector to assure quality. A software indicator also displays GPS position quality. When the GPS position is of the highest quality (RTK-fixed) the software indicator is green. When the GPS position is sub-optimal, i.e. in a non-RTK fixed

quality state, the software indicator will turn orange and then red to alert the operator to a degradation in position quality.

Post-processing of EMPACT data occurred shortly after each data collection to produce detection maps and EM sensor noise metrics. The maps were reviewed to assure proper position and EM sensor integration and data collection using proper line spacing. Noise metrics were reviewed to assure proper EM sensor operation.

### **5.5.3 Data Summary**

All data were backed up to multiple hard drives during the demonstration. Redundant copies reside on a White River Technologies networked attached storage system raid. Data were compiled from the following survey days:

2-4 November 2016: shakedown surveys at Blossom Point and Duck FRF sites

7-10 November 2016: surfzone and sound demonstration surveys

The primary datasets include all raw and processed system navigation and EM data. The raw data files are mixed ASCII and BINARY format. Processed data are saved in binary matlab .MAT files. Auxiliary data from on-board and local site monitoring stations are also compiled with the primary data. These include FRF meteorological and oceanographic data from wind and acoustic doppler measurement stations around FRF as well as base station and geodetic survey control GPS data (HyPack format). On-board auxiliary data included the following:

- single-beam sonar (Echologger) full waveform data files 7-9 November 2016
- self-logging accelerometer data (Hobo) and self-logging conductivity, salinity, and temperature data (Hobo CST) from 7-9 November 2016
- the crawler-EM mission planner Navigation lines as saved on the OCS mission and trackline guidance user interface computer
- on-board acoustic doppler velocimeter data (Vector ADV)

## **6.0 DATA ANALYSIS AND PRODUCTS**

Data analysis was performed using custom preprocessing, detection, and discrimination software developed using the Matlab software environment. Flex-EM data pre-processing, gridding, and detection were also performed using the Geosoft Oasis Montaj UX-Detect software module.

### **6.1 PREPROCESSING**

#### **6.1.1 Navigation and Control Data**

A custom software application imports the raw log files recorded during the test and analyze the data to produce statistics describing the noise and bias of the individual sensors, the vehicle navigation, and the control system performance. RTK-DGPS, GPS heading, and tow point encoder data were synchronously acquired and inserted directly into the archived EM data files. No further preprocessing of the Navigation data is required

### **6.1.2 EM Sensor Data**

The preprocessing of Flex-EM data included median filtering of each data channel to remove intermittent spikes found in the raw data. To remove any temporal drift, the data were sent through a linear piece-wise detrending algorithm to center the noise of the data at an amplitude of zero. Navigation and EM data were correlated in time through interpolation of the EM data with time samples that match the navigation data.

## **6.2 DETECTION**

The Flex-EM post-processing software implements data filtering, position and EMI data merging, and detection routines to provide anomaly locations. A physics-based inversion routine determines accurate target locations as well as classification features corresponding to detected anomalies. Dipole parameters are selected to minimize misfit between dipole model outputs and the Flex-EM data. Classification features based on these dipole-fit parameters are compared to those of known library targets to determine a target or clutter classification. The inversion of Flex-EM data can be performed on-site immediately after surveying an anomaly with very little input from the analyst.

Each time channel of the Z-oriented receiver data is passed through a median filter to remove noise spikes. A 2-D map is created using the sum time decay for the Transmit-Z/Receive-Z data channels. Data are gridded, a 2-D interpolation is applied, and a 2-D spatial filter is applied to spatially smooth the data.

A peak detection algorithm is applied to the generated grid using a threshold based on the data noise floor standard deviation or site-specific TOI detection thresholds. A detection radius is applied to identify the ROI surrounding each peak. The radius size is based on the local gradient associated with the peak and the number of peaks associated with an anomaly (1 peak for Z-data; 2 peaks for X- and Y-data). If ROIs associated with multiple peaks overlap, a combined ROI is generated that encompasses the multiple detections. Finally, across track and along track indices are generated for each alarm in an ROI. These indices correspond to the receiver cube and sounding number associated with each alarm and provide the initial starting parameters for the inversion. Each ROI is saved as a data volume (number of soundings x number of time gates x number of data channels) in .MAT format. Alarm indices and UTM coordinates are saved as part of the data structure as well.

## **6.3 PARAMETER ESTIMATION**

Parameters are estimated using physics-based models to support discrimination of targets from potential clutter items. The primary discrimination method uses a least-squares fit to library polarizabilities. Secondary discrimination methods apply a Gaussian mixture model to the 2-D (size and rate of decay) feature spaces generated from the discrimination parameters.

All features are derived from a least-squares fit to a dipole model. The bases for the discrimination features are the object polarizabilities. Polarizabilities are estimated from a linear least-squares inversion of the dipole forward model:

$$\begin{bmatrix} H'_x & H'_y & H'_z \end{bmatrix} = \frac{1}{4\pi R^3} \begin{bmatrix} m_x & m_y & m_z \end{bmatrix} \begin{bmatrix} \frac{3x^2}{R^2} - 1 & \frac{3xy}{R^2} & \frac{3xz}{R^2} \\ \frac{3xy}{R^2} & \frac{3y^2}{R^2} - 1 & \frac{3yz}{R^2} \\ \frac{3xz}{R^2} & \frac{3yz}{R^2} & \frac{3z^2}{R^2} - 1 \end{bmatrix}$$

where  $m_x$ ,  $m_y$ , and  $m_z$  are the object principal polarizabilities scaled by the transmitter field:

$$\begin{bmatrix} m_x & m_y & m_z \end{bmatrix} = \begin{bmatrix} L_x & L_y & L_z \end{bmatrix} \begin{bmatrix} H'_{Tx} & 0 & 0 \\ 0 & H'_{Ty} & 0 \\ 0 & 0 & H'_{Tz} \end{bmatrix}$$

The primed coordinates denote the target frame of reference where the magnetic field data are transformed using the Euler rotation angles  $\phi$ ,  $\theta$ ,  $\psi$ :

$$\begin{bmatrix} H'_x & H'_y & H'_z \end{bmatrix} = \begin{bmatrix} H_x & H_y & H_z \end{bmatrix} \begin{bmatrix} \cos(\phi)\cos(\theta) & \cos(\phi)\sin(\theta)\sin(\psi) - \sin(\phi)\cos(\psi) & \cos(\phi)\sin(\theta)\cos(\psi) + \sin(\phi)\sin(\psi) \\ \sin(\phi)\cos(\theta) & \sin(\phi)\sin(\theta)\sin(\psi) + \cos(\phi)\cos(\psi) & \sin(\phi)\sin(\theta)\cos(\psi) - \cos(\phi)\sin(\psi) \\ -\sin(\theta) & \cos(\theta)\sin(\psi) & \cos(\theta)\cos(\psi) \end{bmatrix}$$

The rotation angles and the target location ( $x$ ,  $y$ ,  $z$ ) are estimated using a non-linear least squares inversion.

## 6.4 CLASSIFIER TRAINING AND DISCRIMINATION

Historic data collected using the sensor and data collected during preliminary tests performed in-air on at test stand at White River Technologies New Hampshire test facility were used to develop polarizability libraries.

## 6.5 DATA PRODUCTS

Data products consist of calculated metrics as well as figures to illustrate the data used to calculate the metric.

### 6.5.1 Stability and Mobility Data

Metrics emanating from these tests result from the comparison of a true value to a value estimated by the navigation system. These can be represented by plots of time versus the navigation system data and time versus the ground truth data or desired data. For stability (roll, pitch, yaw) data the navigation output will be compared to the desired parameters. For northing and easting data the navigation output was compared to target ground truth of the northings and eastings of the target locations. Figure 70 illustrates an example of these data products.

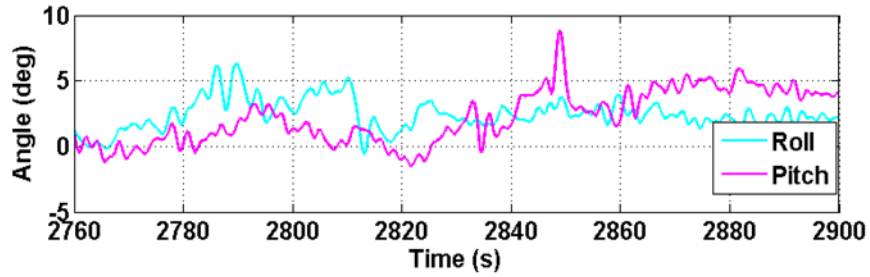


Figure 70. Examples of stability and mobility data products.

### 6.5.2 Detection Accuracy

The estimated detection location (N, E) were compared to the ground truth location of the target interrogated. This resulted in a two-dimensional location error plot (Figure 71) showing the location of the estimate versus the ground truth to reveal error trends and bias. Halos of different sizes are shown to illustrate scale.

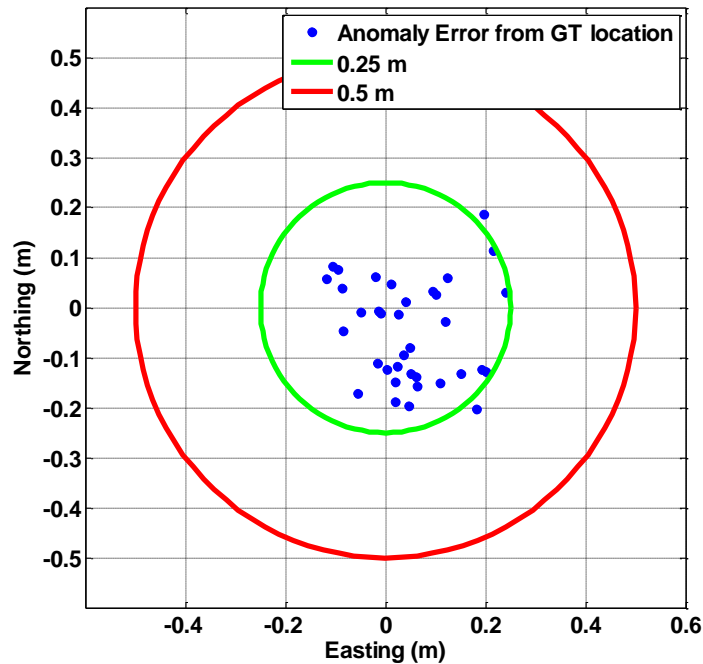


Figure 71. Data product illustrating the detection location accuracy metric.

### 6.5.3 EMI Sensor Data

Data from the Flex-EM was periodically checked including all data channels comprising 18 receivers with  $N$  time gates each. Survey data maps (Figure 72) and channel-based profile plots are used to assess data quality. An example of this is shown in Figure 73.

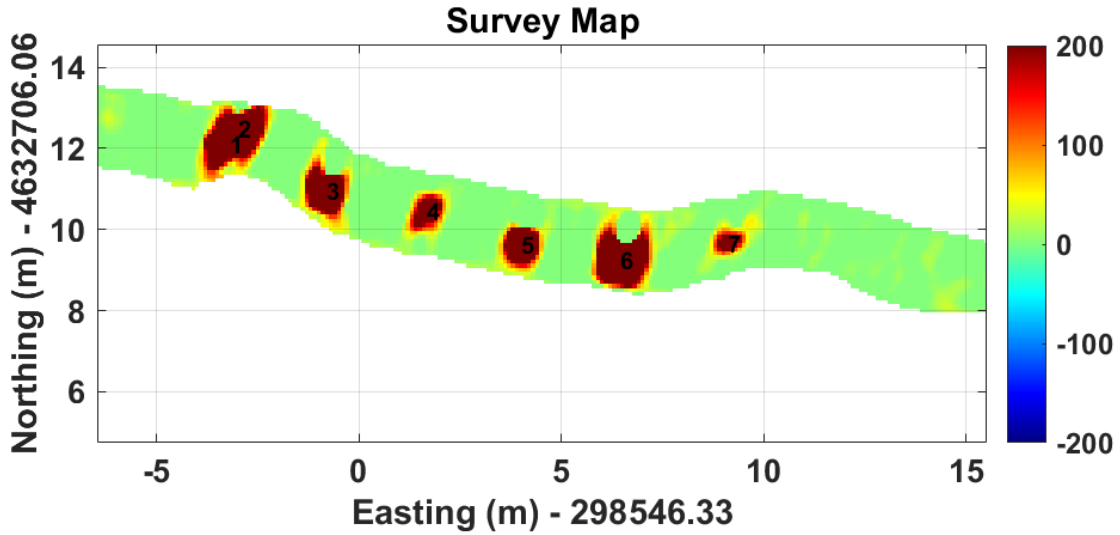


Figure 72. Survey map created using a single pass over six emplaced targets.

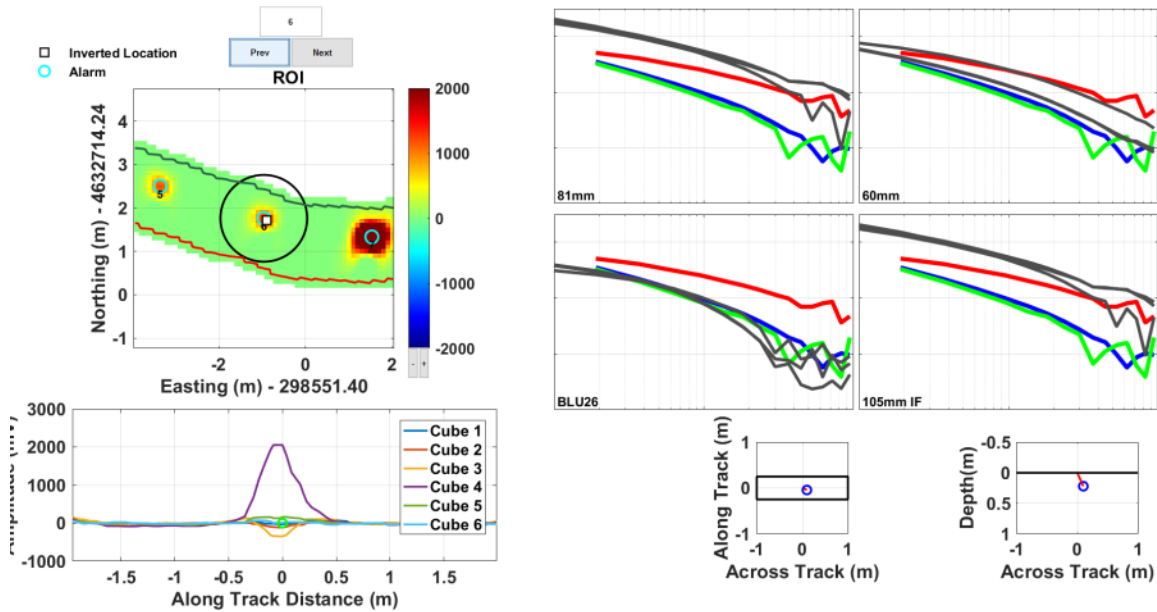


Figure 73. Example data product illustrating the map and inverted polarizability analysis information to be supplied along with the EMI array data quality checks.

## 7.0 PERFORMANCE ASSESSMENT

We assessed performance using the previously defined test objectives and associated metrics shown in Table 5. These include quantitative metrics related to system stability, navigation and control, and detection/localization as well as qualitative metrics such as those associated with operational use. An assessment of each objective is provided in the following sections.

**Table 5. Summary of target objectives, metrics, and results.**

Performance Objective	Target Metric	Result
Surfzone Stability	$\Delta R < \pm 6^\circ$ , $\sigma R < 3^\circ$ $\Delta P < \pm 6^\circ$ , $\sigma P < 3^\circ$ $\Delta Y < \pm 4^\circ$ , $\sigma Y < 2^\circ$ $\Delta X < 0.20$ m , $\sigma X < 0.15$ $\Delta Y < 0.10$ m , $\sigma Y < 0.07$ $\Delta A < 0.10$ m , $\sigma A < 0.15$	$\max(\Delta R) = 8.6^\circ$ , $\sigma R < 3.5^\circ$ $\max(\Delta P) = 9.0^\circ$ , $\sigma P < 3.4^\circ$ $\max(\Delta Y) = 42.1^\circ$ , $\sigma Y < 17.0^\circ$ $\max[\Delta X \text{ or } \Delta Y] = 0.26$ m , $\max[\sigma X \text{ or } \sigma Y] = 0.04$ m $\max(\Delta A) = 0.06$ m , $\sigma A < 0.01$ m
Area Coverage	Shore-Parallel Adv. Rate $> 0.42$ m/s	Average Shore-Parallel Adv. Rate = 1.09 m/s
On-shore / off-shore Mobility	Shore-Perpendicular Adv. Rate $> 0.28$ m/s	Average Shore-Perpendicular Adv. Rate = 0.32 m/s
Detection of all munitions greater than 60 mm	SNR $> 9$ dB Pd $> 0.95$ (assuming a nonfluctuating target and Gaussian noise a 0.95 Pd at 9 dB corresponds to a pFA of approximately 0.01)	All target SNRs $> 20.7$ dB Pd = 1.0
Detection Location Accuracy	$\Delta TN$ and $\Delta TE < 1.0$ m $\sigma TN$ and $\sigma TE < 0.35$ m	$\Delta TN = 0.29$ m, $\Delta TE = 0.22$ m $\sigma TN = 0.42$ m, $\sigma TE = 0.51$ m
Classification of all munitions $\geq 60$ mm	Probability of Classification, Pclass $> 0.75$ with at least 50% of clutter ranked below the UXO	Data not sufficient to assess, but limited multi-angle illumination data yielded promising results
Ease of use	Ease of use compared to alternate standard marine surveying procedures	OCS very effective, but line of sight valuable; more robust tether or wireless tether needed
Launch and recovery	Time to launch, time to recover, mean down time	Launch and recovery very effective; recharging challenges

### 7.1 SYSTEM STABILITY

Typical surfzone transects began on the beach and ran parallel to the water line and then perpendicular into the surf. Once in the surf, the crawler-EM system generally turned parallel to the water line and wave break and transited either up or down the shore for 10's or 100's of meters before turning landward and transiting back to the beach. An example transect is shown in Figure 74. Example map of GPS profile

transect parallel to the wave break in the surfzone. The crawler and towed EM array transited into the surf to approximately 50 cm water depth before turning north along the shoreline for ~80 meters. The location of the approximate water line is shown notionally and was not measured.

with a starting point on the lower beach and an approximately 80 m long shore-parallel transect through the surf zone.

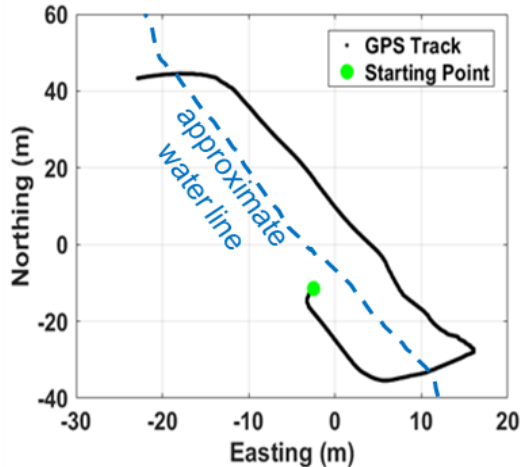


Figure 74. Example map of GPS profile transect parallel to the wave break in the surfzone. The crawler and towed EM array transited into the surf to approximately 50 cm water depth before turning north along the shoreline for ~80 meters. The location of the approximate water line is shown notionally and was not measured.

We calculated EM tow system stability metrics using data collected while the crawler towed the EM array through the surf. The IMU on the tow sled provided roll, pitch, and yaw information and when used in combination with similar IMU data from the crawler, it provides relative angles and translation of the sled during surfzone surveying maneuvers. Stability was determined with respect to relative rotational stability and translational movement of the EM array over the seabed.

Surfzone stability was assessed by analyzing inertial measurement unit and navigation and control observations for traverses of the crawler-EM system between prescribed waypoints. An example of the analysis of roll, pitch, and yaw stability analyses are shown in Figure 75. This example shows the crawler rotational angles (roll, pitch, and yaw) overlain with those from the EM array tow sled. If we use the crawler as a stable reference in the surf, deviations from its rotational angles may indicate instability of the EM array. The objectives are also plotted relative to the instantaneous angle information reported from the IMU on the crawler platform. These are  $\pm 4$  degrees in yaw and  $\pm 6$  degrees in both roll and pitch. It is apparent that the yaw deviations exceeded our objectives for most of the shore-parallel transect, while the roll and pitch deviations are within our objectives.

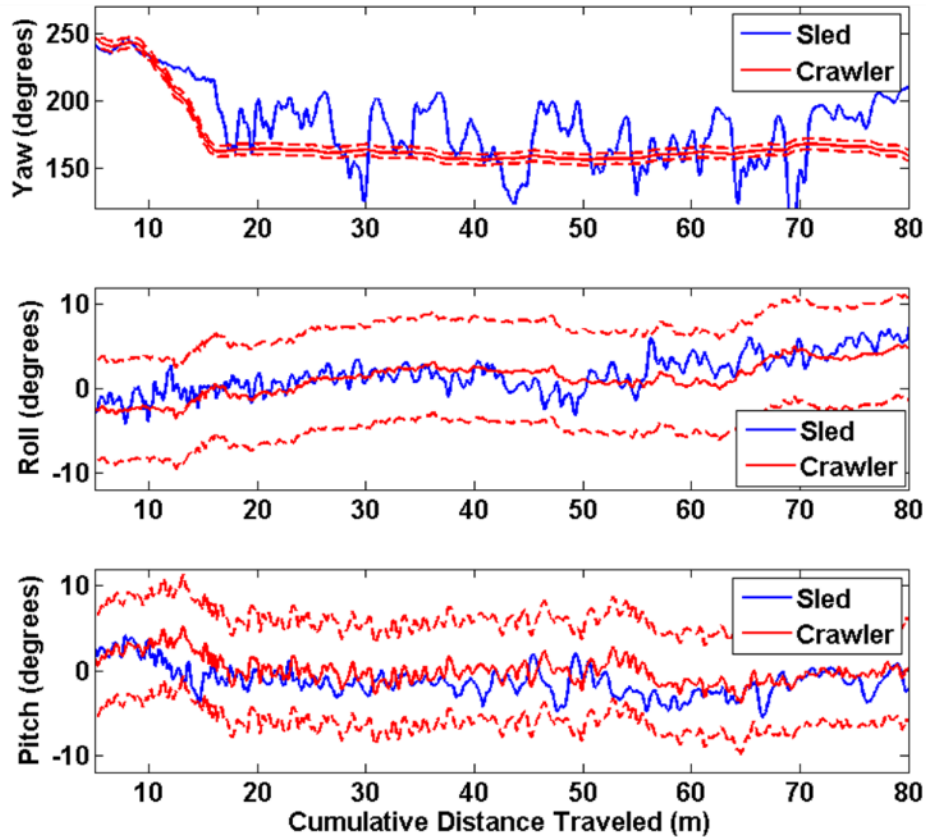


Figure 75. Plots of measured sled yaw (top), roll (middle) and pitch (bottom) are shown in blue. The solid red line is the yaw, roll, and pitch of the crawler. Dashed red lines indicate the performance objectives. Objectives were met for roll and pitch but exceeded in yaw.

By far, the largest instability occurred while the array was oriented parallel to the wave break in moderately deep surf where the ebb and flow of run up wash imparted strong cross currents on the tow platform. This generally manifested as a yaw deviation with the array lifting slightly off the seabed and rotating to a new yaw angle relative to the direction of motion. This heading or yaw deviation is shown in Figure 76 for the shore parallel transect mapped in Figure 74. At approximately 100 seconds, the crawler turned parallel with the wave break and transited north up the shore in the surfzone. Prior to and following this turn maneuver, deviations of the array heading from the crawler's are observed due to swashing of the array to and fro along the direction of the impinging waves and current.

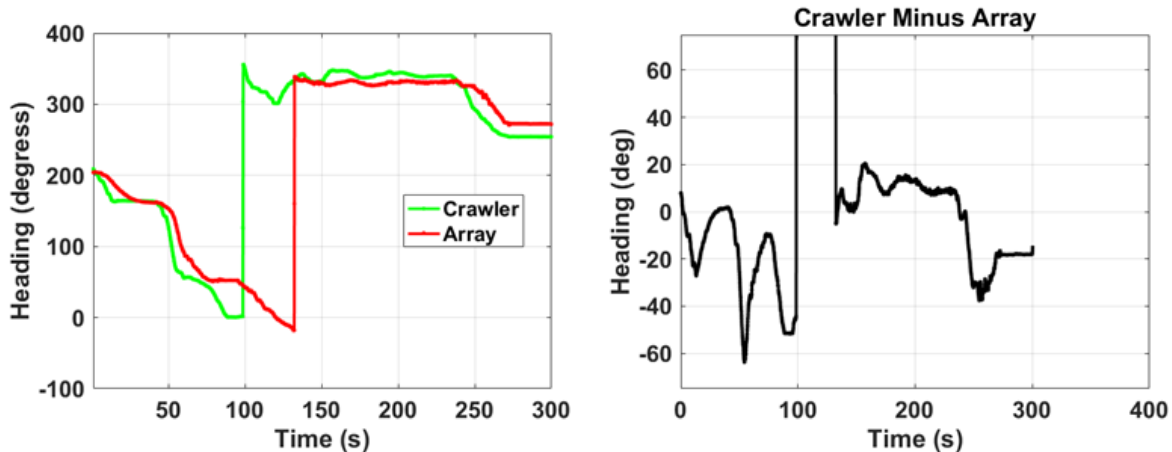


Figure 76. Example of heading deviations between the crawler and the towed EM array during shore-parallel survey maneuvers. Left: Crawler and EM array heading during the transect are shown with a turn from southeast to northwest between 0 and 100 seconds and shore-parallel maneuver from 150 seconds on. Right: Measured deviation between crawler and EM array heading.

During at least one of the surfzone survey transects we attempted to correlate motions on the tow sled to measurements of the local hydrodynamic environment. This was supported by mounting a Nortek Vector triaxial velocimeter to the crawler structural frame. The Vector is a single-point current meter capable of acquiring 3D velocity to depths of 300 m. While we did not fully resolve the vector components relative to the motion of the platform during surveys, we did correlate measurements with corresponding towed array sled motions. Figure 77 shows sled roll, pitch, and yaw measurements as a function of both cumulative distance traveled and as a function of time. This particular survey transect consisted of a shore-normal entrance to the swash and surfzone, followed by a shore-parallel transect and shore-normal return to the beach. The crawler transitioned from the beach to the water at approximately 140 minutes (after 17:00 UTC). The Vector velocimeter instrument was not submerged until 30-40 seconds later (~140.6 minutes) as indicated by the observed water velocity and pressure profiles. Wave and current events in the surfzone are evident from impulse-like velocity profiles and corresponding pressure spikes. The timing of these events is consistent with acoustic doppler (ADOP) measurements acquired from the USACE FRF 3.5 meter buoy array. ADOP data over our survey period at approximately 17:00, 18:00, and 19:00 hours UTC indicated wave heights of 1.96, 1.93, and 1.91 meters, and wave periods of 7.7, 6.5, and 8.7 seconds, respectively.

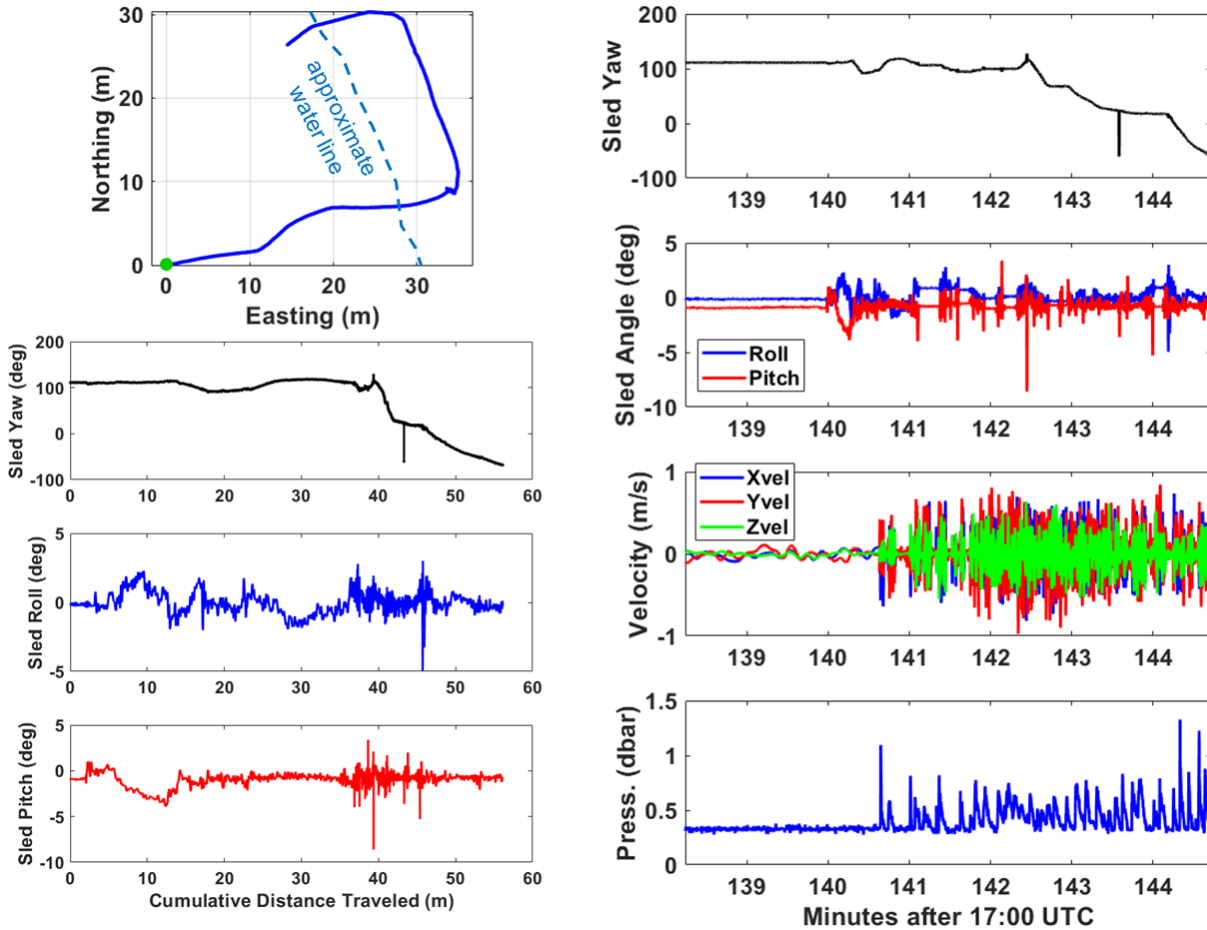


Figure 77. Example survey transect roll, pitch, and yaw stability measurements during surfzone demonstrations on 11/7/2016.

To estimate the overall stability metrics, we compiled all surfzone transects from the afternoon of 7 November 2016. This included nearly 2 km of transects. A map of the transects along with roll and pitch deviation histograms are shown in Figure 78. The maximum roll deviation over these transects was  $8.6^\circ$  while the standard deviation of the roll was  $3.5^\circ$ . For average pitch deviation over these transects we computed a maximum pitch deviation of  $9.0^\circ$  with standard deviation of  $3.4^\circ$ . Figure 79.

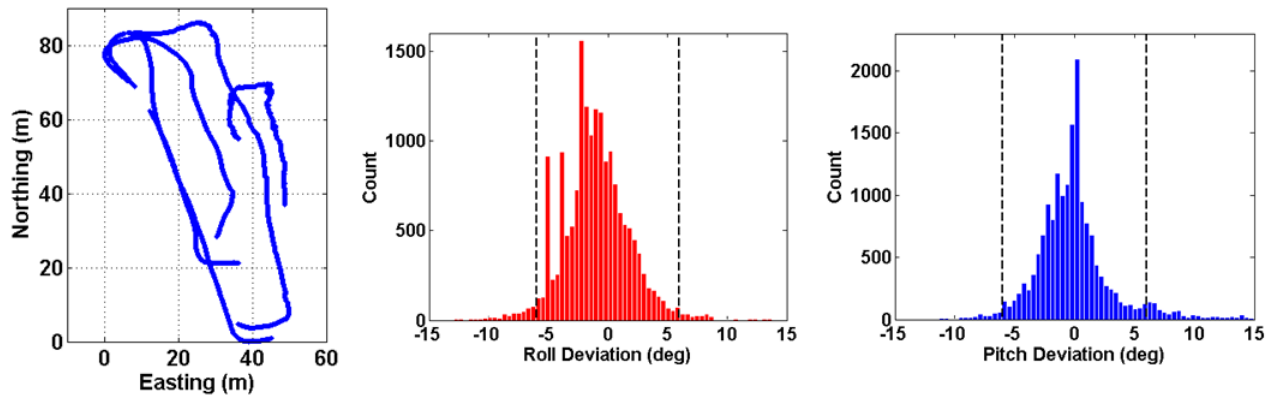


Figure 78. Compilation of ~2 line km of transects conducted in or around the surfzone on 11/7/2016. The western-most transect extending from northwest to southeast was performed in the shallow swash zone and the eastern-most transect extending from northwest to southeast was performed just landward of the wave break area. Compiled statistics for angular stability in terms of roll and pitch are exemplified in the histograms along with the  $\pm 6$  degrees objectives.

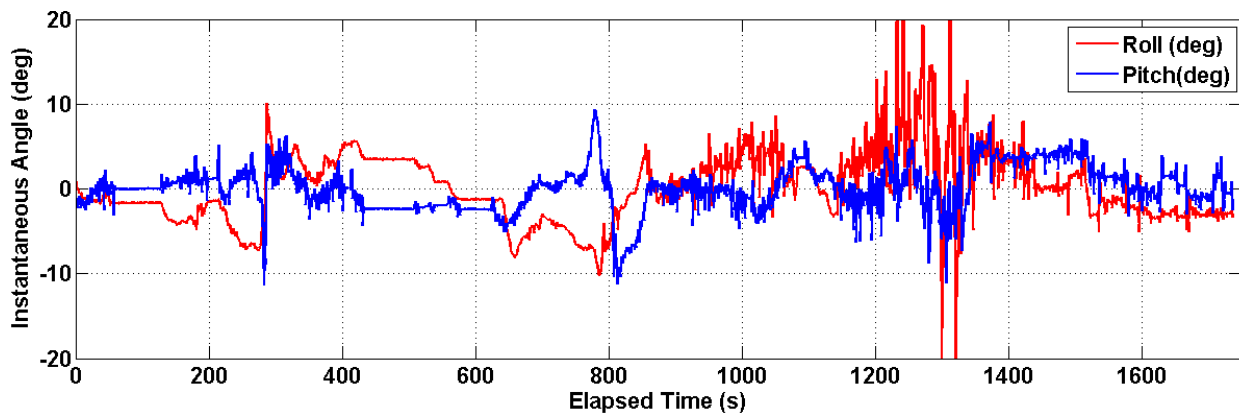
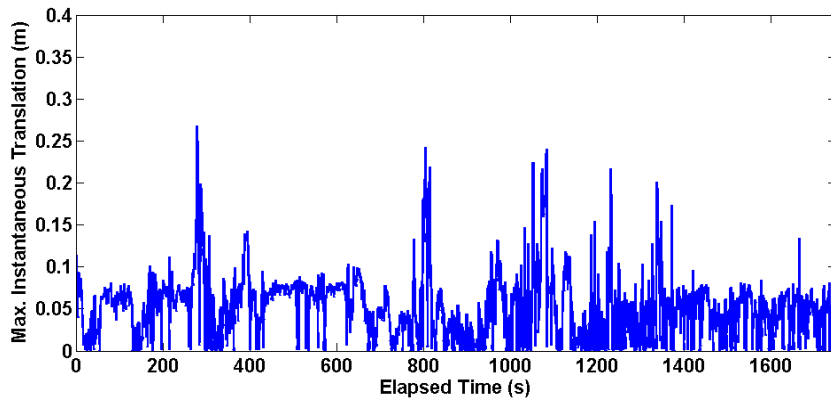


Figure 79. Roll and pitch deviations over the surfzone surveying transects. A variety of crawler system maneuvers and events are represented: from extended durations of the static surveying (400-600 seconds) to rapid maneuvers in high energy surf areas (1200-1400 seconds).

Translational deviations were also computed by examining the instantaneous longitudinal and transverse (i.e., athwartship) deviations. The maximum translational deviations are shown in Figure 80.



**Figure 80.** Maximum instantaneous translational motion measured from GPS and IMU data on the EM array sled. These data include motions associated with normal "straight & level" survey transiting, so a 0.1 m forward translation bias was subtracted from the overall motions to reflect the translational motion deviation.

We contrast the analysis of stability in the surfzone to that in the sound. To assess roll, pitch, and yaw dynamics of the towed array sled relative to that of the crawler, we examine one of the transects from the sound surveys. We selected a nominal east-west transect across the target grid area. This transect is shown in Figure 81 and begins from the east trending to the northwest and then turning slightly toward the southwest about halfway along its traverse.

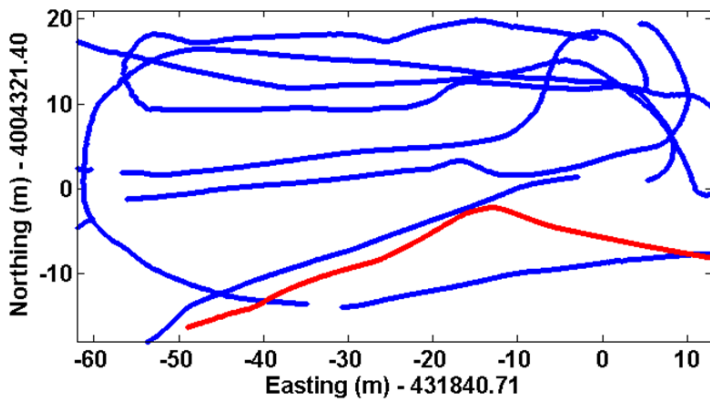


**Figure 81.** Map of the selected GPS profile transect (red) across the Currituck Sound target area transects (blue) used for analysis of array sled stability.

Rotational angles measured during this transect for both the crawler and towed array sled are shown in Figure 82.

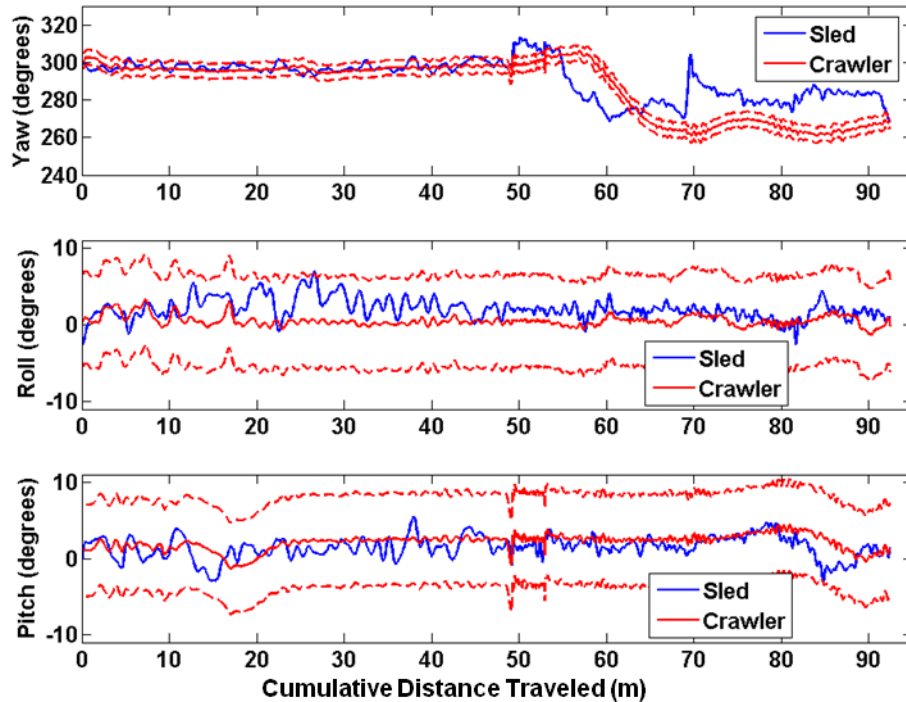


Figure 82. Rotational angle variation of the system during survey operations in the sound. Plots of measured sled yaw (top), roll (middle) and pitch (bottom) are shown in blue. The solid red line is the yaw, roll, and pitch of the crawler. Dashed red lines indicate the performance objectives. Objectives were met for roll and pitch but exceeded in yaw.

Similar to the analysis of the overall stability metrics in the surfzone shown in Figure 83, we estimated the compiled roll and pitch statistics for a group of transects over the target area in the sound. This included over 3 km of data from transects surveyed on 9 November 2016 as shown in Figure 84. We computed the roll and pitch deviations of the towed array sled during. The maximum roll deviation was  $1.18^\circ$  with  $2\sigma$  (i.e., 95<sup>th</sup> percentile) within  $0.159^\circ$  and the maximum pitch deviation was  $0.85^\circ$  with a  $2\sigma = 0.17^\circ$ . These were well within the performance objective limits of  $\pm 6$  degrees. As anticipated, the calmer conditions in the sound produced much more stable operation with respect to roll and pitch of the sled.

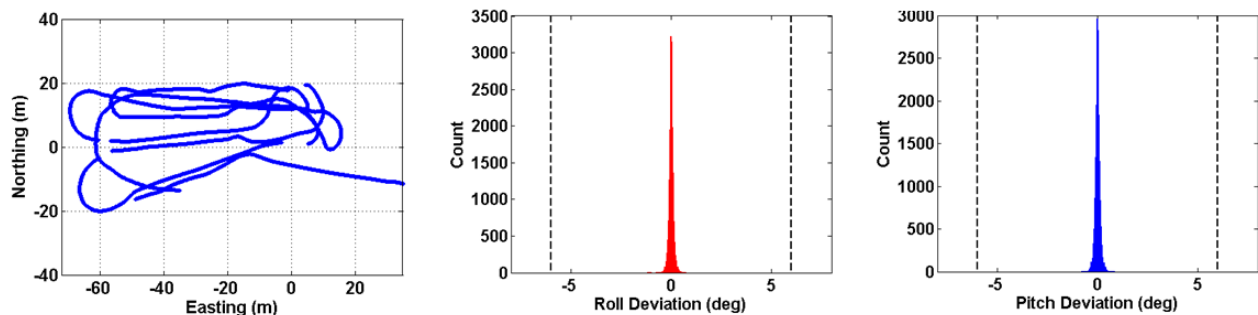


Figure 83. Compilation of ~3 line km of transects surveyed in the Currituck sound directly adjacent to the FRF site on 11/9/2016. Water depths extended from 1.4 to 2.6 meters in this area. Compiled statistics for angular stability in terms of roll and pitch are exemplified in the histograms along with the  $\pm 6$  degrees objectives. Both roll and pitch deviations were very small (within 1.5 degrees). Yaw stability was also much better than that exhibited in the surfzone, although multiple turns led to offsets between crawler and tow sled yaw (i.e., crabbing).

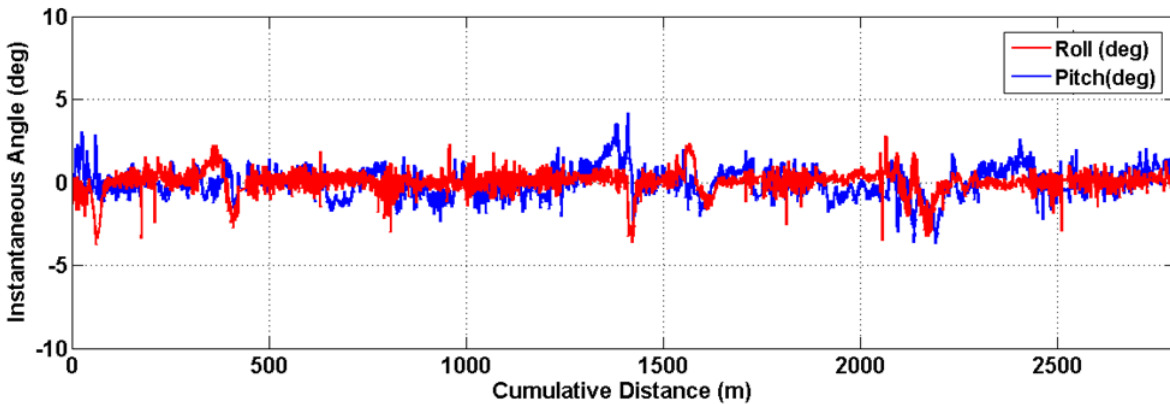


Figure 84. Roll and pitch deviations over the sound surveying transects. Multiple turns and maneuvers were conducted while the roll and pitch remained relatively stable.

## 7.2 AREA COVERAGE RATE

Area coverage was primarily gauged by assessing shore-parallel advance rates for surveys in both the surfzone site and the intertidal sound site. In the surfzone, the distance between EM data samples was approximately 4-5 cm with an overall mean value of 10.5 cm (see Section 5.5.1). At 100% coverage rate using the 2-meter wide array, we achieved an average advance rate of 3.8 line km per hour, which equates to approximately 1.2 acres/hour.

To assess area coverage and on-shore/off-shore stability we parsed the surfzone transects into portions associated with shore-parallel traverses and portions associated with shore-perpendicular transits. Figure 85 shows a map view of the apportioned transects from which we computed shore-parallel and shore-perpendicular advance rates.

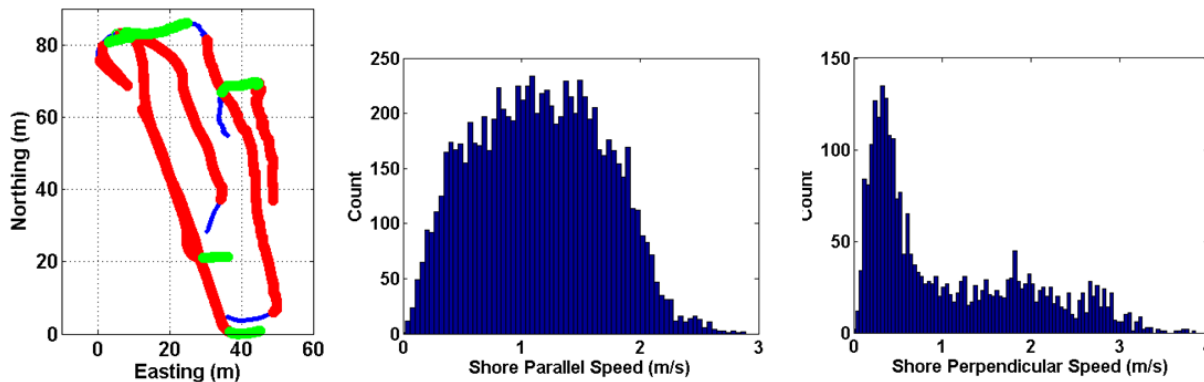


Figure 85. Compilation of offshore and onshore transects used for computing coverage metrics. Left: transects divided into shore parallel (red) and shore-normal (green) transects. Histograms of averaged advance rate for both directions of transects are shown in the middle and right. Shore perpendicular speeds were noticeable slower and had a wider variation compared to shore parallel speeds.

To assess coverage rate for sound surveys, we examined a subset of the total survey tracklines represented in Figures 81. For these surveys, we covered approximately 3 line kilometers over an area of 6,000 m<sup>2</sup> in 27.4 minutes of continuous running time that was spread over a 94 minute period. The average instantaneous speed of the system was 1.85 m/s (mode=0.45 m/s,

median=2.0 m/s). The speed histogram reveals a discernable bimodal distribution with some slower advances of around 0.35 m/s during start/stop and turn maneuvers, but mostly straight-and-level survey transects at speeds of approximately 1.9 m/s. Using the continuous running time, this would equate to approximately 3.25 acres/hour. If we factor in the down time during operation and use the total elapsed time, we estimate 0.94 acres/hour coverage rate. Alternatively, if we use the average instantaneous advance rate of 1.85 m/s (or equivalent instantaneous coverage rate or 3.7 m<sup>2</sup>/s), we estimate approximately 3.23 acres/hour. Considering a more realistic 50/50 split between straight survey operations at 1.5-2.0 m/s (averaging ~1.75 m/s) and slow or fully stopped operations during turns and maneuvers (0-0.5 m/s; average 0.25 m/s) yields a projected estimate of 1.78 acres/hour.

### **7.3 ON- AND OFF-SHORE MOBILITY**

The mobility of the integrated system perpendicular to shore was shown in Figure 82. Due to challenging surf weather we had limited opportunities to conduct survey traverses perpendicular to the shore into the surfzone. Because our primary metric was an assessment of the average forward velocity of the system perpendicular to the shore to submergence of 2 meters of water, we were not able to rigorously test this objective. We were able to average 4 partial perpendicular traverses extending from on-shore to off-shore to compute an average velocity of 0.32 m/s, which exceeded our objective of 0.28 m/s (or 1 mph or 0.54 knots).

### **7.4 DETECTION**

Detection metrics were calculated using the SNR and location of detections output from the detection processing and ground truth information. The target detection objective was target SNR greater than 9 dB for all targets greater than 60 mm in size. We achieved the objective with SNR greater than 20.7 dB for all targets including data from sensor altitudes between 20 cm and 60 cm. The largest detection SNR value was 84 dB for the large ISO and the smallest was 20.7 dB for the 60mm mortar.

A map of the Z-oriented integrated time decay data for the array are shown in Figure 86. This survey consisted primarily of shore-parallel passes over the target grid and return passes over the IVS on the beach. Only 9 of the 16 targets were traversed as the deepest set of targets were in water deemed too challenging for safe operations during our demonstration (see Figure 86, which illustrates surf weather conditions). Target signatures tend to be weaker for targets in deeper water. We believe (but were not able to confirm) that the rough surf produced conditions that accelerated scour and burial of the deepest row of targets over the duration of our surveys and thus modified their original burial depths. It is suspected that the installed target depths of 25 cm beneath the seafloor may have been extended up to 45-55 cm from overwash, scour, and burial. We did not see any evidence of mobility of the targets during our experiments.

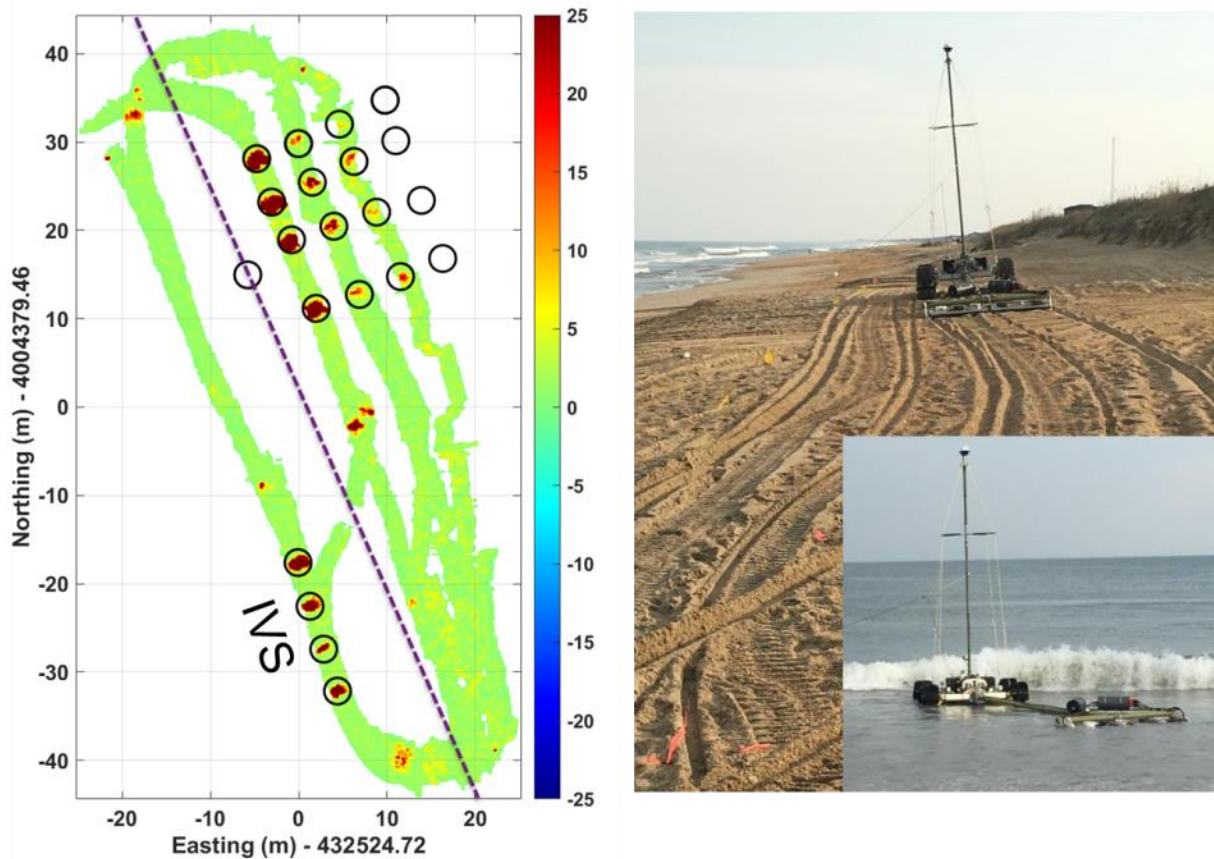


**Figure 86. Example EM data map from Z-oriented receiver data along the shoreline and during shore-parallel surveys in the surfzone. Photographs of the system on the beach and in the surf during EM surveying.**

Detections were scored as TOI detections if the detection location was within a radius of 1.5 m of the TOI ground truth location. Five non-TOI alarms were generated at SNR values greater than 9 dB; three were from emplaced clutter targets and 2 were from natural clutter (assumed but not confirmed) within the survey area.

Figure 87 shows the SNR and offset from the estimated target location to the ground truth location for all of the TOI. All IVS passes yielded SNR values that exceeded 24 dB. For target detections in the surfzone, we found a greater variability and generally lower SNR values. Challenges with lateral control and limited time surveying over the targets prevented us from getting full coverage over the targets as originally intended. This was a primarily a function of the challenging surfzone weather during our demonstration timeframe.

While the map data show that the multiple passes are properly aligned, stable positioning of the sled during passes was a challenge in some cases. This is exemplified in Figure 88, where shifts in the sled lateral position are evident. As surfzone turbulence and forces associated with the flooding and regression of runup increased deeper in the surfzone, the sensor array sled tended to slide across the seafloor along with the current. This resulted in the observed lateral shifts of the sled in the EM map data.

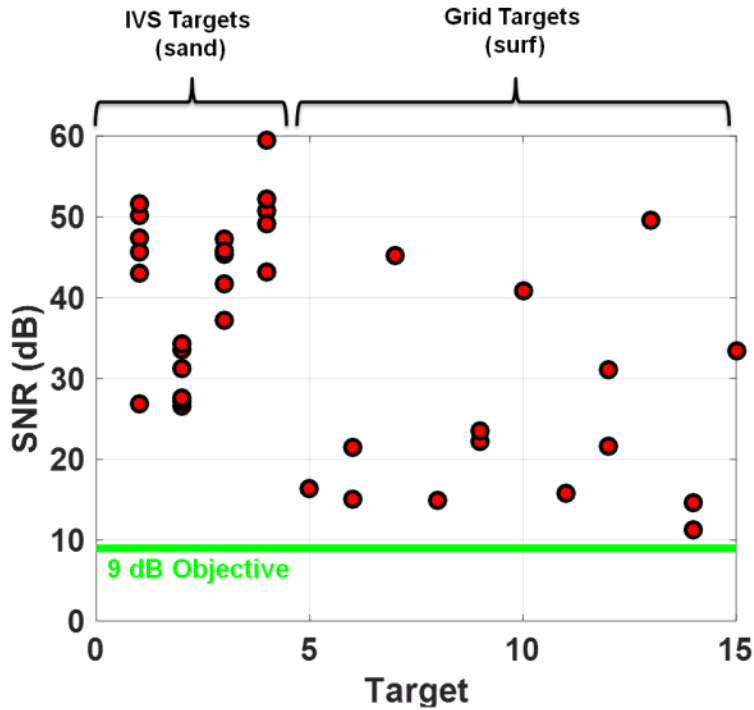


Figure 87. Detection performance results. The signal-to-noise ratio (SNR) is plotted against target index showing that all detections exceeded the 9 dB SNR objective. Targets in the surf yielded lower SNR values as might be expected. We attribute this to the the targets extending deeper below the seafloor than originally planned due to wave induced scour. In addition, lack of horizontal control prevented multiple passes for full coverage surveying.

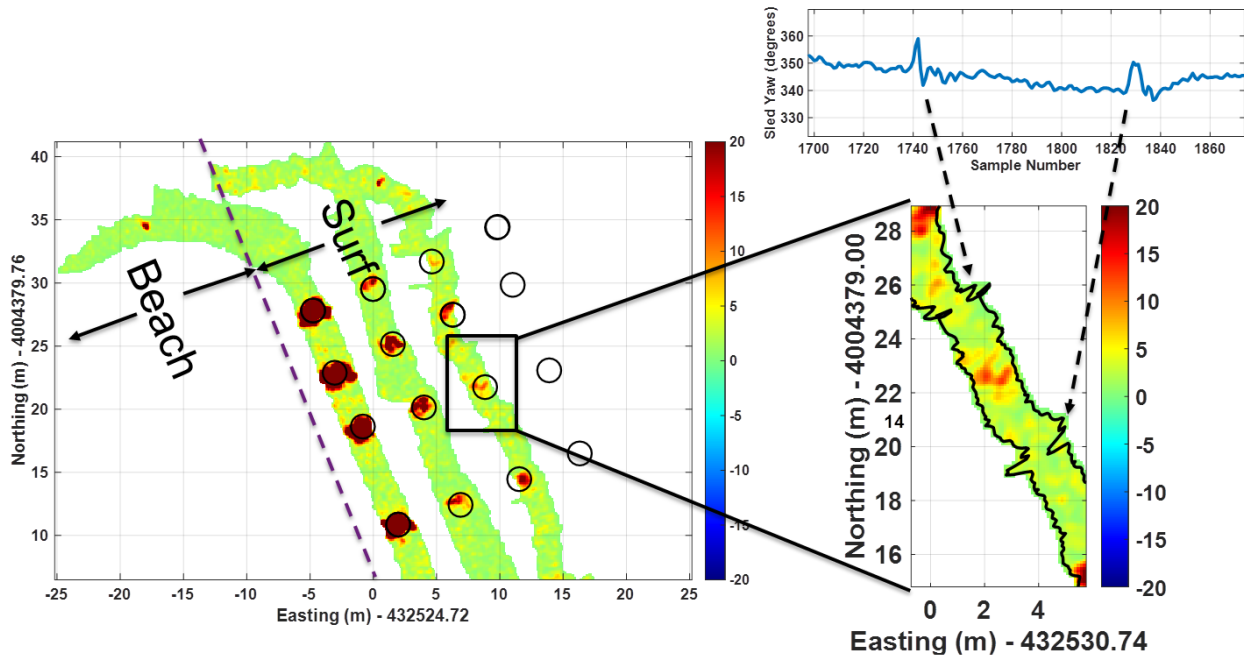


Figure 88. Left: Zoom-in of coverage map over emplaced surfzone targets. Right: Zoom-in showing calculated EM array location while surveying in the surfzone. Fast changes in the sled yaw were due to sudden lateral movements due to breaking waves and swash.

Currents were greatly reduced during surveys conducted in the sound. This enabled efficient surveying with more uniform and complete coverage over the target area. A map of the Z-oriented receiver channel data is shown in Figure 89. The magenta "X" symbols show the locations of emplaced targets. The easternmost "X" symbols are the locations of rebar rods

installed in the seafloor to anchor tie lines extending out between the targets and are indicators of obstacles and not targets to be scored as part of our assessment. The basic configuration of the target layout was oriented exactly the same as those installed in the surf. The same targets were used.

In addition to the anomalies produced by the emplaced targets a number of other anomalies are observed in the map data. For instance, a linear feature extending from the center of the map to the northwest is apparent. Many other large anomalies are also observed. Although, they were not confirmed, these anomalies are considered clutter items.

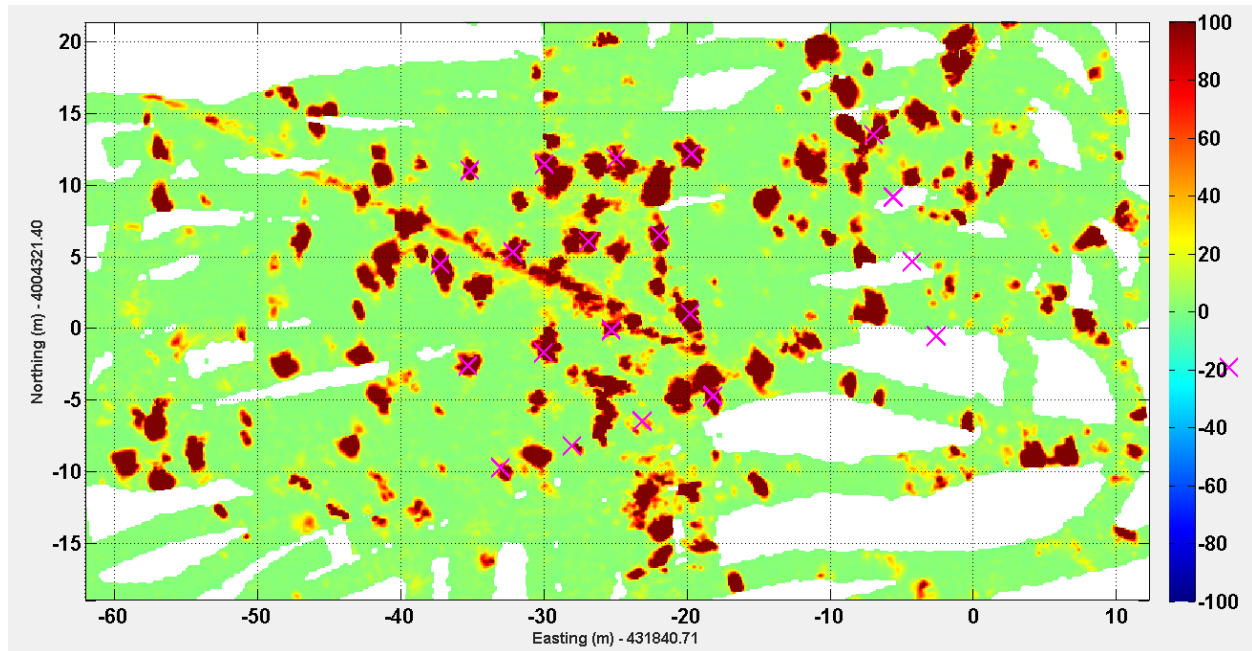


Figure 89. Coverage map over the Currituck Sound. Mapped data are integrated vertical axis array responses only. Emplaced target locations are shown by the magenta Xs. The survey reveals large amounts of clutter in the sound. The four target location furthest to the east were associated with long pieces of metal rebar inserted vertically into the seabed. These were generally avoided by system and should not be considered targets of interest, but instead mark known emplaced metal items in our test area. See Figure 92 for a zoomed-in map of the emplaced UXO target grid.

Overlapping passes produced nearly complete coverage over the grid area. All targets emplaced in the sound were detected with >20 dB SNR. Figure 90.

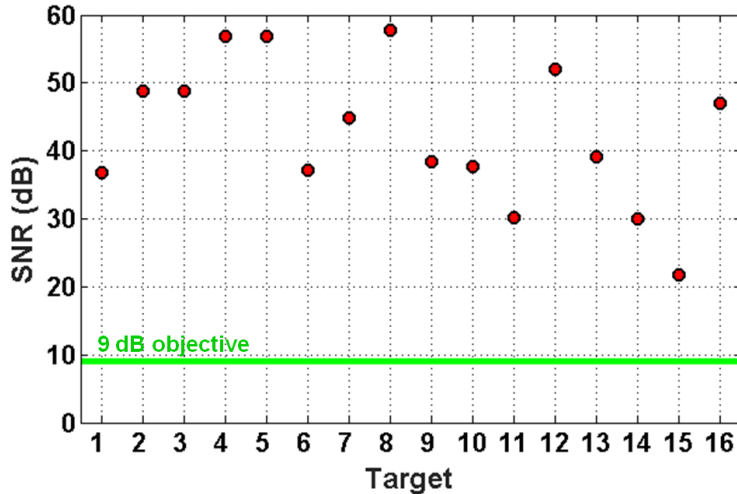


Figure 90. Detection performance results for the sound target grid surveys based on the signal-to-noise ratio (SNR). All target SNR values exceeded the 9 dB SNR objective.

### 7.5 LOCALIZATION ACCURACY

Detected anomalies from the surfzone surveys were used to estimate target locations. The estimated detection locations were compared with those from GPS-based surveying of groundtruth locations.

Overall, the performance objective of mean and standard deviation of emplaced target locations (Easting and Northing estimates) less than 100 cm was achieved. The detection location errors for both IVS (beach) and surfzone grid targets are show in Figure 91. The "bullseye" plot shows no particular statistical offset bias to the location errors. The maximum RMS average error in either northing or easting was 29 cm with a maximum standard deviation of 51 cm. The maximum standard deviation exceeded our objective of 35 cm. Retrospective analysis revealed that heading errors from the tow point encoder were likely the largest factor affecting the overall localization accuracy.

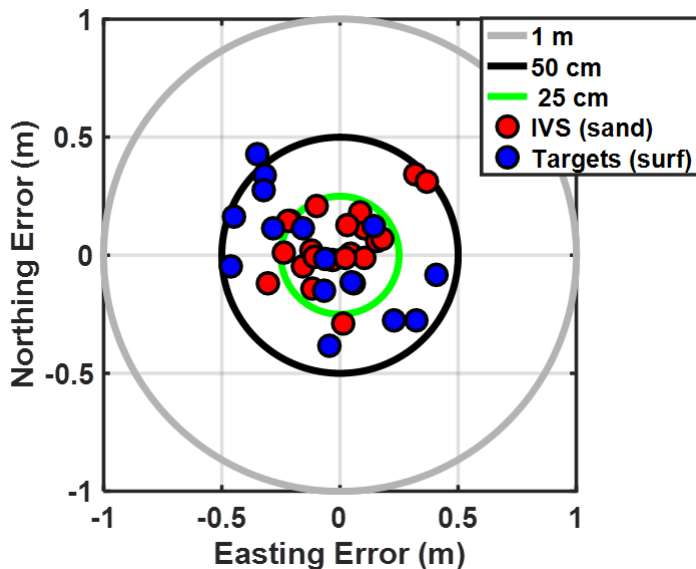


Figure 91. Detection location errors for IVS (red circles) and emplaced surfzone grid targets (blue circles) location estimates.

The emplaced target detection localization accuracy for the sound surveys was not as accurate as those in the surf. A map of the detection and plot of localization errors are shown in Figure 92. The "bullseye" plot shows no particular statistical offset bias to the location errors. The maximum error in either northing or easting was 58.1 cm with a maximum standard deviation of 26 cm. The maximum standard deviation was within our objective of 35 cm. Retrospective analysis revealed that heading errors from the tow point encoder were likely the largest factor affecting the overall localization accuracy. In addition, the presence of non-emplaced (native) magnetic anomalies throughout the surveyed area complicated analyses involving ground truth locations, i.e., in certain local areas with multiple magnetic anomalies present it was difficult to determine which anomaly corresponded to the emplaced (ground truth) item.

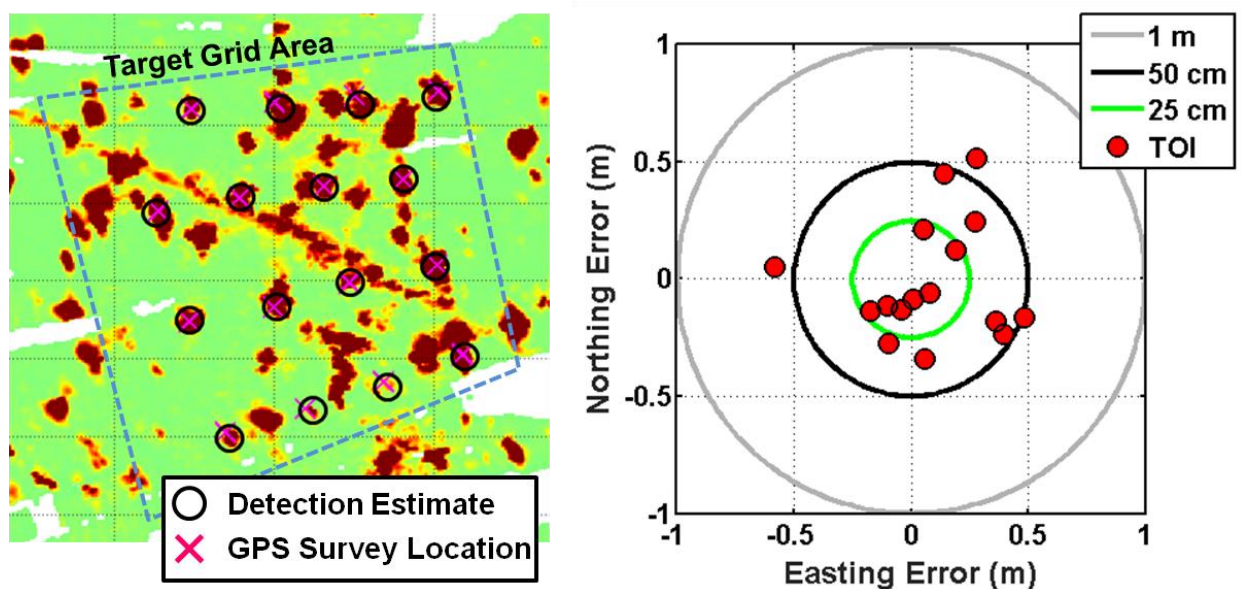


Figure 92. EM anomaly map with GPS groundtruth survey locations and estimated detection locations overlain. Numerous clutter items, densely cluttered areas, and a linear anomaly are evident in addition to the 16 emplaced UXO simulant and ISO targets. Detection location errors for IVS (red circles) and emplaced sound grid targets (blue circles) location estimates. All targets were localized to within 1m of the groundtruth locations and all but two were within 50 cm.

## 7.6 UXO CLASSIFICATION

For effective discrimination, the post-processing software must create polarizabilities that produce repeatable features for UXO targets and clutter. Because the FlexEM towed array sensor has only one transmitter coil, we aggregate the data from consecutive soundings along the transect line (i.e., line methodology) to ensure the target receives the required multi-axis illumination from the transmitter. As the transmitter passes over the target, any offset of the sensor from directly over the target produces a different angle of incidence between the impinging transmitter field and the target. For optimal classification results, we have found that it is best to include soundings from adjacent transect lines in the composite data set to ensure complete three-axis characterization of the target. Greater overlap in adjacent transects yields higher quality classification; however, we have shown that it is possible in certain cases to achieve effective clutter rejection (classification) without overlap in sensor coverage.

Our surfzone survey coverage was not sufficient to produce comprehensive high-quality classification data for all targets. Where overlapping surveys or some degree of angular transmitter offset occurred relative to a target, polarizability inversions generated classification-quality results. An example of this shown in Figure 93. Although we only aggregate data over a single pass over the target, the inverted polarizabilities match very closely (96.4% match) to the library produced for the groundtruth target indicated: a 60 mm mortar. The position estimate also matched very closely with indicated by the groundtruth information including the estimated 25 cm burial depth. This shown in the lower right portion of the analyst graphical user interface.

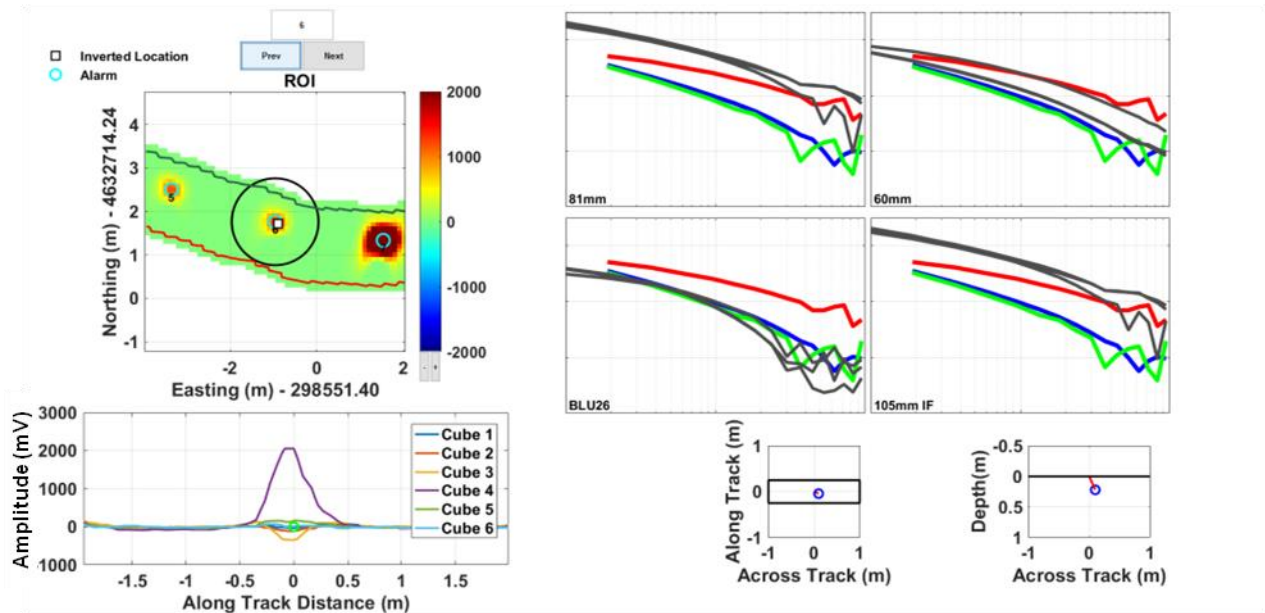


Figure 93. Example of the classification analysis user interface for the FlexEM crawler system. The map view region-of-interest (ROI) is shown in the upper left with threshold alarm and inverted location markers overlain on the Z-axis data image. Bottom left shows the raw EM data profile over the ROI. The upper right panels show a basic set of four polarizability time evolution libraries (gray curves) with the current set of inverted triaxial polarizabilities overlain (red, green, and blue curves). The bottom right panels show map view and cross-section views of the inverted target (here a 60 mm mortar) location relative to the array center.

Two additional classification examples are shown in Figure 94 and Figure 95. Here we show strong library matches to the medium ISO target and 105mm projectile target. For the 105mm projectile, we observe that the primary and secondary polarizabilities match well, although the tertiary polarizability exhibits a noisy evolution with time.

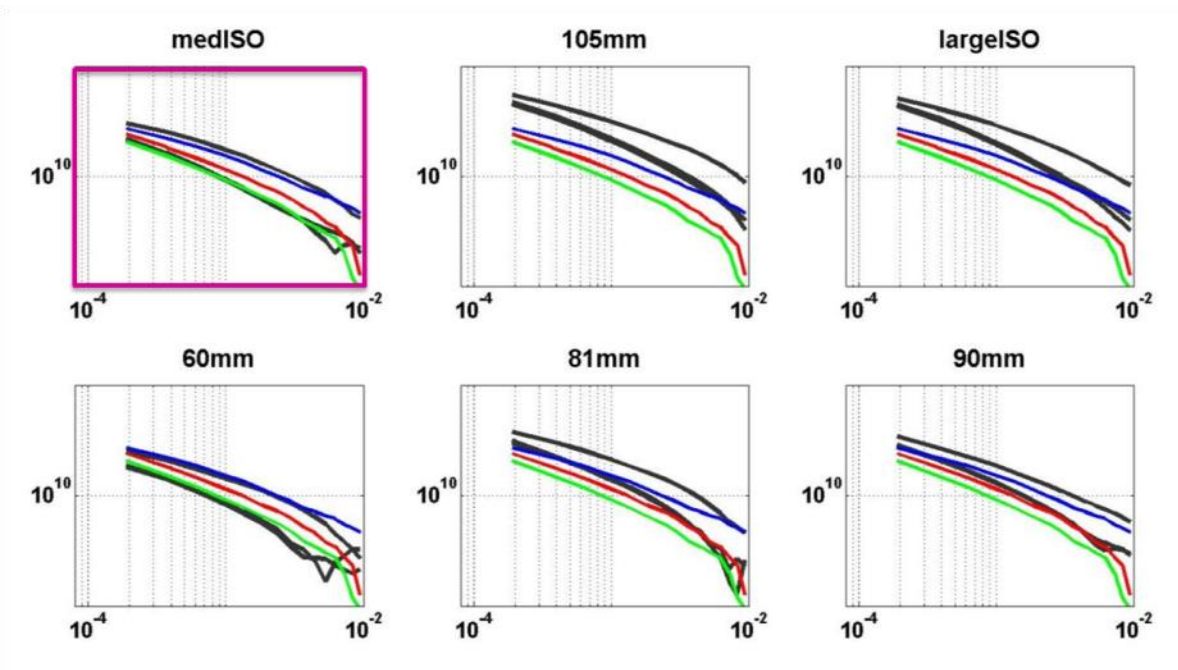


Figure 94. Polarizability library match for a medium ISO target from surfzone grid coverage data.

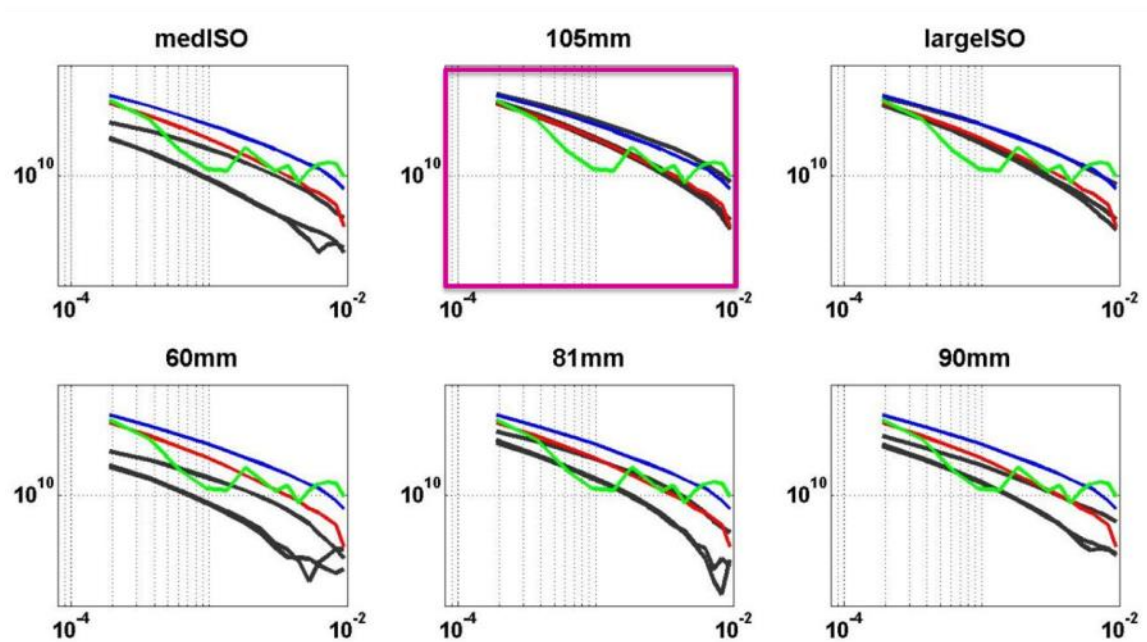


Figure 95. Polarizability library match for a 105 mm projectile based on target grid coverage data in the surfzone.

Although coverage over the sound survey area was significantly higher than that achieved in the surf zone, the density of clutter (see Figure 92) prohibited comprehensive assessment of the inverted polarizabilities for classification. Despite the clutter density, there were a number of polarizability match examples. For example, Figure 96 shows a good polarizability library match for an emplaced 60mm mortar and Figure 97 shows a similar match for an 81mm mortar.

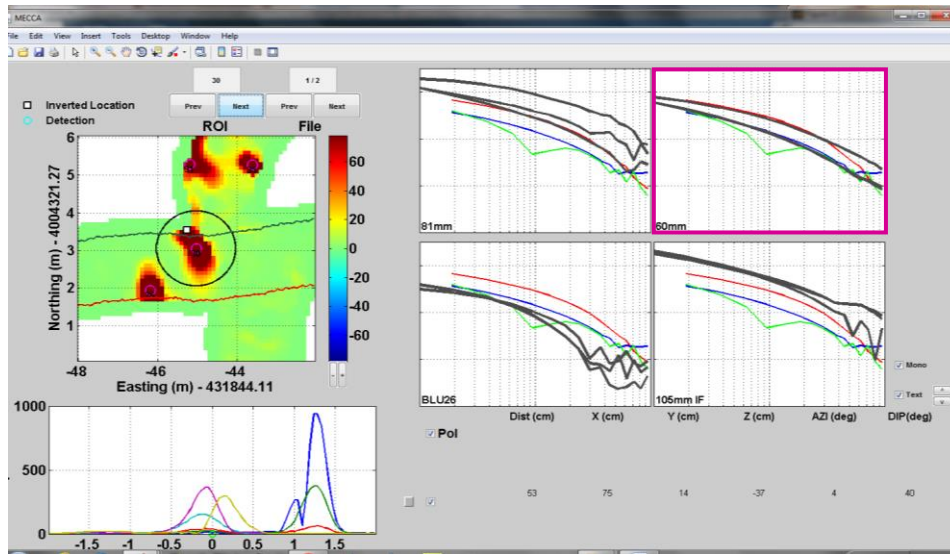


Figure 96. Polarizability library match for a 60 mm mortar based on target grid coverage data in the sound. The target was estimated to be 37cm below the array based on the inversion.

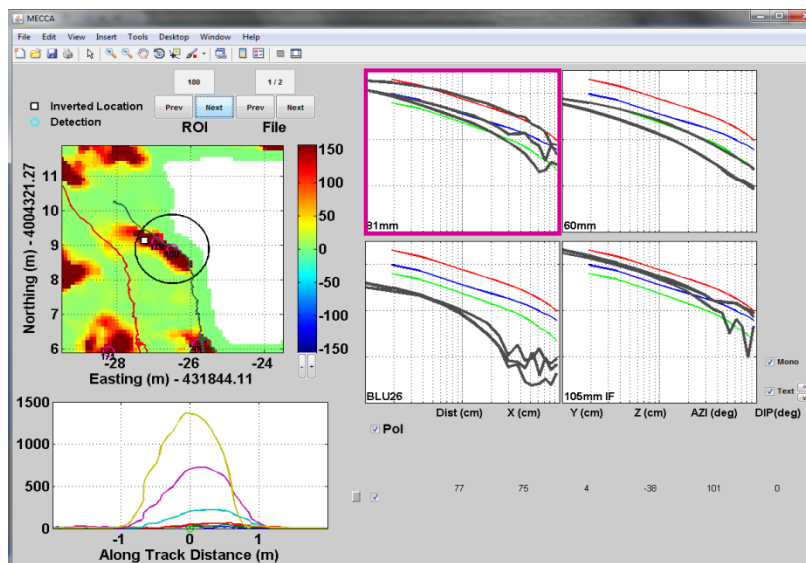


Figure 97. Polarizability library match for a 81 mm mortar based on target grid coverage data in the sound. The target was estimated to be 38cm below the array based on the inversion.

We analyzed a total of 300 anomalies in the sound based on inverted polarizabilities. In addition to emplaced targets, we assessed sound anomaly polarizabilities and noticed some potential groupings based on similar polarizability curve characteristics (i.e., features). We specifically investigated features related to size, shape, symmetry, and aspect. A feature scatter plot showing one realization of the size and shape feature space is shown in Figure 98.

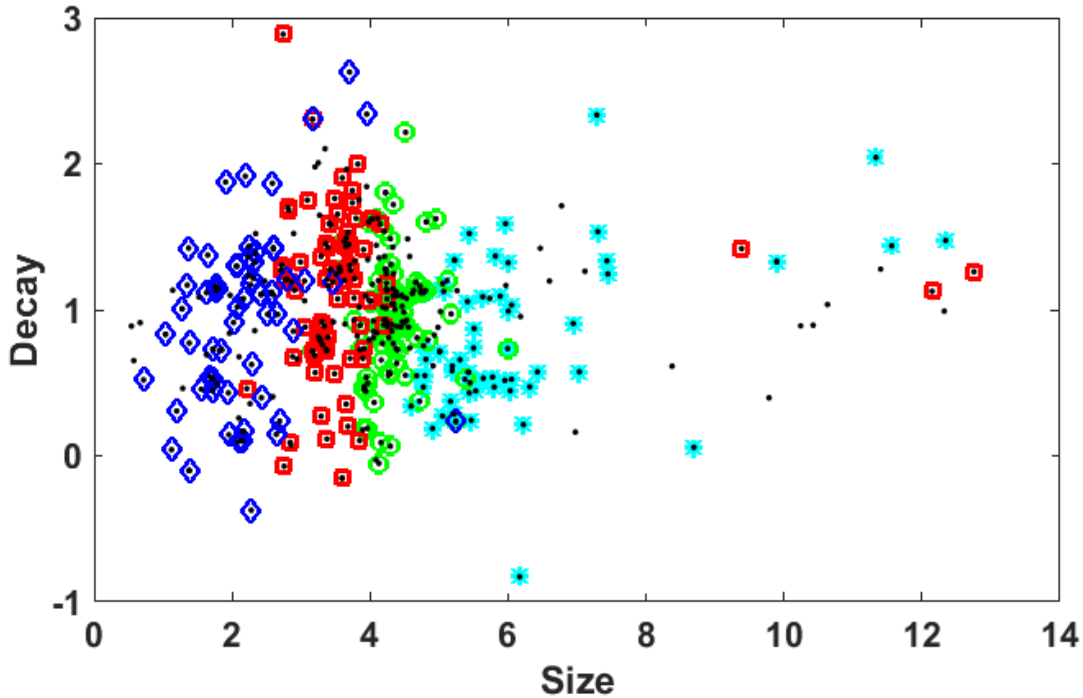


Figure 98. Feature space scatter plot comparing the size and decay distribution computed from polarizability curve characteristics. Cluster analysis was used to group anomalies into 4 classes.

Although the groupings are not particularly strong (i.e., may not uniquely define a target class), when we examine the polarizabilities from each group, we can discern similar characteristics of each group of curves. Figure 99 shows three of the groupings of polarizability curves relative to their averages and the 105mm projectile library curve. Group 1 and 2 exhibit slightly smaller size and faster decay when compared to Group 3 and the 105mm library curves.

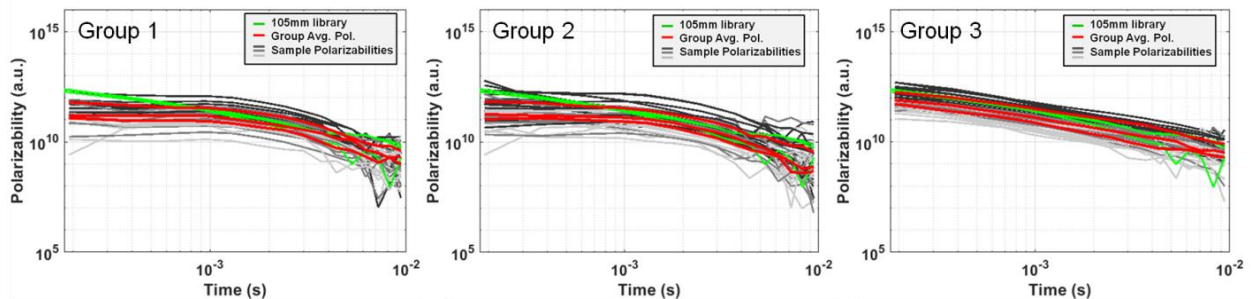


Figure 99. Comparisons of groupings of polarizability curves determined from analysis of size and decay amongst all anomalies identified in the sound surveys.

## 7.7 OPERATIONAL EASE OF USE

We determined the ease of use of the system by overseeing and reviewing operations including system deployment, recovery, and data collection. Deployment and data collection using the integrated crawler-based towed EM array provided information on launch and recovery (LAR) requirements, topside support, and data processing and analysis toward survey mapping and detection list production.

Two technical implementation issues were observed during our demonstration. The first was related to the battery management system for the subsea crawler power supply. The custom SeaView system contains two battery pods that are independently managed and jointly coordinated through the battery management system (BMS). The BMS serves multiple functions related to managing the charging processing and monitoring and optimizing the batteries during operations. The total energy available on the crawler is over 14.5 kiloWatt hours, thus the BMS also provides a means of controlling and managing the potential rapid dissipation of the power over time. In addition, monitoring each of the 40P cell packs wired in series, the BMS also maintains cell balancing and monitors for overcurrent and short circuiting. We observed frequent faults due to potential overcurrent or overvoltage indicators. However, it is unlikely that these frequent faults were due to actual overcurrent/voltage issues and more likely from sporadic noise being imparted on the BMS and falsely causing the faults. This became a nuisance to the operator, who had to reset the BMS frequently. This issue should be addressed in future demonstrations and operations. A challenging case occurred when faults occurred on both battery pods at the same time. This caused a case where the mobility subsystems were not able to receiver power. This should be remedied by implementing a third and separate power supply that can independently retain power to restart the system regardless of the fault condition on the main power supplies.

The second issue was related to operations with fiber optic system. The tether and related subsea topside-subsea communications system functioned without exception, but management of the tether while make turns required some additional procedures for preventing the tether from getting wrapped around the GPS mast. In addition, the tether connection at the subsea crawler may be susceptible to water ingress and failure without redundant strain relief and more robust attachment.

The operator control (Figure 100) of the crawler system was relatively straightforward. It was observed that continuous turning with the tow system took some practice. The challenge is that the crawler essentially executes skid-steer control of turning maneuvers. This involves disproportional effort being supplied to the right and left motors to make the turn. Optimization of the motors may be required to improve continuous turning.



**Figure 100. Operator control station showing the helmsman with joystick control and multiple screens with camera views and system feedback. The operator can access 3 or 4 camera views, scanning sonar range and bearing display, crawler status interface (displaying real-time battery status, navigation, and radio communications information) crawler and tow sled navigation - waypoint tracking software interface, and the FlexEM data acquisition and configuration control user interface from the top side control station**

## **7.8 LAUNCH AND RECOVERY**

The initial deployment of the system was very straightforward and relatively fast, taking fewer than 3 hours. The crawler was remotely controlled to dismount if from its carrying trailer and mechanically connected to the EM array tow sled. The electrical connections were made and tested and the GPS mast was erected and secured in place. Operation of the crawler-based EM system during our demonstration was relatively straightforward overall. Data collection involved minimal interaction from the system operator (helmsman) and sensor system analyst.

## **8.0 COST ASSESSMENT**

### **8.1 COST MODEL**

The cost elements that were tracked during the demonstration at the Duck FRF site are detailed in Table 6. The provided cost elements are based on a simple and incomplete cost model developed for the integrated crawler-EM system used in our demonstrations. The integrated system does not yet have a price developed for purchase or lease. Therefore, some aspects of the price elements must be estimated for the purposes of cost assessment.

**Table 6. Cost Model for a Detection/Discrimination Survey Technology**

Cost Element	Data Tracked	Estimated Costs
Instrument cost	N/A (See description below)	All major equipment and instrumentation are on-loan to the project by participating performers; estimated costs of the Flex-EM or similar array are \$500/day or \$2,500/wk
Support equipment lease rates	Lease rates for major components Engineering estimates based on current development Lifetime estimate Consumables and repairs	RTK-GPS: \$ 1,200/wk
Mobilization and demobilization	Cost to mobilize to site Derived from demonstration costs	Equipment Prep (est.): \$ 3,600 Shipping (MI-NC-MI): \$ 4,110 <i>TOTAL Mob/Demob: \$ 7,710</i>
Site preparation	Time and cost to setup test site (relates to beach IVS set up)	Test Target Prep: \$ 550
System setup costs	Unit: \$ cost to set up and calibrate Data requirements: Hours required Personnel required Frequency required	Crawler System Setup: \$ 5,250 EM Array Setup/QA: \$ 1,275 RTK-GPS Setup: \$ 1,750 <i>TOTAL Setup: \$ 8,275</i>
Survey costs	Unit: \$ cost per acre Data requirements: Hours per acre Personnel required	1.1 acres/hour at 100% coverage 100% coverage (\$/acre): \$ 571 50% coverage (\$/acre): \$ 286 25% coverage (\$/acre): \$ 143
Detection data processing costs	Unit: \$ per hectare as function of anomaly density Data Requirements: Time required Fixed costs and Personnel required	Fixed Costs: \$ 1,250 1 person (analyst at \$100/hr) 2 mins. / anomaly (average) Per anomaly (100/acre): \$ 3.33 Per acre (100/acre): \$ 333

**Instrument Cost:** EM sensors applicable for underwater UXO applications vary in size and complexity. Although we do not have lease prices for the Flex-EM sensor, we estimate costs based on the commercially available similar sensor arrays. The EM-61S has a daily rate of \$95 and fixed mobilization charge of \$125. Two EM-61S systems would then be \$250/day. The Geometrics G-882 TVG array rents for \$375/day (plus \$750 mobilization cost).

**Support Equipment Lease Rates:** Support equipment includes the RTK-GPS and, as such, has associated lease rates that were tracked. This equipment is categorized as required. All associated labor costs were tracked and aggregated to form the cost element assessment.

**Mobilization and Demobilization:** The cost for mobilization and demobilization activities are derived from actual costs including packing and shipping from Dexter, MI to Duck, NC. The number of personnel and labor hours were tracked for specific mobilization /demobilization tasks.

**Site Preparation:**

The cost for site set up and preparation including target seeding were tracked based on actual labor hours and logistical costs associated with this cost element. This included the use of a 2 people for at least one-half of a day to install and survey IVS targets and associated calibration fiducials.

**Instrument Set Up Costs:** The cost for preparation and set up of instrumentation including the crawler-based EM system, topside control components, launch and recovery, and supporting equipment. Time associated with non-recurring engineering or additional set-up required for engineering analyses was not included. We estimate 8 hours of labor for initial setup of the operator control station, subsystem mounting and cabling, and GPS mast setup. We estimate 4 hours labor for EM array setup and QA including EM array mounting and cabling. Configuration, setup, and checkout of the RTK-GPS system will take approximately 4 hours. Overall, this results in an estimated instrument setup cost of \$8,275.

**Survey Costs:** Costs are estimated from the incurred cost of labor and equipment (based on day-rate lease estimates) during survey mode operations. Area was calculated based on data acquired from the system navigation data.

**Detection Data Processing Costs:** Detection-level processing costs will be pro-rated based on the prescribed data flow and standard procedures that are being demonstrated. Costs were estimated based on individual labor hours and any required fixed costs (e.g., for software licensing). Our estimate for data processing costs are \$333 per acre assuming approximately 100 anomalies per acre.

## 9.0 SYNTHESIS AND CONCLUSIONS

Nearshore environments such as swash zone, surf zone with breaking waves, and shallow tidal areas provide hydrodynamic and bottom conditions that machinate to challenge geophysical survey operations. Forces present both in the water column and seafloor substrates can be difficult to manage due to their variability in both space and time. To date, extensions of terrestrial or open ocean survey configurations such as man-portable, diver-based, or surface vessel towed sensor arrays have had little success in effectively surveying these areas. To overcome the limitations of these current configurations, we evaluated both platform and sensor performance to demonstrate and characterize a tailored and integrated robotic bottom crawler towed sensor solution in representative nearshore UXO sites. The tests and demonstrations reported on here are among the first of their kind in terms of quantification of UXO detection survey performance metrics for a system that can traverse back and forth between fully submerged and dry land environments (i.e., completely amphibious). We had to overcome a number of challenges related to system integration and validation, preparation of a nearshore test site, and execution and analysis of field tests in the transitional shoreline zone.

We showed preliminary engineering evaluation results from experiments conducted on land at test sites in New Hampshire and Maryland, on the shore and waters of western Lake Erie, and at the USACE FRF surf zone site in North Carolina. These early shakedown tests highlighted system improvements that were needed in order to demonstrate an effective integrated bottom crawling survey system in our interim demonstration. The SurfROVer platform was tailored for towing of the FlexEM TDEM array. The array sled was developed, modified, instrumented, and validated at the FRF before fully integrating with the SurfROVer platform. The SurfROVer was also modified iteratively to enhance the drive motors and topside control system. The drive motors were up-scaled and tested to provide over 573 kgf (1264 lbf) of pulling force. The maximum load force from independent sled tests at the FRF was 170 kgf during uphill climbs out of the wave trough just shoreward of the breaking waves. Data acquisition and operator/analyst topside user interfaces were optimized and verified. This included development and implementation of a topside helmsman navigation and guidance software interface as well as testing to develop target polarizability libraries for the system.

The SurfROVer crawler platform and integrated tow sled system proved to be a stable operating platform with decent tractive control on all substrates on which it was tested (dry grass and gravel, soft sand, mud and silt, shelly sands, dry and saturated fine to coarse sand). During our interim demonstration of the integrated system at the FRF site, target emplacement as well as crawler system operations were hampered by a strong offshore storm that delivered 20-30 knot winds and waves over 2.2 meters high. Despite this very challenging weather, we were able survey enough area to estimate mobility, stability, and target detection metrics. We are able to show adequate control of system mobility and stability with advance rates exceeding 0.32 m/s (0.62 knots) and detection of all targets target detection within 0.3 m RMS localization accuracy relative to surveyed ground truth locations. The full capability of the 3D EM array system was not completely tested because of our limited areal coverage and associated multi-angle EM illumination of targets. Even though we were not able to conduct overlapping survey transects, single pass transects over the emplaced targets yielded classification quality magnetic polarizability inversions that matched our target libraries within 90% fit RMS fit metrics.

Additional testing was completed over the target grid established in the northwestern portion of the Currituck Sound. During surveys in the sound, we covered approximately 7.3 line kilometers over an area of approximately 12,000 m<sup>2</sup>. Average advance rates of 1.4 m/s enabled efficient surveying at a rate of approximately 1.2 acres/hour. Targets were readily detected with an overall probability of detection of 100%. Follow on classification using three-axis polarizability inversion was adequate to correctly classify many of the anomalies as targets of interest and as clutter. Among the primary challenges we faced in detecting and classifying UXO in the surf zone was tracking of the towed array behind the crawler. Our positioning problem is exacerbated by the fact that we have a two-body system comprised of the crawler itself and the tow platform. Although the tow platform is coupled to the crawler through a rigid tow bar, the tow point has 3 rotational degrees of freedom to allow motion over roll, pitch, and yaw angles. This means that the tow platform is not necessarily following directly in-line with the crawler trajectory. Therefore, we need to provide instantaneous relative position and orientation estimates of the tow platform relative to the crawler. This may be accomplished through implementation of an absolute angle encoder at the tow point to measure the yaw (azimuth) and an inertial measurement unit on the tow bar that provides roll and pitch angles. These measurements can be combined with those measured on the crawler platform itself to generate relative orientation between the two bodies. In addition, a shorter tow bar length and moving the center of gravity forward on the tow sled may improve the overall tracking of the towed array.

Overall, the tests reported on here proved that the system could: (i) be transported, launched, and operated for nearshore and marine UXO applications, (ii) survey effectively with adequate stability and mobility in the surf and traction control on the soft muds in the sound, (iii) provide high quality data to topside operators and analysts for detection and localization of UXO of size 60mm to 155mm within 30 cm of surveyed locations, and (iv) discriminate targets of interest from clutter in many cases when EM array positioning control and coverage permitted. To improve classification for single-pass towed EM operations from the crawler, we foresee significant advantages in sequencing primary field transmitters across the array. Although, this is not as effective as a full three-dimensional transmitter configuration for dynamic single-pass classification (such as that implemented in the OPTEMA 5T system), it will lead to significantly more robust and accurate polarizability inversions. Because the current sensor implementation excites both transmitters in series, it effectively operates with only one transmitter coil. Therefore, we need to aggregate data from consecutive soundings along the transect line (i.e., line methodology) in order to ensure the target receives the required multi-axis illumination from the transmitter. As the transmitter passes over the target, any offset of the sensor from directly over the target produces a different angle of incidence between the impinging transmitter field and the target. While this appears to be effective in the along-track direction (i.e., along the direction of motion), it doesn't provide sufficient across-track illumination to robustly resolve all three principal axes of the polarizability tensor. By sequencing the left and right transmitters that are already implemented in the array (or sequencing between opposing and aiding polarities), it is possible to adequately illuminate targets of interest along all three orthogonal directions, and thus resolve polarizabilities more consistently with single-pass crawler-towed EM.

Another challenge we faced in executing marine towed system performance testing was related to controlling the stability of the emplaced test target assets. Highly dynamic and energetic conditions in the surf zone at the FRF site presented a challenge for installation of simulant UXO

targets and keeping them from moving. We attempted to use "target string" by connecting each simulant UXO along a line together with a weighted rope line that was attached to each UXO. In the most energetic region of the surf zone near the wave break and swash region, we found that it was not possible to keep UXO from mobilizing over a 24-hour period (or more likely over a diurnal tidal cycle). This has illuminated a need for improved installation and target tracking methods for future tests. The implementation of "smart UXO" that contain MEMS sensors to detect self-movement and burial may be advantageous to track simulant targets and estimate changes in their burial depth. In addition, we advocate for the development of improved simulant target installation methods as hand digging in saturated submerged substrate such as fine sands in the surf zone while under the influence of strong currents and waves is not ideal. Alternate methods such as water jetting or caisson installation techniques may prove useful.

Two technical implementation issues were observed during our demonstration. The first was related to the battery management system for the subsea crawler power supply. We observed frequent faults due to potential overcurrent or overvoltage indicators that moderately impacted operations and should be addressed in future tests/operations. The second issue was related to operations with fiber optic system. The tether and related subsea topside-subsea communications system functioned without exception, but management of the tether while make turns required some additional procedures for preventing the tether from getting wrapped around the GPS mast. Although, the operator control of the crawler system was relatively straightforward, continuous turning with the tow system took some practice. Optimization of the crawler track drive motors may be required to improve continuous turning and overall maneuverability of the integrated system.

## 10.0 REFERENCES

- Bachman, C.M., Abelev, A., Bounds, M.T., Fusina, R.A., Kremens, R., Difrancesco, G., Vermillion, M., Mattis, G., Edwards, K.B., and Estrada, J., 2016, Ssan Yong 2014 Remote Sensing Experiment, Naval Research Laboratory Memorandum Report NRL/MR7230-16-9667, 282 pp.
- Bellis, V., O'Connor, M.P., and Riggs, S.R., 1975, Estuarine shoreline erosion in the Albemarle-Pamlico region of North Carolina: North Carolina Sea Grant Publication UNC-SG-75-29, 67p.
- Birkemeier, W.A., Miller, H.C., Wilhelm, S.D., DeWall, A.E., Gorbics, C.S., 1985. A User's Guide to the Coastal Engineering Research Center's (CERC's) Field Research Facility, IR CERC-85-1. U.S. Army Corps of Engineers, Vicksburg, MS (p. 136).
- Byrnes, M. R. 1989. SuperDuck Beach Sediment Sampling Experiment, Report 1, Data Summary Report. Miscellaneous Publication CERC-89-18, U.S. Army Engineer Waterways Experiment Station, Coastal Engineering Research Center, Vicksburg, MS.
- Coastal Planning & Engineering of North Carolina, Inc., 2014, Environmental Assessment For the Town of Duck Shoreline Protection Project, 167 pp.
- Coastal Planning & Engineering of North Carolina, Inc., 2015, Comprehensive Marine Sand Search and Borrow Area Design Report: Towns of Duck, Kitty Hawk, and Kill Devil Hills, North Carolina. 48p. (Prepared for the Towns of Duck, Kitty Hawk, and Kill Devil Hills, North Carolina).
- Drake, T.G., 1997, Final Report for Field Studies of Nearshore Sedimentary Structures, Miscellaneous Report CHL-97-3, North Carolina State University, 155 pp.
- Dolan, R., Lins, H., 2000, The Outer Banks of North Carolina, USGS Professional Paper 1177-B, Prepared in cooperation with the National Park Service, 43 pp.
- Eames, G.B., 1983, The late Quaternary seismic stratigraphy, lithostratigraphy, and geologic history of a shelf-barrier-estuarine system, Dare County, North Carolina: M.S. Thesis, Department of Geology, East Carolina University, Greenville, NC, 196p.
- Haines, J.W., and G. Gelfenbaum, 1995, Field measurements of turbulent stresses during the Duck94 nearshore processes experiment, EOS Transactions of American Geophysical Union, [#O22B-10], 76 (46), pp. 298.
- Inman, D.L. and Dolan, R., 1989, The Outer Banks of North Carolina: Budget of sediment and inlet Ivantysynova, M. 2000. Displacement Controlled Linear and Rotary Drives for Mobile Machines with Automatic Motion Control. 2000 SAE International OFF-Highway & Powerplant Congress, Milwaukee, Wisconsin, USA. SAE Technical Papers 2000-01-2562. doi:10.4271/2000-01-2562.
- Ivantysynova, M. 2000. Displacement Controlled Linear and Rotary Drives for Mobile Machines with Automatic Motion Control. 2000 SAE International OFF-Highway & Powerplant Congress, Milwaukee, Wisconsin, USA. SAE Technical Papers 2000-01-2562. doi:10.4271/2000-01-2562.
- Laudato, S.J., Schultz, G., Keranen, J., and Miller, J, 2016, Dynamic EMI sensor platform for digital geophysical mapping and automated clutter rejection for CONUS and OCONUS applications, Proceedings of the SPIE, Defense and Security Symposium 9823, 982305-982305-10.
- Leatherman, S.P., K. Zhang, and B.C. Douglas. 2000. Sea level rise shown to drive coastal erosion. EOS, Transactions American Geophysical Union 81(6):55-57.

- Leatherman, S.P., T.E. Rice, and V. Goldsmith, 1982. Virginia barrier island configuration: a reappraisal. *Science*, 215: 285-287.
- Mallinson, D., Riggs, S., Thieler, R., Culver, S., Foster, D., Corbett, R., Farrell, K., and Wehmiller, J., 2005, Late Neogene and Quaternary evolution of the northern Albemarle Embayment (mid-Atlantic continental margin, USA), *Marine Geology*, 217: 97-117.
- McNinch, J.E. 2004. Geologic control in the nearshore: shore-oblique sandbars and shoreline erosional hotspots, Mid-Atlantic Bight, USA. *Marine Geology* 211: 121-141.
- Meisburger, E.P., C. Judge, and S.J. Williams, 1989. Physiographic and geologic Setting of the Coastal Engineering Research Center's Field Research Facility. Miscellaneous Paper CERC-89-9, U.S. Army Corps of Engineers, Waterway's Experiment Station, 28p.
- O'Connor, M.P., Riggs, S.R., Winston, D., 1972. Recent estuarine sediment history of the Roanoke Island area, North Carolina. In: Nelson, B.W. (Ed.), *Environmental framework of coastal plain estuaries*. Geological Society of America Memoir, 133, pp. 453-463.
- Riggs, S.R., Belknap, D.F., 1988. Upper Cenozoic processes and environments of continental margin sedimentation: eastern United States. In: Sheridan, R.E., Grow, J.A. (Eds.), *The Atlantic Continental Margin*, U.S. Geological Society of America. *The Geology of North America*, pp. 131-176.
- Riggs, S.R. and O'Connor, M.P., 1974, Relict sediment deposits in a major transgressive coastal system: North Carolina Sea Grant Publication UNC-SG-74-04, 37p.
- Riggs, S.R., 1996, Sediment evolution and habitat function of organic-rich muds within the Albemarle estuarine system, North Carolina: *Estuaries*, v.19, p.169-185.
- Riggs, S.R., Cleary, W.J., Synder, S.W., 1995. Influence of inherited geologic framework on barrier shoreface morphology and dynamics. *Mar. Geol.* 126, 213- 234.
- Riggs, S.R., York, L.L., Wehmiller, J.F., Snyder, S.W., 1992. Depositional patterns resulting from high-frequency Quaternary sea-level fluctuations in northeastern North Carolina. In: *Quaternary Coasts of the United States: Marine and Lacustrine Systems*. SEPM Spec. Publ. No. 48, 141-153.
- Rogers, S. and D. Nash. 2003. *The Dune Book*. North Carolina Sea Grant, Raleigh, North Carolina, 28 pp.
- Schlee, J.S., Manspeiser, W., and Riggs, S.R., 1988, Paleoenvironments offshore Atlantic U.S. margin: In
- Schultz, G., Keranen, J., Miller, J., and Shubtiidze, F., 2014, Acquisition and processing of advanced sensor data for ERW and UXO detection and classification, *Proceedings of the SPIE, Defense and Security Symposium 9072*, 90720H-90720H-9.
- Schultz, G., Shubitidze, F. J. Miller, and Evans, R., 2011, "Active source electromagnetic methods for marine munitions", *Proceedings of the SPIE, Defense and Security Symposium*, 8017, 8017OU; doi:10.117/12.884023.
- Sheridan, R.E. and Grow, J.A. (eds.), *The Atlantic continental margin of the United States: Geology of North America*, Geological Survey of America *Decade of North American Geology v.I-2*, p.365- 385.
- Smith, G.M., Thomson, A.G., Wilson, A.K., Hill, R.A., and Purcell, P.W., 2007, Airborne remote sensing for monitoring the impact of coastal zone management, *International Jour of Remote Sensing*, 28, 1433-1435.
- Staube, D.K., Holem, G.W., Byrnes, M.R., Anders, F.J., Mesiburg, E., 2993, SUPERDUCK Beach Sediment Experiment: Beach profile change and foreshore sediment dynamics, Coastal Engineering Research Program Report, CERC-93-4, May 1993, 51 pp.

- Thieler, E.R., D.S. Foster, E.A. Himmelstoss, 2014. Geological framework of the northern North Carolina, USA inner continental shelf and its influence on coastal evolution. *Marine Geology* 348: 112-130.
- USACE (United States Army Corps of Engineers). 2010. Final Environmental Impact Statement May 2010. Beach nourishment project, Town of Nags Head, North Carolina. U.S. Army Corps of Engineers, Wilmington District. Washington, NC. 172 pp.
- USACE (United States Army Corps of Engineers). 2000. Final feasibility report and environmental impact statement on hurricane protection and beach erosion control: Dare County beaches (Bodie Island portion), Dare County, North Carolina. Vol I and Vol II, US Army Corps of Engineers, Wilmington District, South Atlantic Division.

*Relevant websites referenced or accessed:*

[www.frf.usace.army.mil](http://www.frf.usace.army.mil)  
[navigation.usace.army.mil/CHL\\_Viewers/FRF](http://navigation.usace.army.mil/CHL_Viewers/FRF)  
[www.bluecdesigns.com/blueDrop.aspx](http://www.bluecdesigns.com/blueDrop.aspx)